

PERFORMANCE ASSESSMENT OF A NATURAL CONVECTION
SOLAR TUNNEL DRYER THROUGH EXPERIMENTATION AND
CFD SIMULATION OF TEMPERATURE AND AIR FLOW

By

MAONA MUKANEMA

A Dissertation Submitted to the University of Zambia in Partial Fulfilment of the
Requirements for the Award of the Degree of Master of Engineering in Renewable
Energy Engineering

The University Of Zambia

2022

DECLARATION

I **MAONA MUKANEMA** do hereby declare that the contents in this dissertation are my original work and have not been previously submitted to any University for the award of a degree or any other qualification.

MAONA MUKANEMA

Signature..... Date

CERTIFICATE OF APPROVAL

This dissertation submitted by **MAONA MUKANEMA** has been approved as fulfilling the requirements for the award of the degree of Master of Engineering in Renewable Energy Engineering at the University of Zambia.

.....

Supervisor Signature

.....

Chairperson (Board of Directors) Signature

.....

Co-Supervisor Signature

Examiner 1: Sign..... Date

Examiner 2: Sign Date.....

Examiner 3: Sign Date.....

CERTIFICATION

This is to certify that this research entitled “Performance assessment of a natural convection solar tunnel dryer through experimentation and CFD simulation of temperature and air flow” was carried out by **MAONA MUKANEMA** in the school of Engineering at the University of Zambia for the award of the degree of Master of Engineering in Renewable Energy Engineering.

.....

Dr. Isaac N. Simate (Supervisor)

.....

date

.....

Dr. Edwin Luwaya (Co-Supervisor)

.....

date

ABSTRACT

Natural-convection solar tunnel dryers capable of achieving greater drying rates when drying products. The increased temperature decreases the relative humidity of the air, thereby allowing the air to more efficiently dry the product. However, it is necessary to provide an appropriate solar air heater in order to achieve the required drying air temperature distribution for improved performance of such a dryer. In order to predict variation of moisture content with time during the drying process, it is necessary to have an appropriate drying model. The purpose of this study was to investigate the performance of dryer and apply Computational Fluid Dynamics simulations in visualizing the air flow and temperature. In this study experiments were carried out at the University of Zambia, Department of Agricultural Engineering under natural conditions. Simulations of temperature and air flow within the model of the dryer were done and the results showed average air temperature of up to 70°C was attained at the drying unit. The average air temperature obtained in the process of the Computational Fluid Dynamics (CFD) simulation was in agreement with the experimental temperature for drying the banana slices with an error of 5.1%. The dryer model describes the transfer process and flow field pattern of air in the tunnel dryer and predicts the instantaneous temperature, air velocity, pressure field pattern at any location of the dryer with emphasis on the collector, drying unit and chimney. From the simulations it was observed that the increasing the collector length from 1.5 to 2 m had a collector temperature percentage increment of 8.98%. The simulation results shows that temperature obtained inside the chamber increases with increase in exposed surface area of collector. A mass of 0.943 kg of banana slices were dried from an initial moisture content of 73.89% (w.b.) to 4.39% (w.b.) in 13 hours. The performance of the dryer was analysed by calculating the collector and drying chamber efficiencies. The efficiencies were found to be 33.09% and 13.5% for the collector and drying chamber, respectively. To find an appropriate thin layer model, 11 thin layer models from literature were analysed using Matlab R2018A curve fitting tool and the best model was determined based on three statistical parameters: coefficient of determination (R^2), Sum of Square Error (SSE) and Root Mean Square Error ($RMSE$). Among the 11 thin layer mathematical models which were established to help predict the drying of banana slices, the Midilli et al and Page models provided excellent fits to the experimental

data with a value of R^2 of **0.9990** and **0.9933**, respectively. The values of *SSE* and *RMSE* obtained from both models were less than **0.008335** and **0.02753**, respectively. This research also presents an energy and exergy analysis of the solar drying process. From the energy and exergy analysis, the average collector efficiency during the experiment was 33.09 % while the average collector exergy and drying chamber efficiencies were 1.91 % and 63.20%, respectively. On the basis of temperatures obtained from the simulation and experiment results, the drying time achieved for 3 mm banana slices and the collector efficiencies, the dryer performed well. Cost based optimization of the dryer is recommended for further study.

Keywords

CFD simulation, Temperature and air flow, Natural convection, Solar tunnel dryer, Chimney

DEDICATION

This research work is wholeheartedly dedicated to our parents Clement and Ireen C. Mukanema who have been a source strength, who continually provide their unconditional spiritual, emotional and financial support.

To my sisters (Mwiza and Thandiwe Mukanema) for always cheering me on, my late brother (Taonga Mukanema) for always believing in me, My Niece Victoria Mukanema may this be stepping stone for you and the generations to come, my family members and friends for their prayers and words of encouragement during the study period, thank you!

To my love Mwaka Chizi for your patience, unconditional love and support, thank you!

May the almighty God bless and protect you all.

Lastly of a greater magnitude, I dedicate this research to God Almighty for his sustenance, provision and grace. All the Glory I give to you.

ACKNOWLEDGEMENTS

My deepest gratitude is directed towards the Almighty God for the Grace and strength He bestowed upon me throughout the progress of this research, the opportunity He made possible as well as the art of approach he continually fills me with. It wasn't easy but made it possible

I would like to offer my special thanks to my supervisor, Dr. I.N. Simate and co supervisor Dr. E. Luwaya for their willingness to devote their time and help me with valuable and constructive suggestions. May the almighty God bless your endeavours!

I would also like to acknowledge the heads of Department of Agricultural and Mechanical Engineering, University of Zambia Dr. V. Kaluba and Dr. V. Musonda together with their entire members of staff, technical and support staff for their generous input.

TABLE OF CONTENTS

DECLARATION.....	ii
CERTIFICATE OF APPROVAL	iii
CERTIFICATION	iv
ABSTRACT	v
DEDICATION	vii
ACKNOWLEDGEMENTS	viii
TABLE OF CONTENTS	ix
LIST OF FIGURES	xii
LIST OF TABLES	xiv
LIST OF ABBREVIATIONS	xv
NOMENCLATURE.....	xvi
1. CHAPTER ONE: GENERAL INTRODUCTION.....	1
1. Chapter introduction.....	1
1.1 Background.....	1
1.2 Statement of the problem.....	2
1.3 Justification of the study.....	3
1.4 Objectives of the study	3
1.5 Research questions	4
1.6 Scope of the study	4
1.7 Ethical considerations.....	4
2. CHAPTER TWO: LITERATURE REVIEW	5
2. Introduction	5
2.1 Overview	5
2.1.1 Drying.....	5

2.1.2	Open sun drying (OSD).....	5
2.1.3	Types of solar drying systems	7
2.2	Drying efficiency	12
2.3	Banana drying.....	13
2.3.1	Drying Models for the Description of Drying Kinetics of Banana	14
2.4	Computational fluid dynamics	16
2.5	Temperature distribution	18
2.6	Governing equations.....	19
2.6.1	Heat transfer	19
2.7	Simulation.....	24
2.8	Energy and exergy analysis	25
2.9	Closing remarks.....	26
3.	CHAPTER THREE: METHODOLOGY	28
3.	Introduction	28
3.1	Description of the dryer and its mode of operation	28
3.2	Determination of the temperatures and air velocity	29
3.3	Simulation procedure.....	33
3.4	Setup.....	36
3.5	Thin layer modelling of the drying curve.....	43
3.6	Performance evaluation	46
3.7	Energy and Exergy analysis	47
3.8	Closing remarks.....	51
4.	CHAPTER FOUR: RESULTS AND DISCUSSIONS	52
4.	Introduction	52
4.1	Heat transfer analysis	52

4.2 Relative humidity	55
4.3 Moisture content changes with time	57
4.4 Airflow	58
4.5 Simulations	59
4.6 Comparison of experimental and simulation results	72
4.7 Effects of varying the collector and drying chamber lengths through simulation	73
4.8 Evaluation of the dryer performance	76
4.9 Thin layer modelling	79
4.10 Energy and exergy analysis	83
4.11 Closing remarks	87
CHAPTER FIVE: CONCLUSIONS AND RECOMMENDATIONS.....	88
5. Introduction	88
5.1 Conclusions	88
5.2 Recommendations	89
5.3 Closing remarks	89
REFERENCES	90
Appendix I: Solar dryer	104
Appendix II: The banana slices after drying	105
Appendix III: Sample calculation of the heat transfer rate.....	106
Appendix IV: The best fitting thin layer models midilli et al and page models.	107
Appendix V: Simulation input and output variables	108
Appendix VI: Approval of Study	109
Appendix VII: Article.....	112

LIST OF FIGURES

Figure 2-1: Working principle of open sun drying (Sharma, 2009).....	6
Figure 2-2 Classification of Solar dryers based on designs (Ekechukwua & Norton, 1999).....	7
Figure 2-3 Working principle of a direct solar dryer (Sharma, 2009).....	9
Figure 2-4 Working principle of an indirect solar dryer (Sharma, 2009)	10
Figure 2-5 Forced convection mixed mode solar tunnel dryer used to dry hot chilli	12
Figure 2-6 Hierarchical classification of various methods in CFD (Hossain & Fdhila, 2015).....	18
Figure 2-7: Time Rate of Change of Energy in a System	23
Figure 3-1 Air flow in the solar tunnel dryer (source: Cherotich, (2016)).....	29
Figure 3-2 Experimental set-up of the solar tunnel dryer and the equipment (1) Collector unit, (2) Drying unit, (3) Bare flat-plate chimney unit, (4) Solar pyranometer, (5) Data logger, (6) Computer.	30
Figure 3-3 Solar tunnel dryer loaded with the sliced bananas.....	33
Figure 3-4: Solar dryer components	34
Figure 3-5: Solar dryer component dimensions	35
Figure 3-6: Visualization of computational domain.....	37
Figure 3-7: Arrangement of the bananas on the mesh.....	40
Figure 3-8: Porous medium in the solar dryer.....	40
Figure 3-9: Generated mesh of the solar dryer.....	41
Figure 3-10: Flow chart of pre and post processing stages of simulation	43
Figure 4-1: Air temperatures and solar radiation on the Day 1 of the drying Experiment	53
Figure 4-2: Air temperatures on the Day 2 of the drying Experiment	55
Figure 4-3: Variation of relative Humidity and Solar Insolation during the banana drying experiment.....	56
Figure 4-4 Banana drying curve	58
Figure 4-5 Velocity through the solar tunnel dryer chimney	59
Figure 4-6 Simulated temperature flow trajectories	61
Figure 4-7 Temperature cut plots	63

Figure 4-8 Surface temperature contours at collector	64
Figure 4-9 Velocity flow trajectories	66
Figure 4-10 Velocity cut plots	68
Figure 4-11 Relative Humidity.....	71
Figure 4-12 Average simulated and experimental temperatures in the drying unit	72
Figure 4-13 Average simulated and experimental temperatures at the collector outlet .	73
Figure 4-14 Buoyancy pressure head and solar insolation	78
Figure 4-15 Pressure drop in the chimney.....	79
Figure 4-16 Experimental and predicted MR model	82
Figure 4-17 Energy efficiency	83
Figure 4-18 Collector exergy input, exergy output and exergy loss	84
Figure 4-19 Collector efficiency	85
Figure 4-20 Drying chamber exergy inflow, exergy loss and exergy outflow.....	86
Figure 4-21 Drying chamber exergy efficiency	87

LIST OF TABLES

Table 3-1 Computational domain Size	37
Table 3-2 Material properties	38
Table 4-1 Increasing the Collector Length to 1.5m.....	74
Table 4-2 Increasing the collector Length to 2m.....	75
Table 4-3 Increasing the drying chamber length to 2m.....	75
Table 4-4 Increasing the drying chamber length to 3m.....	76
Table 4-5 Thin layer model results.....	81

LIST OF ABBREVIATIONS

CFD	Computational Fluid Dynamics
EEA	Energy and Exergy analysis
Etc	et cetera
FCISD	Forced convection indirect solar dryer
GI	Galvanized Iron
ISD	Indirect solar dryer
MR	Moisture Ratio
NCISD	Natural convection indirect solar dryer
RMSE	Root Mean Square Error
R^2	The correlation coefficient
SAC	Solar air collector

NOMENCLATURE

A_{cz} area of convective zone, m^2	T_{do} temperature at the exhaust side of the dryer, $^{\circ}K$
A_i inlet area, m^2	T_{∞} reference temperature, $^{\circ}K$
C_{pa} specific heat of air, $kJ\ kg^{-1}\ K^{-1}$	V velocity, $msec^{-1}$
E_i emissive power at inlet, Wm^{-2}	g gravitational acceleration, $msec^{-2}$
\dot{E}_{x_i} exergy inflow, W	g_c constant in Newton's Law
\dot{E}_{x_o} exergy outflow, W	m_{da} mass flow rate of air in the dryer, $kg\ s^{-1}$
Ex_{ci} exergy inflow for collector, W	m_{cai} mass flow rate of drying air at the inlet of collector, $kg\ s^{-1}$
Ex_{co} exergy output for collector, W	m_{cao} mass flow rate of drying air at the outlet of collector, $kg\ s^{-1}$
Ex_{do} exergy outflow for collector, W	m_{dao} mass flow rate of drying air at the outlet of dryer, $kg\ s^{-1}$
$EX_{sol-in-col}$ solar exergy, W	s specific entropy, $kJ\ kg^{-1}\ K^{-1}$
\dot{E}_{XL} exergy loss, W	s_{∞} specific entropy at ambient, $kJ\ kg^{-1}\ K^{-1}$
E_{net} net solar radiation, Wm^{-2}	u_0 specific internal energy, $kJ\ s^{-1}$
F_i inlet shape factor	u_{∞} specific internal energy at ambient, $kJ\ s^{-1}$
J joule constant	v specific volume, $m^3\ kg^{-1}$
P_{∞} pressure for ambient, kPa	v_{∞} specific volume at ambient, $m^3\ kg^{-1}$
T temperature, $^{\circ}C$, $^{\circ}K$	z altitude coordinate, m
T_0 reference temperature, $^{\circ}C$	
T_{ci} temperature at the inlet of collector, $^{\circ}K$	
T_{co} temperature at the outlet of collector, $^{\circ}K$	

z_{∞} altitude coordinate at ambient, m

μ_c chemical potential, kJ kg^{-1}

μ_{∞} chemical potential for ambient,
 kJ kg^{-1}

$\eta_{\text{collector}}$ exergetic efficiency of the
collector

η_{dryer} exergetic efficiency of the dryer

CHAPTER ONE: GENERAL INTRODUCTION

1. Chapter introduction

This chapter begins by describing solar energy in food drying and goes on to emphasize on the importance and use of computational Fluid dynamics in heat and mass transfer related to food drying. It highlights the current preservation techniques used to process freshly produced foods before narrowing down to solar drying as the preferred method of food preservation. It also describes in detail the limitations of use of solar dryer and justifies the need to investigate the temperature and air flow distribution in Solar Dryers as way of improving their performance.

1.1 Background

A. Solar energy in food drying

In many parts of the world, there is a developing recognition that renewable energy has an important function to play in extending technology to the farmers in the developing nations to amplify their productivity (Bolaji & Olalusi, 2008). Solar thermal technology is a technology that is rapidly gaining acceptance as an energy saving measure in agricultural application. The seasonal characteristics of crops makes preservation necessary to assure a regular and continuous supply to the consumers throughout the year. There are numerous methods of food preservation but drying is the oldest and most practical method. Sun drying of agricultural produce has been practiced as a preservation method in quite a number of parts of the world (Sacilik, et al., 2006).

Solar dryers incorporating thermal energy storage are quite effective for continuously drying agriculture and food products at steady state in the temperature range of 40°C to 60°C (Kant, et al., 2016). Solar dryers are being studied broadly as an alternative to the conventional techniques (open sun drying, hot air drying, oven drying etc) of crop drying (Pangavhane & Sawhney, 2002). Solar drying has been applied to a range of products including; cereals, nuts, oil crops, fruits and vegetables among others. Solar drying of fruits is one way of keeping fruits in a good quality for consumption and for any required subsequent processing (Cherotich, 2016).

B. CFD in food processing

Computational fluid dynamics, as a tool of research for enhancing the design process and understanding of the basic physical nature of fluid dynamics can provide benefits through improved design to the food processing industry in many areas, such as drying, sterilization, mixing, refrigeration and other application areas (Kaushal & Sharma, 2012). Drying is a common food manufacturing process. The drying rate is a strong function of air flow or air velocity. Therefore, it is of great importance to know the air flow and velocity in the drying chamber, thus leading to know the areas of adequate air velocities for proper drying (Xia & Sun, 2002). Computational fluid dynamics is a powerful tool to aid the prediction of drying process therefore can be used to predict the air flow and velocity during drying. Mathioulakis, et al (1998) used CFD to simulate the air movement inside an industrial batch-type, tray air dryer. Drying tests of several fruits were performed and the result showed that the degree of fruit dryness depended on its position within the dryer. According Kaushal & Sharma, (2012) the determination of pressure profiles and air velocities by CFD showed that the main cause of the variations in drying rates and moisture contents was the lack of spatial homogeneity of air velocities within the drier.

1.2 Statement of the problem

In practice, solar dryers, especially those that operate in natural convection mode, face some challenges which include uneven drying of food products. For the solar tunnel dryer, the effectiveness of the dryer depends on the temperature of the air, natural convection flow rate, initial moisture content and the type of crop to be dried. Uneven drying of food products is as a result of non-uniformity in the air and temperature distribution in the solar dryer. Commonly, the efficiency of solar dryers is evaluated either based on the thermal performance or drying rates of the products. However, several problems might exist such as low drying efficiency, leading to low product quality due to uneven distribution of temperature and air flow in the solar tunnel dryer. These problems attract the attention in the academic and industrial fields. The monitoring of the drying process is in most cases complicated since the temperature and air usually varies from location to location in the dryer, flow simulations allow the temperature and air distribution in the dryer to be visualized, facilitating the identification of possibilities for

design changes. Then, the performance of modified designs can also be simulated without the need to physically construct the model and test it.

While studies have been done on natural convection solar tunnel drying primarily focusing on banana drying and use of CFD in the drying process. In Zambia, it appears little or no studies have been undertaken on natural convection solar tunnel drying of banana and the application of CFD simulations in visualizing the air flow and temperature in the solar tunnel dryer.

The lack of understanding of the factors that affect performance of solar tunnel dryers prevents improvement in their designs. Therefore there is a need to study the performance of Natural Convection Solar Tunnel Dryer.

1.3 Justification of the study

The quality of food depends on the effectiveness of drying which means longer shelf life and maintaining the intended nutritional value. Banana is a fruit widely consumed in the world. However, it is very perishable, causing great waste and financial loss. Convective drying is a simple and low-cost method, widely used in fruit processing to produce new products and extend the shelf life of food. The dried banana is a product of good sensory acceptance and therefore drying is a good alternative for processing the banana slices. The temperature of the drying air is one of the principal parameters of this process since it influences the drying kinetics and the physicochemical properties of the dry product. Therefore, it is important to study different drying air temperatures to determine the best drying condition for dried banana production, to optimize the dried banana process and properties. The application of drying systems in developing communities can greatly reduce postharvest losses of agricultural commodities and significantly contribute to food availability in these areas.

1.4 Objectives of the study

To investigate the temperature and air flow distribution in a Natural Convection Solar Tunnel Dryer using CFD

1.4.1 Specific objectives

The specific objectives of the study were to:

- i. Evaluate the of temperature and airflow distribution in the natural convection solar tunnel dryer,
- ii. Evaluate the collector efficiency, drying efficiency and buoyancy pressure by the chimney of the natural convection solar tunnel dryer ,
- iii. Determine an appropriate mathematical thin layer model to predict the drying characteristics of the banana slices and validate it against experimental results, and
- iv. Evaluate the energy and exergy of the natural convection solar tunnel dryer.

1.5 Research questions

To achieve the objectives of the study, the following questions were to be answered:

- 1) How is the temperature and airflow distributed in the natural convection solar tunnel dryer?
- 2) What is collector efficiency, drying efficiency and buoyancy pressure by the chimney of the natural convection solar tunnel dryer?
- 3) Which mathematical thin layer model best predicts the drying characteristics of the banana slices?
- 4) What is the energy and exergy of the natural convection solar tunnel?

1.6 Scope of the study

This research dealt with a natural convection solar tunnel dryer utilizing solar air heating. Simulation of temperature and air flow through the dryer was done using SOLIDWORKS flow simulation software. The study sought to evaluate the dryer performance using bananas as a product. The mathematical thin layer models were established from existing models in literature. The thin layer model was determined, and validated against experimental results.

1.7 Ethical considerations

In this study, no ethical considerations were considered, as no participants were involved.

CHAPTER TWO: LITERATURE REVIEW

2. Introduction

This chapter begins with a description of the principles of food drying, then principles of CFD and its use in food processing and goes on further to explain the types of solar dryers. It then narrows down to Natural circulation Solar Dryers and proceeds to cite the relevant literature on drying of different food products. Finally, mathematical modelling of mass and heat transfer is discussed in this chapter.

2.1 Overview

2.1.1 Drying

Drying is the basic process to reduce moisture from a product, which is one of the oldest techniques used for food or agricultural products storage (Kant, et al., 2016). It is a classical method of food preservation, which provides longer shelf-life and lighter weight for transportation and small space for storage (El-Sebaei & Shalaby, 2012). Heat and mass transfer phenomena which include the heating of the product, vaporization of water from liquid state on the surface and within the product, diffusion of vapours, mixing the vapour with air and removing the moisture is known as drying (Abdel-Galil, 2007). It extends shelf-life of the harvested products, improves the bargaining power of farmers by maintaining relatively constant price of the agricultural products. Finally, drying reduces post-harvest losses and lowers the transportation cost (Chavan, et al., 2020). The simplest way to dry a product is to expose it to a stream of air whose temperature and humidity conditions allow the water contained in the product to evaporate. The desired moisture content varies depending on the fruit properties, initial moisture content, and the final use of the product, i.e. replanting of grains or drying fruit for consumption (Ekechukwua & Norton, 1999). Indirect solar drying uses a convective drying method where heated, low moisture air is used to transfer heat to the product and evaporation takes place at the product surface (Belessiotis & Delyannis, 2011)

2.1.2 Open sun drying (OSD)

The working principle of open sun drying by using only the solar energy is shown in figure 2.1. The crops are generally spread on the ground, mat or cement floor where they receive short wavelength solar energy during a major part of the day and also natural air circulation (Visavale, 2012). There is partial reflection and absorption of solar radiation

falling on the surface in which the absorbed radiations and surrounding air heat up the surface. Moreover, the moisture from the surface of the product is evaporated, by the produced heat, to the surrounding air although some of this heat is lost through long wavelength radiation to the atmosphere and through the conduction to the ground (Sahdev, 2004). The absorbed radiation is converted into thermal energy and the temperature of the material starts to increase. During sun drying, products are placed on the ground where they are unprotected from contamination and attack by bacteria, infestation by insects, birds, animals and rodents and also it is laborious as the drying product layers have to be turned over and over again periodically to ensure undeviating drying (Abdulmajid, 2015). The process is independent of any other source of energy except sunlight and hence the cheapest method. In general, the open sun drying method does not fulfil the required quality standards and sometimes the products cannot be sold in the international market. With the awareness of inadequacies involved in open sun drying, a more scientific method of solar-energy utilization for crop drying has emerged termed as solar drying (Visavale, 2012).

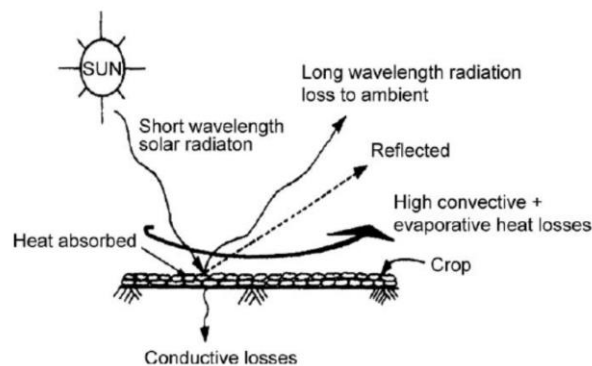


Figure 2-1: Working principle of open sun drying (Sharma, 2009)

To achieve this effect, the air temperature is increased by energy intake from solar radiation (Romero , et al., 2014). The volume of the dried materials is reduced by the drying process thus improving the efficiency of storage and transportation. Also, drying is influenced by air humidity, velocity and temperature (Agarry, et al., 2013). Solar drying of agricultural products in enclosed structures by forced convection is an attractive way of reducing post-harvest losses and low quality of dried products associated with traditional open sun-drying methods (Jain & Tiwari, 2003). Well-designed solar dryers

may provide a much-needed suitable substitute for drying of some of the agricultural crops in developing countries (Kant, et al., 2016). As elaborated below, solar energy dryers can broadly be classified into direct, indirect and hybrid solar dryers. The working principle of these dryers mainly depends upon the method of solar energy collection and its conversion to useful thermal energy for drying.

2.1.3 Types of solar drying systems

In the year of 1976, Everitt and Stanley developed the first solar dryer (Chavan, et al., 2020) . Solar dryers exist in a variety of designs and sizes depending on the requirement and drying capability (Kant, et al., 2016). Solar drying systems can be classified as passive or active depending on the mode of air flow. Both passive and active solar dryers are divided into direct, indirect or mixed mode solar dryers. The main features of typical designs of the various classes of solar dryers are illustrated in Figure 2-2, showing three main groups for solar dryers (direct, indirect or mixed mode solar dryers) on the basis of the energy sources used.

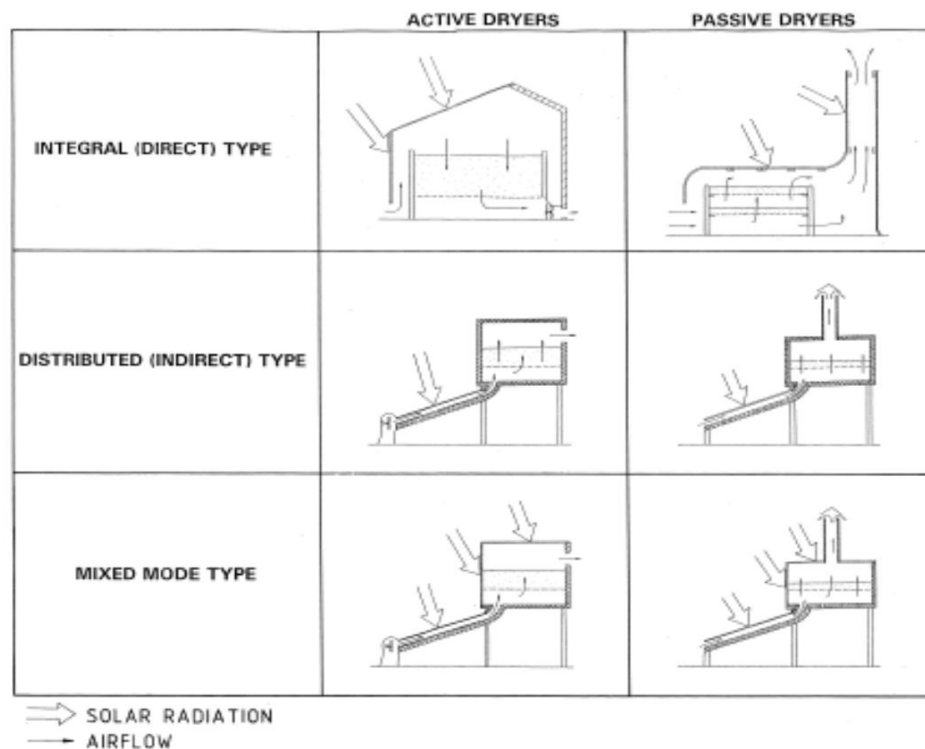


Figure 2-2 Classification of Solar dryers based on designs (Ekechukwua & Norton, 1999)

A. Active or forced convection solar dryers

A typical active solar dryer depends solely on solar-energy as the heat source but employs motorized fans for forced circulation of the drying air (Ekechukwua & Norton, 1999). Active solar dryers are incorporated with a fan or a blower to force the air through the product contained in the dryer, hence, the term forced convection (Leon, et al., 2002). These dryers find major applications in large-scale commercial drying operations in combination with conventional fossil-fuel to have a better control over drying by consolidating the effect of fluctuations of the solar insolation on the drying air temperature (Visavale, 2012). Active solar dryers are known to be suitable for drying higher moisture content foodstuffs such as papaya, kiwi fruits, eggplant, cabbage and cauliflower slices. A variety of active solar-energy dryers exist which could be classified into either the direct -type, indirect-type or hybrid dryers (Visavale, 2012). The requirements for a fan and a source of power to drive the fan make active solar dryers more complex and relatively more expensive than passive solar dryers (Fudholi, et al., 2010).

B. Passive or natural convection solar dryers

Passive solar-energy drying systems are conventionally termed natural-circulation solar drying systems (Visavale, 2012). Natural-circulation solar-energy dryers depend entirely on solar energy for their operation (Maia, et al., 2012; Simate, 2003; Fudholi, et al., 2010). In such systems, solar-heated air is circulated through the crop by buoyancy forces or as a result of wind pressure, acting either singly or in combination (Maia, et al., 2012). The air heated by the solar energy becomes less dense than the ambient air resulting in a difference in air densities which in turn creates a buoyancy force. The buoyancy force or wind pressure or both causes air to be driven in and out of the dryer (Sharma, et al., 2009). Natural circulation solar-energy dryers are the most suitable option for use in remote rural locations where there is no electricity available. They are superior operationally and compete economically with traditional Open Sun Drying (Ekechukwua & Norton, 1999). These are primitive, inexpensive in construction with locally available materials, easy to install and to operate especially at sites far from electrical grid. The passive dryers are best suited for drying small batches of fruits and vegetables such as banana, pineapple, mango, potato, carrots (Hughes & Oates, 2011).

C. Direct solar drying (DSD)

In direct solar dryers, collection of solar energy and drying of the product takes place in an enclosed insulated structure where the food receives direct solar radiation. In direct solar dryers solar energy passes through a transparent cover and is absorbed by the food. Essentially, the heat required for drying is provided by radiation to the upper layers and subsequent conduction into the depth of the food (Bolaji & Olalusi, 2008). The working principle of direct solar crop dryer, also known as a solar cabinet dryer is shown in Figure 2.3. Here the moisture is taken away by the air entering into the cabinet from below and escaping through at the top exit of the dryer. In the cabinet dryer, of the total solar radiation impinging on the glass cover, a part is reflected back to atmosphere and the remaining is transmitted inside the cabinet (Visavale, 2012). When using these types of dryers, the drying process is controlled and the product being dried is protected from damage by insect pests, dust and rain. Also, comparing it to sun drying, the drying time of solar dryers is reduced by about 20% and produces better quality dried products (Hedge, et al., 2015). During drying, heat loss to the ambient is reduced by a glass cover, which is useful for increasing the product and chamber temperature (Mustayen, et al., 2014). The overall phenomena causes the temperature above the crop inside the cabinet to be higher. The glass cover in the cabinet dryer thus serves in reducing direct convective losses to the ambient which plays an important role in increasing the crop and cabinet temperature (Visavale, 2012).

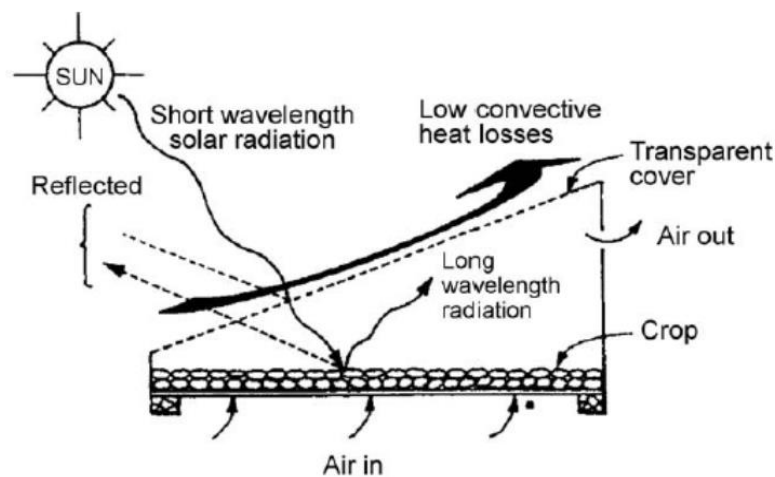


Figure 2-3 Working principle of a direct solar dryer (Sharma, 2009)

D. Indirect solar drying

In indirect dryers, air is heated by solar radiation in an air heater and then flows over the product bed in the drying chamber where the food does not receive direct solar radiation (Patil & Gawande, 2016). Indirect dryers are suitable for colour sensitive food products, as the produce is not exposed directly to sunlight (Zooba & Bansal, 2011). In distributed or indirect solar dryers, the crop is not directly exposed to solar radiation in order to minimize discoloration and cracking of the crop surface. Instead, heated air from a separate solar collector is passed through the crop, placed in a separate chamber. Evaporation of moisture from the crop is obtained as in open sun drying and direct solar drying (Tiwari, 2002). The working principle of an indirect solar dryer is shown in figure 2-4.

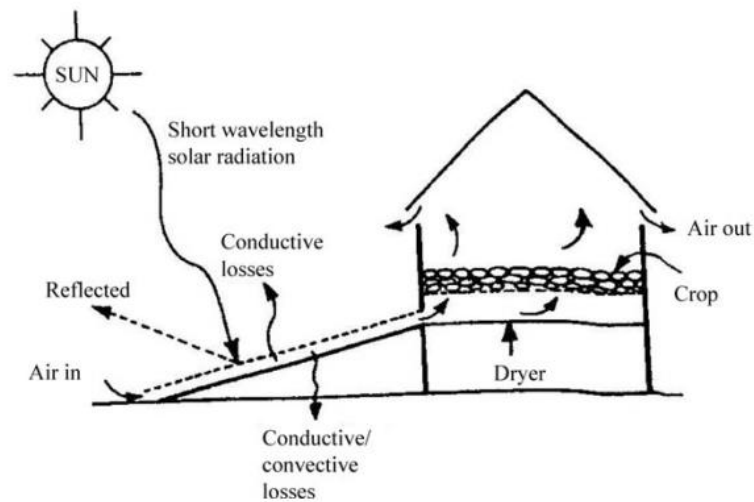


Figure 2-4 Working principle of an indirect solar dryer (Sharma, 2009)

E. Mixed-mode solar drying

In mixed mode solar dryers products are exposed directly to solar radiations and hot air from a solar collector. It is a combination of direct and indirect solar dryers (Patil & Gawande, 2016). Mixed mode dryers have the air heated in two stages, firstly, at the air heating unit and secondly, at the product drying unit. The combined action of incident direct solar radiation on the product to be dried and air pre-heated in a solar collector heater produces the necessary heat required for the drying process (Visavale, 2012). Therefore in the mixed mode dryers, the product being dried benefits from direct solar

energy falling on the drying unit, covered by a transparent cover and the pre-heated air from the air heating unit called a solar collector.

Solar tunnel dryers, a type of mixed mode solar dryers, have a distinct collector unit that serves the purpose of heating air and a drying unit where the product is located. A solar heated tunnel improves the quality of the product being dried by protecting it from foreign matter. It reduces wasted produce and electricity costs, and thus improves the quality and shelf life of the product (Mkhathini & Zulu, 2015). Solar tunnel dryers have some advantages over sun drying when correctly designed. They give faster drying rates, by heating the air to 10-30°C above ambient, reducing its humidity and deterring foreign objects that can spoil the produce. The faster drying reduces the risk of spoilage, improves quality of the product and gives a higher throughput, so reducing the drying area that is needed (Mkhathini & Zulu, 2015). In its simplest form the solar tunnel dryer is usually a hooped framed structure with one or two layers of glazing. There are several reasons why such structures are attractive for use in crop drying. These have an ability to generate high internal temperatures when sealed well and unventilated. They have low capital cost, are easy to construct, and have structural stability. They can also hold commercial size quantities of a crop compared to other forms of solar dryers (Fuller, 1995). Hossain & Bala, (2007) used a mixed mode type forced convection solar tunnel dryer to dry hot red and green chillies under the tropical weather conditions of Bangladesh. The dryer had a loading capacity of 80 kg of fresh chillies. Moisture content of red chilli was reduced from 2.85 kg/kg to 0.05 kg/kg (dry basis) in 20 hours in solar tunnel dryer and it took 32 hours to reduce the moisture content from 2.85 kg/kg to 0.09 kg/kg and 0.40 kg/kg (dry basis) in improved and conventional sun drying methods, respectively. In the case of green chilli, about 0.06 kg/kg (dry basis) moisture content was obtained from an initial moisture content of 7.6 kg/kg (dry basis) in 22 hours in solar tunnel dryer and it took 35 hours to reach the moisture content to 0.10 kg/kg and 0.70 kg/kg (dry basis) in improved and conventional sun drying methods, respectively. The design of the solar tunnel dryer used by Hossain & Bala, (2007) is shown in Figure 2-5.

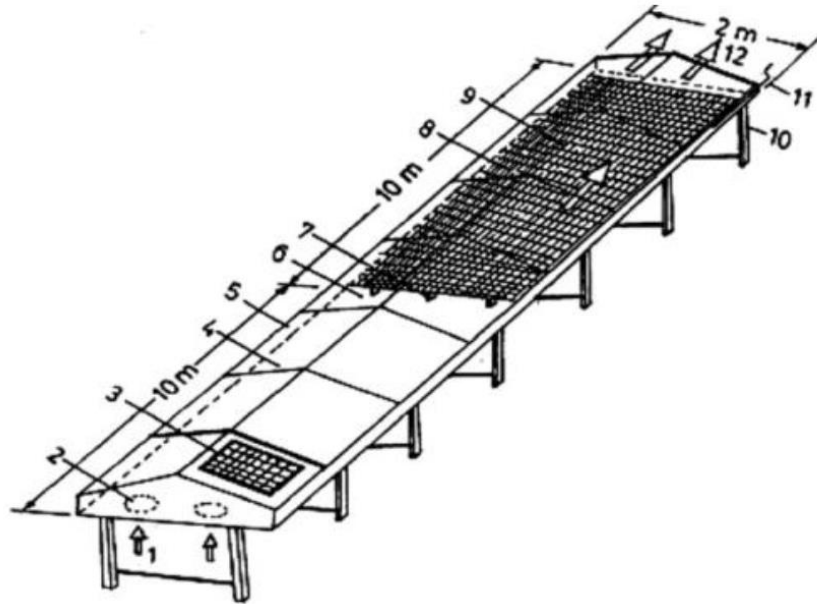


Figure 2-5 Forced convection mixed mode solar tunnel dryer used to dry hot chilli

2.2 Drying efficiency

The drying efficiency is a parameter that indicates the overall performance of the solar dryer and it is defined as the ratio of energy required to evaporate the moisture to the energy supplied for drying (Lingayat, et al., 2017). The major parameters that influence the drying efficiency include the temperature of the air in the drying unit, the mass flow rate, the air speed and the collector design (Leon, et al., 2002). When these parameters are considered under the same solar insolation for a passive drying system and an active drying system, it can be observed that passive drying systems tend to have a lower drying efficiency than active solar drying systems. This is because there is no control on the air flow rates in passive drying systems, hence they normally tend to suffer low flow rates. Aissa, et al., (2014) found overall system drying efficiency (ratio of energy required to evaporate moisture to that supplied to solar dryer, including that consumed by the blower) varied from 1.85 % to 18.6 % and was higher for increased air flow rate. Cherotich, (2016) dried mango using a natural convection solar tunnel dryer and found the dryer efficiency to be 11.3% under solar insolation of between 470 and 1070 W/m^2 . Lingayat, et al., (2017) found the average thermal efficiency of the collector to be 31.50% and that of drying chamber to be 22.38% in an indirect type solar dryer for banana drying.

2.3 Banana drying

Banana (*Musa parudisiaca*) is consumed directly as raw, ripe fruit or processed into pulp-liquid fruit, canned slice, deep-fried chips, toffees, fruit-bars, brandy, etc (Kachru., et al., 1995). It is a tropical climacteric fruit, rich in carbohydrates, dietary fibres, certain vitamins, minerals, phenolic compounds and antioxidants. They are often eaten raw as a dessert fruit, because in the ripe state they are sweet and easily digested. Bananas have therapeutic values in many special diets (Omolola, et al., 2015). As a result, banana consumption is associated with health promotion and the reduction of disease risks. Furthermore, because of these properties, the banana has good sensory acceptance and low cost. These characteristics make bananas one of the most consumed fruits in the world, with an average annual consumption of approximately 12 kg per capita (Macedo, et al., 2020; Khoozani, et al., 2019). The banana pulp represents about 60% of the total weight, being the main part of the fruit. Through the processing of banana pulp the aim is to produce other products and contribute to minimizing waste (Khoozani, et al., 2019). The dried banana is one of the products obtained by drying the banana pulp. Generally, this product has 20–25% moisture, lower than that of fresh pulp (between 70 and 80%) (Sidhu & Zafar, 2018; Borges, et al., 2010). Thuwapanichayanam, et al., (2011) reported by that effective moisture diffusivity of banana ranged between 8.5×10^{-11} - 2.29×10^{-10} at 70-100°C. Macedo, et al., (2020) reported that in convective drying of banana at 40°C, 60°C, and 80°C, the temperature of 80°C showed the highest overall desirability value (0.65). Therefore, 80°C was the ideal drying air temperature for dried banana production.

Drying is one of the oldest methods of preservation and widely applied to banana fruits owing to its simplicity, ease of operation and cost-effectiveness. Besides these advantages, drying decreases the bulk of foods by reducing the volume which reduces packaging, handling and storage and transportation costs as well as ease of handling and processing operations (Gatea, 2011; Gupta, et al., 2011; Radhika, et al., 2011). Drying is necessary to make them available all year round and at locations where they are not produced. Several researchers have carried out studies on drying of bananas. Mowlah, et al., (1983) studied the modelling of the drying kinetics of banana. Krokida, & Maroulis, (1999) studied the effect of microwave and microwave- vacuum on increased product porosity and colour changes.

2.3.1 Drying Models for the Description of Drying Kinetics of Banana

Drying of agricultural materials usually occurs under two drying regimes, namely constant rate and falling period. In the constant rate phase, the surface of the product is saturated with vapour and evaporation takes place continuously whereas in the falling rate period, the surface of the product is not saturated and the moisture diffusion is controlled by internal liquid movement as the surface dries. The second falling rate is typical of hygroscopic products. In this phase, the moisture content decreases until equilibrium is attained at which point the drying ceases (Cherotich, 2016). Studies conducted on drying kinetics of banana by various researchers (Dandamrongrak, et al., 2002; Ganesapillai, et al., 2011) revealed that drying of banana usually takes place under the falling period and that diffusion mechanisms (movement of moisture from a region of higher concentration to a region of lower concentration) is the dominant physical mechanism prevailing during the moisture removal process in bananas. However, drying of banana could also occur under the falling and constant rate period drying regimes in a single drying operation.

The removal of water in a foodstuff during drying occurs via two mechanisms: migration of water within the foodstuff and evaporation of moisture from the foodstuff into the air. The migration of water within the foodstuff is considered as the most common moisture migration during drying, and has been used to explain the drying kinetics of banana (Mowlah, et al., 1983; Sankat, et al., 1996). Mowlah, et al., (1983) reported a constant rate period followed by a falling rate period during drying of banana dices at 60°C and relative humidity of 9%.

Thin layer drying modelling contributes to understanding of the drying characteristics of the product being dried and therefore provides a viable way to control drying (Lahsasni, et al., 2004). The thin layer drying characteristics of most agricultural products, which includes banana, could be described using drying models. These drying models are of two main groups, including the empirical models (Diamante, et al., 2010; Mundada, et al., 2011; Silva, et al., 2013) and diffusion models (Nguyen & Price, 2007; Silva, et al., 2013). The thin layer drying models that describe the drying characteristics of agricultural

materials are sub-divided into three categories, namely theoretical, semi-theoretical and empirical (Midilli, et al., 2002).

The theoretical approach is concerned with either the diffusion equation or simultaneous heat and mass transfer equation and only takes into account the internal resistance to moisture transfer. On the other hand the semi-theoretical approach deals with approximated theoretical equations and considers only the external resistance to moisture transfer between the product and the air. Semi-theoretical models are developed by simplifying general series solution of Fick's second law and they offer a compromise between theory and ease of use. These models are only valid within the temperature, relative humidity and airflow velocity and moisture content range for which they were developed (Akpinar., 2006).

Empirical models derive a direct relationship between average moisture content and drying time but neglect fundamentals of the drying process and their parameters. Empirical models therefore do not give an accurate interpretation of the important processes occurring during drying. However they describe the drying curve for the conditions of the experiments (Akpinar., 2006). Silva, et al., (2014a) used several empirical models to simulate the thin layer drying of whole bananas at temperatures of 40, 50, 60 and 70°C. Their results showed that Page and Silva *et al.* models were the best models to describe the drying kinetics of whole bananas. Olawoye, et al., (2017) performed an experiment on Modelling of thin-layer drying characteristic of unripe Cardaba banana (Musa ABB) slices. The drying kinetics of Carbada banana were investigated using sun and hot air-drying at the temperature of 50°C, 60°C and 70°C. The drying rate of the convective hot air oven was kept constant at 1.2 m²/s. Among the thin-layer models, Wang and Singh model was found to best explain the drying behaviour of the Cardaba banana slices. Macedo, et al., (2020) reported that the Midilli model best represented the kinetics of the moisture ratio in the convective drying banana at 40°C, 60°C, and 80°C.

The simplest model for describing thin layer drying characteristics of agricultural products is in the form of the exponential model (Equation 2-1). It assumes negligible resistance to moisture movement to the surface of the material and that the resistance to

moisture movement is concentrated on the surface of the material and is referred to as ‘simple lumped’ model (which is analogous to Newton's law of cooling) (Aregbesola, et al., 2015)

$$MR = \frac{M - M_e}{M_i - M_e} = \exp(kt) \quad (2.1)$$

Where MR is the moisture ratio, M the moisture content at any time t (% db), M_e the equilibrium moisture content (emc) at the conditions of the drying air (% db), M_i the initial moisture content of the sample (% db), t is the drying time (min), and k is the drying constant (min^{-1}).

2.4 Computational fluid dynamics

Computational Fluid Dynamics (CFD) is a numerical approach for simulating fluid flow (Kayne, Alexander, 2012). Computational Fluid Dynamics is a tool for solving conservation equations for mass, momentum and energy in flow geometry of interest. Flows and associated phenomena can be described by partial differential equations, which are in many cases extremely difficult to solve analytically due to the non-linear inertial terms. To obtain accurate results, the domain in which the partial differential equations are described, has to be discretized using sufficiently small grids. Therefore, accuracy of numerical solution is dependent on the quality of discretization used (Sharafani, 2015). It allows the practitioners and researchers to predict characteristics of a system, including flow velocity, pressure, temperature and heat transfer (Kayne, Alexander, 2012). Many different numerical methods have also been developed by researchers to use this robust tool to simulate a wide range of complex flows and heat transfer problems (Hosain & Fdhila, 2015). Increasingly, CFD is becoming a vital component in the design of industrial products and processes (Ingle, et al., 2013). Advanced Engineering methods such as CFD are extensively used to solve, design and model complex industrial applications. Computational Fluid Dynamics is an effective and powerful tool to simulate fluid flow and heat transfer numerically (Hosain & Fdhila, 2015). Simulation is an important tool for design and operation control. For the designer of a drying system, simulation makes it possible to find the optimum design and operating parameters (Ingle, et al., 2013). According to Hosain & Fdhila, (2015) CFD methods can be categorized into two major groups as “conventional methods” and “accelerated methods”. In CFD, most

of the methods solve the Navier-Stokes equations either in Eulerian or in Lagrangian approach. Apart from that, some methods solve the Boltzmann equations instead of Navier-Stokes equations. In many instances, other equations are solved simultaneously with the Navier-Stokes equations.

Different CFD methods have also been developed by researchers to simulate a wide range of complex flows and heat transfer problems. These methods are shown in figure 2.5. The conventional methods are highly accurate and the most widely used in the commercial software packages. However, the conventional methods are extremely slow in terms of computation time which makes it almost impossible to solve large problems within a reasonable time (Hosain & Fdhila, 2015). Conventional methods may include finite volume method, finite difference method, finite element method, spectral methods and many more. The Acceleration Methods are further categorized into two major groups: Advanced Numerical Methods and Hardware techniques. Hardware acceleration techniques are usually used together with both Conventional and advanced numerical methods. Advanced numerical methods can be classified as Mesh based, Mesh free and Hybrid methods (Hosain & Fdhila, 2015). Classification of various methods in CFD is shown in figure 2.6

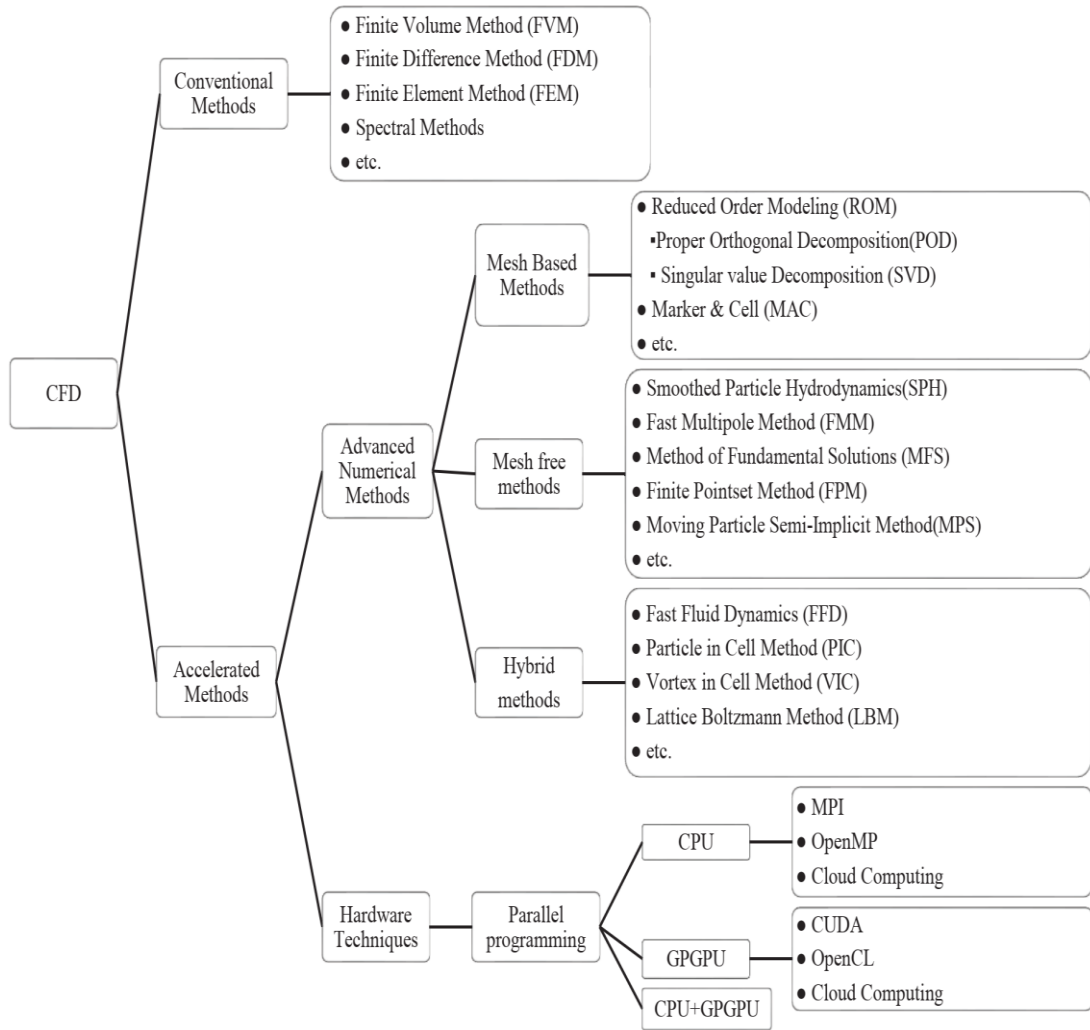


Figure 2-6 Hierarchical classification of various methods in CFD (Hossain & Fdhila, 2015)

2.5 Temperature distribution

A solar dryer creates an increase in air temperature but a reduction in the air humidity. Hence a solar dryer reduces the equilibrium of moisture content and increases the free humidity and drying air velocity (Rigit & Patrick, 2010). Rigit & Patrick, (2010) deduced that heat and mass transfer by natural convection is more suitable for drying pepper berries with solar radiation. In the natural convection model, the thermal heat distribution in the drying chamber was uniform and suitable for drying the pepper berries. The uniform heat distribution at the center of the drying chamber with a range from 62.25 °C to 78.85 °C was sufficient for drying the pepper berries to the moisture content of 12% wet basis. Sharma, et al., (1990) found that the predicted plate temperature for no load

reached a maximum of 80°C to 85°C during the noon hours, while with a load of 20 kg of wheat, the maximum temperature was 45°C to 50°C. Bolaji, (2005) investigated an indirect solar dryer using a box type absorber collector. He found also that the maximum average temperatures inside the collector and drying chamber were 64°C and 57°C, respectively; while, the maximum observed ambient temperature was 33.5°C. Daud & Simate, (2017) used sliced pineapples to evaluate the performance of a Solar Conduction Dryer (SCD) and found that for the period of the experiment, ambient temperature and temperature in the dryer ranged from 24°C to 37 °C and 25°C to 46 °C, respectively.

Madhlopa, et al., (2002) developed a solar dryer which had composite absorber systems based on the principles of psychrometry. The dryer comprised of a flat plate collector, wire mesh absorber, glass cover, chimney and drying chamber. The heater was integrated to a drying chamber for food dehydration. The performance of the dryer was evaluated by drying fresh samples of mango. Results showed that the temperature rise of the drying air was up to 40°C above ambient during noon hours. Minka, (1986) reported that temperatures in the cabinet dryer were 20°C to 30°C above ambient temperature and that the cabinet dryer should be useful in drying a variety of products. Schirmer, et al., (1996) developed a multi-purpose solar tunnel dryer that could dry up to 300 kg of ripe bananas in each drying batch. They found that the temperature of the drying air from the collector varied between 40°C and 65°C, and that the bananas could be dried within 3 to 5 days, compared to the 5 to 7 days needed for open drying.

2.6 Governing equations

The fundamental governing equations of Computational fluid dynamics simulation modelling are the Navier-Stokes equations which were derived from the basic mass conservation and continuity equations applied to properties of fluids.

2.6.1 Heat transfer

Heat transfer is a method in which energy is transferred between two different bodies due to a difference in temperature between the two. There are three different modes in which this transfer of energy can take place: conduction, convection and radiation.

A. Conduction

Conduction deals with the energy transfer from energetic particles to the less energetic particles surrounding it. This transfer of energy is quantified by Fourier's Law shown in Equation 2.2.

$$\dot{q}_x = -k \frac{dT}{dx} \quad (2.2)$$

Equation 2-1: Fourier's law of heat conduction

Where \dot{q}_x = Heat flux in the x-direction, W

k = Thermal conductivity, W/mK

T = Temperature, K

B. Convection

Convection heat transfer is the energy that is transferred between a solid and a moving fluid, each being at different temperatures. The rate at which this exchange of energy occurs is given by Newton's law of cooling, shown in Equation 2.3.

$$\dot{q} = h (T_s - T_f) \quad (2.3)$$

Where: \dot{q} = Convective heat flux W/m²

h = Convective Heat transfer coefficient, W/m²K

T_s = Temperature of the solid body, K

T_f = Temperature of the fluid body, K

C. Radiation

Thermal radiation is the energy transfer between two bodies via electromagnetic waves. This form of energy transfer is exhibited by all bodies, and requires no medium for the heat to be transferred. It can even be seen to occur in a vacuum. The amount of energy that can be radiated by a surface is given by the Stefan-Boltzmann law shown in Equation 2.4.

$$\dot{q} = \epsilon \sigma T^4 \quad (2.4)$$

Where: \dot{q} = Radiative heat flux, W/m^2

ϵ = Emissivity

σ = Stefan-Boltzmann constant $5.67 \times 10^{-8} \text{W}/\text{m}^2 \cdot \text{K}^4$

T = Surface temperature of the radiating body, K

Here, emissivity is a measure of a material's ability to radiate energy as compared to that of a perfectly radiating black surface. This value can range from 0, a non-radiating body, to 1, a perfectly radiating black surface.

D. First Law of Thermodynamics

The first law of thermodynamics states that the energy of any system must be conserved. This means that the amount of energy entering a system must equal the amount of energy leaving the system (Rajput, 2012). This energy balance, along with Equations 2.1-2.3, makes up the system of equations that are used to solve general heat transfer problems.

E. Fluid flow

The material presented in the previous section only applies to a system consisting of solid bodies in which there is no fluid flow. For systems in which there is fluid motion present, a different set of equations must be introduced that relate to the conservation principles that must be met by a system.

F. Continuity equation

Conservation of mass must be satisfied in any closed system. Mass must not be created or destroyed. The equation governing this principle is known as the continuity equation and is shown below in Equation 2.5:

$$\frac{\partial \rho}{\partial t} + \nabla \cdot (\rho \mathbf{V}) = 0 \quad (2.5)$$

Where: ρ = Density, kg/m^3

t = Time

$$\nabla = \text{Del operator} = \frac{\partial}{\partial x} \mathbf{i} + \frac{\partial}{\partial y} \mathbf{j} + \frac{\partial}{\partial z} \mathbf{k}$$

$V = \text{Velocity vector} = V_x i + V_y j + V_z k$

This equation can be expanded and becomes,

$$\frac{\partial \rho}{\partial t} + \frac{\partial \rho V_x}{\partial x} + \frac{\partial \rho V_y}{\partial y} + \frac{\partial \rho V_z}{\partial z} = 0 \quad (2.6)$$

G. Navier-Stokes equations

The Navier-Stokes equations are a collection of the 3-dimensional momentum equations for any Newtonian fluid. In fluid dynamics, a Newtonian fluid is one in which the stresses at each point in the fluid are linearly proportional to the strain rates at that point. These equations ensure that in any system, the momentum is conserved. This means that the total force generated by the momentum transfer in each direction must be balanced by the rate of change of momentum in each direction (Coleman, 2010). The Navier-Stokes equations are provided below:

$$\frac{\partial \bar{u}}{\partial t} = \nabla \cdot \left(\frac{\mu}{\rho} \nabla \bar{u} \right) - \bar{u} \cdot \nabla \bar{u} + \dot{F} - \nabla P \quad (2.7)$$

H. Energy Conservation

The equation for the conservation of energy is derived from the consideration of the first law of thermodynamics:

Time Rate of Change of Energy = Net Rate of Heat Added + Net Rate of Work Done

$(\Sigma \dot{Q})$

$(\Sigma \dot{W})$

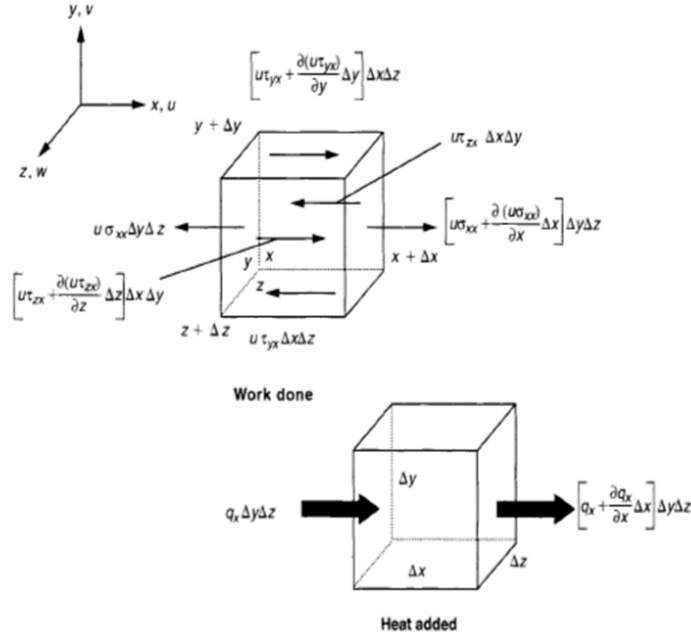


Figure 2-7: Time Rate of Change of Energy in a System

With regard to the surface forces (pressure plus shear and normal stresses), considering the forces in the x, y and z directions, the time-rate-of-change of energy of the fluid element is denoted by Equation (2.8).

$$\begin{aligned} \rho(DE/DT) = & \partial(u\sigma_{xx})/\partial x + \partial(v\sigma_{yy})/\partial y + \partial(w\sigma_{zz})/\partial z + \partial(u\tau_{yx})/\partial y + \\ & \partial(u\tau_{zx})/\partial z + \partial(v\tau_{xy})/\partial x + \partial(v\sigma_{zy})/\partial z + \partial(w\sigma_{xz})/\partial x + \\ & \partial(w\sigma_{yz})/\partial y - (\partial q_x/\partial x + \partial q_y/\partial y + \partial q_z/\partial z) \end{aligned} \quad (2.8)$$

The energy fluxes q_x, q_y and q_z in the equation above are expressible through employment of Fourier's law of heat conduction, which relates heat flux to the local temperature gradient as shown in equation 2.9:

$$q_x = -k\partial T/\partial x, q_y = -k\partial T/\partial y, q_z = -k\partial T/\partial z \quad (2.9)$$

Where k is thermal conductivity. Substituting equation (2.9) into equation (2.8) and with application of normal stresses, the energy equation is now:

$$\begin{aligned} \rho(DE/DT) = & \partial[k\partial T/\partial x]/\partial x + \partial[k\partial T/\partial y]/\partial y + \partial[k\partial T/\partial z]/\partial z - (\partial u p/\partial x + \\ & \partial v p/\partial y + \partial w p/\partial z) + \Phi \end{aligned} \quad (2.10)$$

The dissipation function, Φ , describe the effect on the energy equation that viscous stresses have,

$$\Phi = \frac{\partial(u\tau_{xx})}{\partial x} + \frac{\partial(u\tau_{yx})}{\partial y} + \frac{\partial(u\tau_{zx})}{\partial z} + \frac{\partial(v\tau_{xy})}{\partial x} + \frac{\partial(v\tau_{yy})}{\partial y} + \frac{\partial(v\tau_{zy})}{\partial z} + \frac{\partial(w\tau_{xz})}{\partial x} + \frac{\partial(w\tau_{yz})}{\partial y} + \frac{\partial(w\tau_{zz})}{\partial z} \quad (2.11)$$

2.7 Simulation

Simulation is a mathematical model that describes or creates computationally a system process. Simulations are our best cognitive representation of complex reality, that is, our deepest conception of what reality is (Vallverdú1, 2014). Simulation involve the modeling of the system to be studied. The model may itself be another physical system, or it may be a mathematical model.

Simulation softwares come in different forms. SOLIDWORKS® Flow Simulation is an intuitive Computational Fluid Dynamics (CFD) solution and a general parametric flow simulation tool that uses the Finite Volume Method (FVM) to calculate product performance, it is embedded within SOLIDWORKS 3D CAD that enables to quickly and easily simulate liquid and gas flows through and around your designs to calculate product performance and capabilities. SOLIDWORKS Flow Simulation takes you through the steps of creating the SOLIDWORKS part for the simulation followed by the setup and calculation of the SOLIDWORKS Flow Simulation project. The results from calculations are visualized and compared with theoretical solutions and empirical data. Comsol Multiphysics software is a general purpose software platform based on advanced numerical methods and is used for modelling and simulating physics based problems. It is suitable for electrical, mechanical, fluid flow and chemical applications, among others. In addition, the user is able to include their own equations that may describe a material property, boundary, source or even a unique set of partial differential equations. The user can then create new physics interphases from the equations entered (Comsol, 2012). ANSYS is a general-purpose, finite-element modelling package for numerically solving a wide variety of mechanical problems. These problems include static/dynamic, structural analysis, heat transfer, and fluid problems, as well as acoustic and electromagnetic problems. There are two methods to use ANSYS. One method is to use the graphical user interface (GUI) (Nakasone, et al., 2006).

Omolola, et al., (2015) to conducted a CFD analysis of a solar dryer using SolidWorks Flow Simulation. They investigated the effect of air flow distribution, flow velocity, and pressure field on transient moisture within the dryer. Some of the simulation parameters such as air temperature were accurately predicted, resulting in small deviations of about 0.02%. Their simulation of drying process for the green bell pepper was conducted using the standard turbulence model under steady state conditions. Zoukit, et al., (2019) used solidworks and presented a numerical simulation of a hybrid solar-gas dryer operated under forced convection with an air mass flow rate of 0.025kg/s.

2.8 Energy and exergy analysis

Energy and exergy analysis (EEA) is useful in thermodynamic for forecasting the thermal performance of complete drying processes (Lingayat, et al., 2019). In order to find out the energy interactions and thermodynamic behaviour of drying air throughout a drying chamber, the energy and exergy analyses of the drying process should be performed (Chowdhury, et al., 2011). The energy analysis is based on the conservation of energy principle which is the first law of thermodynamics. It does not provide any information about the irreversibility and also, it is not possible to find the different energy qualities within system and process like the quality of heat which is a function of source temperature (Lingayat, et al., 2019). So, to overcome the problem in energy analysis, the exergy analysis comes into picture which provides clear idea or view about the process, the influence of thermodynamic phenomena in the drying process, provides new unforeseen ideas for improvement of the system and process (Erek & Dincer, 2009). Exergy is defined as the maximum amount of work that can be produced by a system or a flow of matter or energy as it comes to equilibrium with a reference environment. (Bayrak, et al., 2003; Chowdhury, et al., 2011). Exergy analysis provides information about different losses, their types, magnitudes, and location. It is useful for the design of more efficient thermal systems, its thermal analysis, and process optimization (Haseli, et al., 2010; Dincer, 2011). The exergy method can help further the goal of more efficient energy resource use, because it enables the locations, types and true magnitudes of losses to be determined. As a result, exergy analyses can reveal where and by how much it is possible to design more efficient thermal systems by reducing the sources of existing inefficiencies (Chowdhury, et al., 2011). A number of studies have been performed on

the energy and exergy analyses of the solar drying process of agricultural products. Chowdhury, et al., (2011) performed EEA in solar drying of jackfruit leather in a solar tunnel dryer and reported that the exergy input and exergy loss for the dryer increased with increasing solar radiation. The energy efficiency of collector and dryer varied between 27.45% and 42.50% and between 32.34% and 65.30% respectively for the variation in solar radiation between 100 W/m² and 600 W/m². The overall energy efficiency of the solar dryer was 42.47%. The exergetic efficiency of collector and the mean value of the exergetic efficiency of dryer were 32% to 69% and 41.42% respectively.

Lingayat, et al., (2019) reported that bananas got sufficiently dried at temperatures between 28°C and 82°C with solar radiation ranging from 335 W/m² to 1210 W/m² while the exergy losses varied from 3.36 kJ/kg to 25.21 kJ/kg. In particular, the exergy efficiency values varied from 7.4% to 45.32%.

Panwar, (2014) performed EEA in NCISD dryer during the drying of coriander leaves and reported the air temperature to have varied from 36°C to 56°C. The initial moisture content of coriander leaves was 7.33 kg/kg of dry basis (db) and was reduced to a final moisture content of 0.8181 kg/ kg of dry basis db in drying time of 7.5 hours. Midilli model was found to be best to describe the drying kinetics. The energy efficiency values were in a range of 7.81% to 37.93%, while exergy efficiency values were in a range of 55.35% to 79.39%.

Kesavan, et al., (2019) developed a FCISD which consisted of triple-pass solar air collector with sand as sensible heat storage material. The optimum mass flow rate of air was found to be 0.062 kg/s. The thermal efficiency of the solar air collector was in the range of 12% to 66% with an average of 45%. The exergetic efficiency of the dryer varied between 2.8% and 87.02% with an average of 53.57%.

2.9 Closing remarks

It was noted that solar drying has a huge role in crop drying including fruits and vegetables due to its capability to maintain quality while reducing the drying time significantly. From the several classifications and designs of solar dryers in literature, active solar dryers are more common than natural convection dryers and this is

attributable to better and controllable air flow rates in the active systems. Computational Fluid Dynamics (CFD) is an important tool in the improvement of solar drying technology. Simulation of air flow and temperature may be used to improve the design of a dryer so that uneven drying may be reduced. Use of actual measurement to facilitate such design is not only difficult, but it would also be expensive and time consuming. Studies have been carried out to select from the existing thin layer drying models the one that best fits drying curves for different products. It was observed that that the best model not only depended on the product and type of dryer, but also on drying conditions such as drying air temperature and velocity. It is thus necessary to select and verify a thin layer drying model for banana slices in a natural convection dryer. The focus of this study was on experimental and CFD investigation of a natural convection solar tunnel fruit dryer.

CHAPTER THREE: METHODOLOGY

3. Introduction

This chapter describes how the entire research work was carried out in order to fulfil the objectives of the study. It gives a detailed account of all the procedures and the types of equipment that were used for the research.

3.1 Description of the dryer and its mode of operation

The fabricated solar tunnel dryer developed by (Cherotich, (2016) consists of three major components: the collector unit, the drying unit, and a bare flat-plate chimney unit. Each of the units has been described in detail in the following sections.

3.1.1 *The collector unit*

The solar collector unit was a flat-plate type with air flow above the absorber plate while the cover was a transparent 200 μm polythene sheet. The reason for using this type of collector unit is because of their low thermal losses. The absorber plate was made from Galvanized Iron (GI) sheet and in order to increase the solar absorptivity of the absorber plate, it was painted black using mat black paint. The overall dimensions of the collector unit were 1.0 m \times 0.75 m (L \times W).

3.1.2 *The drying unit*

The drying unit, adjacent to the collector unit was made from the same materials as the collector unit and in the same configuration as the collector unit. To provide for the drying of the product, the drying unit was mounted with a removable wire mesh tray to hold the product during the drying as shown in Figure 3.2. The overall dimensions of the drying unit were 1.0 m \times 0.75 m (L \times W) while the tray had an effective area of 0.69 m². The end of the dryer unit was mounted with a vertical bare flat-plate chimney described in the following section.

3.1.3 *The chimney unit*

The chimney unit which serves the purpose of reheating the air exiting the drying unit was a bare flat-plate type collector. The solar radiation receiving surface of the chimney was painted black with mat black paint to absorb as much of the incident solar radiation as possible during operation. The dimensions of the chimney were 0.75 m \times 0.75 m (L \times W) with an air channel of 0.1 m. It was constructed from 0.3 mm thick GI sheet and

was mounted vertically adjacent to the drying unit in a North-South orientation. The dryer was supported by four dryer legs 0.6 m above the ground and all the units were detachable to allow for easy assembly and re-assembly for transportation purposes.

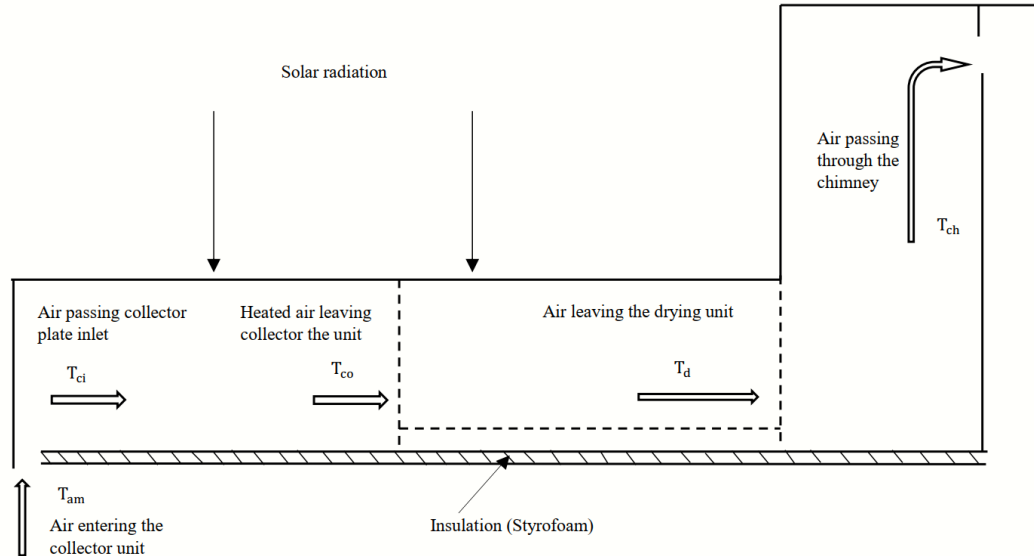


Figure 3-1 Air flow in the solar tunnel dryer (source: Cherotich, (2016))

3.2 Determination of the temperatures and air velocity

The experiments were carried out under load conditions, that is to say, the banana slices was loaded in the drying chamber. From the moisture content results of banana slices, an appropriate thin layer model which best predicts the drying of the product under the observed conditions was obtained and validated against experimental results.

3.2.1 Experimental set-up

The experiments were conducted on the 11th and 12th of April, 2022 at the Department of Agricultural Engineering field station workshop at the University Zambia with coordinates; Latitude 15.3°S; Longitude 28.3°E. The solar tunnel dryer was positioned on an open flat ground surface outside the workshop under natural conditions during the experiments. Figure 3-2 shows the experimental setup.



Figure 3-2 Experimental set-up of the solar tunnel dryer and the equipment (1) Collector unit, (2) Drying unit, (3) Bare flat-plate chimney unit, (4) Solar pyranometer, (5) Data logger, (6) Computer.

A multi probe Campbell Scientific Inc. data logger (model: CR 1000) was connected to the solar tunnel dryer to record the air temperatures and solar radiation. The data logger recorded the air temperatures through thermocouple type temperature probes (model: 108 – L and accuracy of $\pm 0.01^{\circ}\text{C}$). The temperature probes were capable of recording temperature ranging between -5°C and $+95^{\circ}\text{C}$. The air temperatures recorded were: the ambient air temperature (T_{am}), the collector air inlet temperature (T_{ci}), the collector air exit temperature (T_{co}), the drying unit air exit temperature (T_{d}) and the chimney air exit temperature (T_{ch}). These recorded air conditions varied with the time of the day and they define the drying of the product.

The collector air inlet temperature was recorded using a relative a temperature/humidity probe (model: HMP60-L) that was capable of temperature and humidity in the ranges of -40°C to 60°C and 0 and 100 % respectively, whereas the solar insolation was recorded by a pyranometer (model: CMP6-L) placed on a flat horizontal ground surface near the solar tunnel dryer. Finally, the ambient velocity (V_{am}) and inside the chimney unit (V_{ch})

was measured using a digital air flow meter (model: TES 1340) that had an accuracy $\pm 0.01 \text{ m s}^{-1}$ for air velocities between 0 and 30 m s^{-1} .

3.2.2 Determination of the initial moisture content of bananas

The procedure described below was followed to determine the initial moisture content (M_o) of banana.

- i. Ripe banana whose degree of ripeness was not determined experimentally but based on the fact that it was ready and acceptable for consumption by the consumers was purchased locally from the markets
- ii. Using the standard method of moisture content determination (AOAC, 2005) described in steps (iv) – (viii) the initial moisture content was determined.
- iii. Bananas were peeled and sliced into approximately 3 mm thickness using a table knife.
- iv. A clean empty petri dish with known weight was loaded into an oven at 105°C for 3 hours and left to cool.
- v. The banana slices were put into the petri dish in (iv) and 10 g was weighed from a digital weighing balance (model: PE 3000, accuracy, $\pm 0.1 \text{ g}$). The weight of the dish and sample was recorded as (W_1)
- vi. The dish and sample were then loaded into the oven and left to dry for 3 hours at 105°C .
- vii. At the end of the 3 hours, the sample in the petri dish was left to cool and then reweighed for the final dry weight (W_2).
- viii. Using Equation (3.1), the initial moisture content was calculated in wet basis (w.b.).

$$M_o = \frac{(W_1 - W_2)}{W_2} \times 100\% \quad (3.1)$$

$$\% \text{IMC (w. b)} = \left(\frac{(\text{Original weight} - \text{Oven dry weight})}{\text{Original weight}} \right) \times 100\% \quad (3.2)$$

3.2.3 Determination of moisture removal rate

Moisture removal rate is also called drying rate. To determine moisture removal rate (MRR), moisture loss in each drying experiment was calculated from the difference

between the mass of banana slices before and after drying, weighed using a digital balance. MRR was determined using eq. (3.3) and can be defined as the mass of moisture lost during a drying session of time t for every unit mass of wet banana slices or the amount of evaporated moisture content over time. To calculate the drying rate the following formula is used (Dhanushkodi, et al., 2014).

$$MMR = \frac{M_i - M_d}{t} \quad (3.3)$$

Where,

M_i is mass of sample before drying in kg, t is drying period in hours and M_d is mass of sample after drying, in kg.

3.2.4 Procedure of the banana drying experiments

- i. For the experimental setup, ripe banana were purchased from a supplier in Lusaka industrial area on an evening before the day of the experiment and kept under room temperature overnight.
- ii. Starting at 08:00 hrs on the day of the experiment, the equipment was set then bananas were peeled, sliced into approximately 3 mm.
- iii. They were placed onto a square polyethylene nets for the purpose of loading in the drying unit and to prevent them from sticking to the wire mesh (tray).
- iv. The square nets containing the banana slices were then loaded into the wire tray located in the drying unit, the entire wire mesh was covered by a square net where the bananas were evenly spread with as shown in Figure 3-3.



Figure 3-3 Solar tunnel dryer loaded with the sliced bananas

- v. On the first day of the Experiment, the set-up of the equipment and preparation of the product was complete and the drying of the product started. The experiments conducted between 09:00 hours and 16:00 hours due to the abundance of the solar radiation in this period of the day.
- vi. Through the data logger, air temperatures, the collector air exit temperature (T_c), the drying unit air exit temperature (T_a) and the chimney air exit temperature (T_{ch}), the solar insolation were recorded as the drying progressed until the end of the experimental day (16: 00 hours).
- vii. Drying was resumed the following day by unpacking the banana from the polythene bag and reloading into the dryer
- viii. On the second day of the Experiment At 09:00 hrs, the set-up of the equipment and the drying of the product continued.

3.3 Simulation procedure.

A 3-D model of solar tunnel dryer geometry was created using solid works version 2016
CPU Type: Intel(R) Core(TM) i5-5300U CPU @ 2.30GHz, CPU Speed: 2295 MHz,
RAM: 3970 MB, Flow Simulation 2016 SP0.0. Build: 3259 results provides sufficient

practical information to identifying the low temperature spot of the system and consequently this would be useful for improvement of the dryer designs. Mass flow rate and pressure (static and total) boundary conditions were specified at models' inlets and outlets. Steady state Reynolds-averaged 3D Navier-Stokes equations using the $k-\epsilon$ turbulence model were selected to carry out computation as it produces accurate and satisfactory results. The 3D Model of the solar tunnel dryer used in the simulation is shown in Figures 3-4 and 3-5 .The following simulation procedure below was used in this study.

3.3.1 Design and modelling of the solar dryer system

The design for the natural convection solar tunnel dryer presented in this research was provided by the Department of Agricultural Engineering at the University of Zambia and is described in section 3.2. The solar tunnel dryer model supplied was developed in SOLIDWORKS, a computer-aided-drawing (CAD) software.

Figure 3.4 and figure 3.5 show the overall design of the dryer system which consists of several components were designed using SOLIDWORKS, then analysed and simulated using SOLIDWORKS flow simulation.

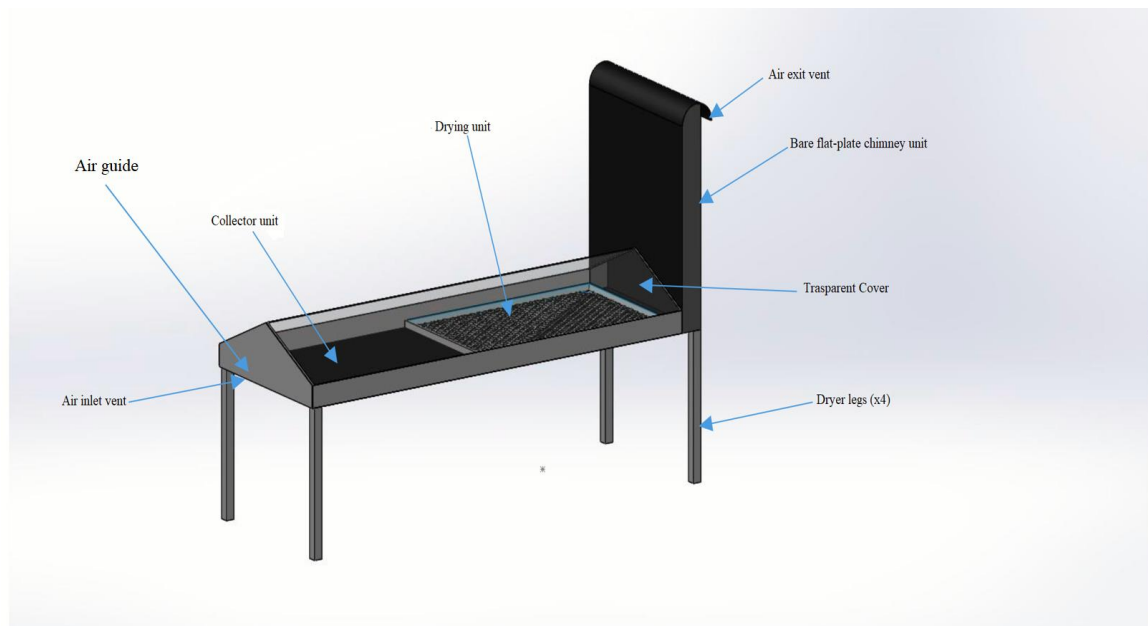


Figure 3-4: Solar dryer components

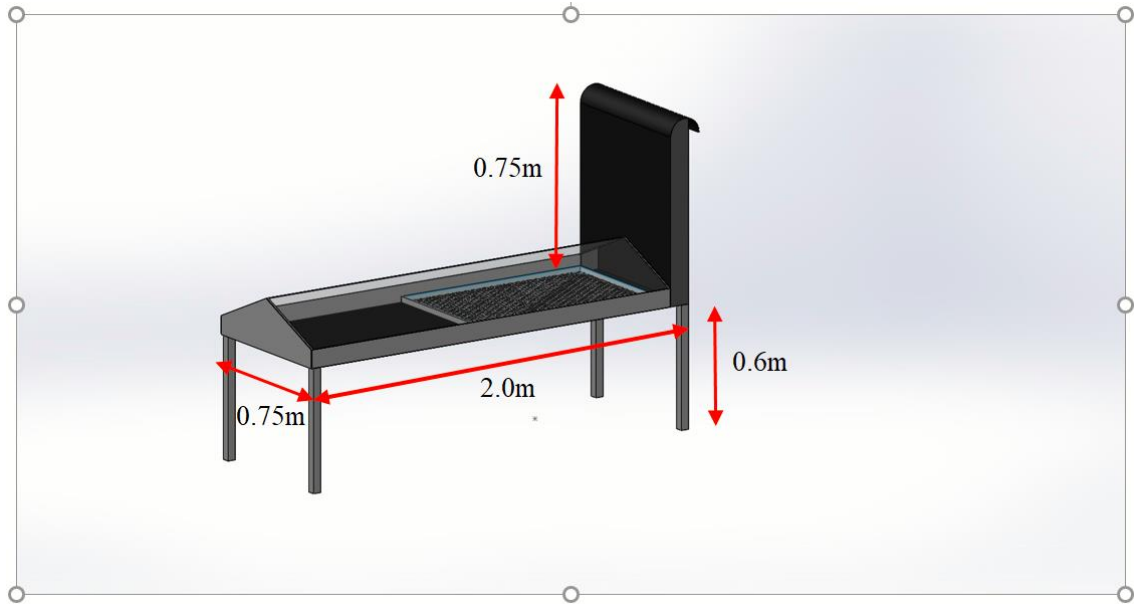


Figure 3-5: Solar dryer component dimensions

3.3.2 Kinetic modelling of fluid movement

After the design, the kinetic modelling of fluid movement inside the dryer and of the bananas were performed. Some assumptions made in simulation were:

- Air flow is laminar.
- Heat conduction takes place under steady state conditions.
- The solar collector and the chimney receive the same amount of insolation.

A. Flow simulation

After the project was generated, the entrance data (articles of the project tree), were defined to develop the simulations which are described below:

B. Project setup

Data related to fall of pressure as a function of the flow of mass $\{\Delta P = (m)\}$ are specified, starting from the results obtained experimentally. The project is created to develop the simulation with the use of Computational Fluid Dynamics (CFD), in Simulation of Fluid, where the following data are defined:

- System of units: The International System of Units is declared;

- Analysis type: an internal analysis is selected because the air flows inside the dryer, excluding the cavities without conditions of flow;
- Fluid: Air, selecting the automatic option of behaviour, either laminar or turbulent, as characteristics of the fluid (in this case laminar);
- Wall conditions: Adiabatic;
- Initial conditions: thermodynamic parameters of pressure and temperature.
- Resolution of the results and the geometry: it is declared as an automatic configuration, a level similar to 5 for the geometry of computational mesh.

3.4 Setup

3.4.1 Project design tree setup

The SolidWorks Flow Simulation design tree provides a convenient specification of project data and view of results. It also allows to modify or delete the various SolidWorks Flow Simulation features.

A. Computational domain

The area around the 3D and 2D models, which defines the flow simulation the restricted area, is known as the Computational Domain. This defines the boundary under which the flow simulation will take place. The flow and heat transfer calculations are performed inside the computational domain. The computational domain is a rectangular prism for both the 3D and 2D analyses. The computational domain boundaries are parallel to the global coordinate system planes. The icon Computational Domain is used to modify the dimensions of the volume that it is being analysed and it allows visualizing the limits of the computational domain. Table 3.1 and Figure 3.6 show the size and visualization respectively of the computational domain used in the simulation. Table 3-1 shows the coordinates of computational domain size.

Table 3-1 Computational domain Size

X min	0.345 m
X max	1.091 m
Y min	1.037 m
Y max	1.789 m
Z min	0.442 m
Z max	2.546 m

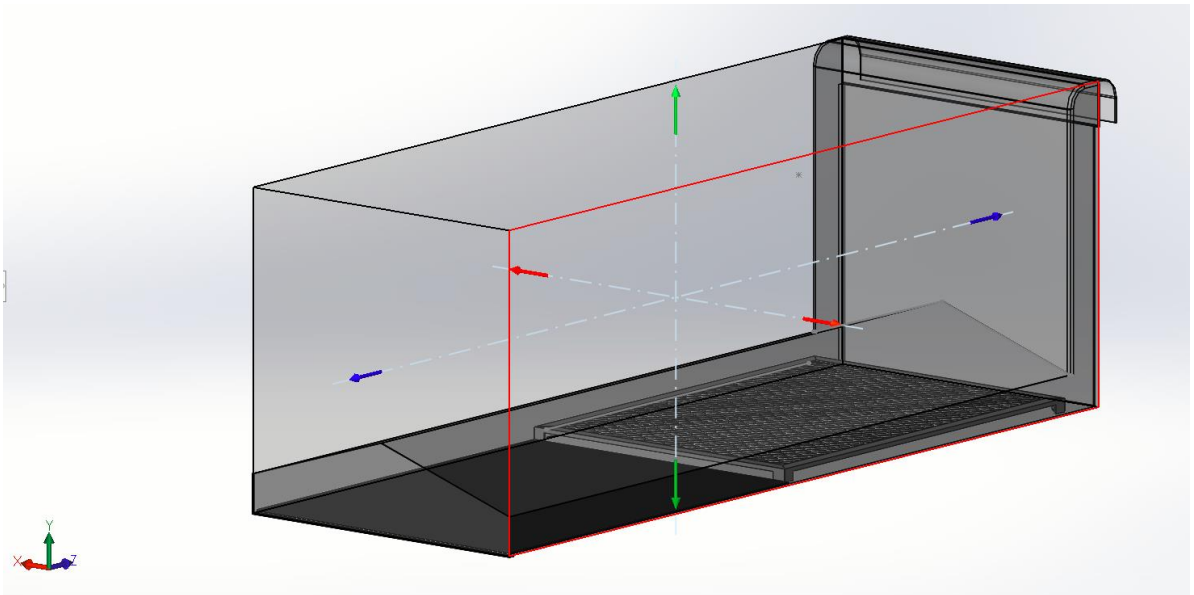


Figure 3-6: Visualization of computational domain

B. Material properties

The parameters used in the simulation study are shown in Table 3-2

Table 3-2 Material properties

Parameter	Value	Units	Source
Banana dimension (D × h)	30 × 3	mm	In this study
Initial moisture content - Ripe banana	73.8	%w.b	In this study
Initial Equivalent porosity - Ripe banana	0.83	-	(Ni, 1997)
Thermal conductivity - Ripe banana	0.97	W/m K	(Udomdejwatana, 1994)
Density - Ripe banana	870	kg/m ³	
Specific heat (Cp) - Ripe banana J kg K	3430	J/kg K	
Ambient pressure	101325	Pa	In this study
Polyethylene Cover			(Román, et al., 2019)
Density	915	kg/m ³	
Thermal conductivity	0.33	W/m K	
Emissivity	0.9	-	
Specific heat (Cp)	1900	J/kg K	
Single layer polyethylene			(Michael, 2014)
Transmittance	85.7	%	
Galvanized iron			(Kumar, et al., 2019)
density(ρ)	7,870	kg/m ³	
Thermal Diffusivity	84.18x10 ⁶	m ² /s	
Specific Heat (Cp)	896	J/kg K	
Thermal Conductivity (k)	204.2	W/m K	

C. Boundary conditions

The amount and type of boundary conditions varies from case to case depending on how the physical geometry is built. Regardless of which boundary condition is chosen there is usually no need to further edit the boundary condition since the default usually are sufficient for all specifications. A boundary condition in SOLIDWORKS flow Simulation is required in any place where fluid enters or exits the model, excluding openings where a fan is specified. Boundary conditions are used to specify the fluid characteristics at the model inlets and outlets in an internal flow analysis or on model surfaces in an external flow analysis (SOLIDWORKS Corporation, 2010). The icon Boundary Conditions allows establishing the parameters to the fluid, in the entrance or exit of the computational domain. A boundary condition can be set in form of Pressure, Mass Flow Rate, Volume Flow Rate or Velocity. You can also use the Boundary Condition dialog for specifying an Ideal Wall condition that is an adiabatic, frictionless wall or a Real Wall condition to set the wall roughness and/or temperature and/or heat conduction coefficient at the selected model surfaces. For internal analyses with Heat conduction in solids enabled, you can also set thermal wall condition on outer model walls by specifying an Outer Wall condition.

In this study the boundary conditions in regard to pressure and mass flow, the dryer's surfaces (top cover, floor, and sides) were considered to be no-slip walls for the purpose of fluid flow analysis. These surfaces also had adiabatic considerations. The top cover had a boundary condition to simulate incident sunlight upon the dryer. The collector was modelled with a radiation absorptivity of 0.65 and an emissivity of 0.07, characteristic of rough galvanised iron (The Engineering Toolbox, 2003). The plastic cover making up the dryer's roof was modelled to have a transmissivity of 0.86, the average light transmissivity for polyethylene plastic film (Sangpradit, 2014). The model geometry was characterized by a laminar flow regime.

D. Porous medium

In this study the bananas were considered as porous media in the solar tunnel dryer. The porous media is modelled by the addition of a momentum source term to the standard

fluid flow equations such as conservation of energy, momentum and moisture transport equation. For this simulation study, the banana porosity was assumed to be constant.

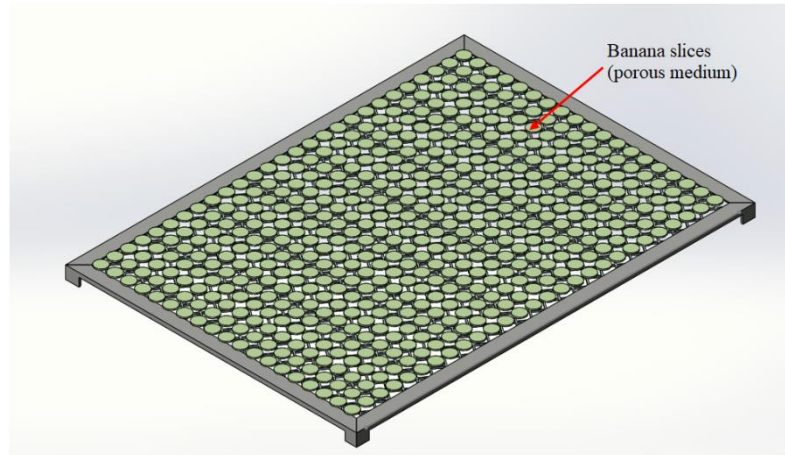


Figure 3-7: Arrangement of the bananas on the mesh

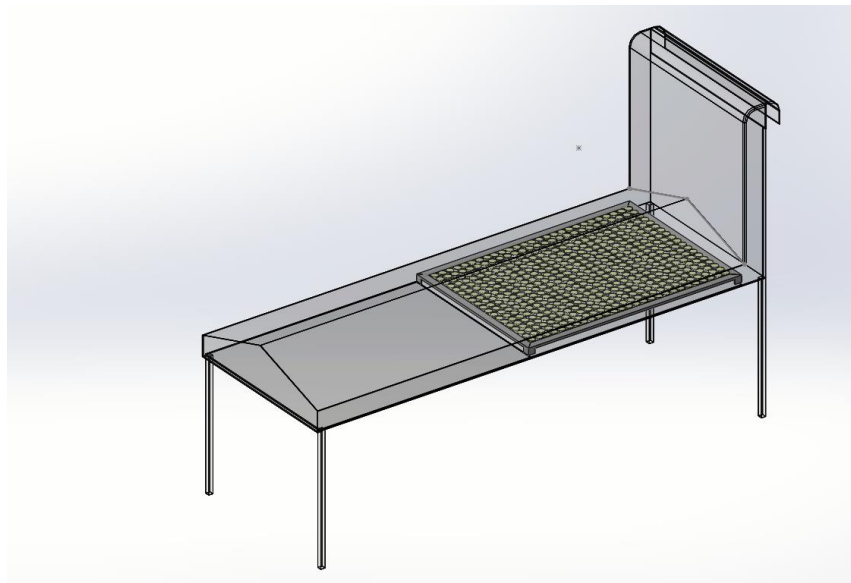


Figure 3-8: Porous medium in the solar dryer

E. Engineering goals

The icon Engineering Goals allows defining what parameters are of interest in order to reduce the time of calculation when reaching the convergence of the solution and to influence in the stop criterion. In this study, temperature, velocity and humidity were considered.

F. Meshing

The process of subdividing machine elements into an organized set of nodes and elements is called meshing, or creating a mesh, on a model of the component to be analysed. As implied above, mathematical solution of a CFD analysis depends upon sets of simultaneous equations that describe small displacement at the element level. Therefore, subdividing a model into a continuous set of nodes and elements, i.e., meshing a model, is a necessary prerequisite in the solution process. Fortunately within SOLIDWORKS, simulation meshing occurs automatically. The operation can be also useful to define the motion of the system and analyses of simulation.

The icon Local Meshes allows diminishing the size of the computational domain in a specific region of the domain for the sake of reaching bigger precision of the results in this region. In order to avoid any numerical problems further on in the CFD process, where the meshes are run through the flow solver, it is most desirable to have mesh with high quality. This decreases the chances for divergences due to poor mesh quality. Depending which type of element is considered, SOLIDWORKS Flow Simulation calculates the quality of the element differently. Generating proper mesh is a must in CFD simulations since the good mesh helps the CFD solver converge to the correct answer while minimizing the computer resources expended. The generated mesh used in this study is shown in figure 3-9.

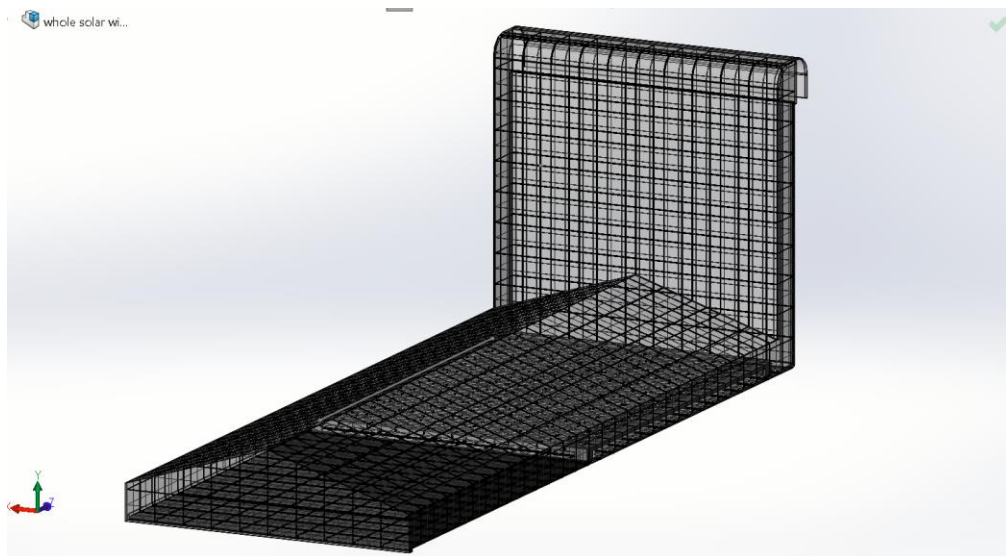


Figure 3-9: Generated mesh of the solar dryer

SolidWorks Flow Simulation 2016, which is based on Finite Volume Method (FVM) was used in order to obtain the correct simulated results. In the course of the solving process, the total cell count, Fluid Cells, Solid Cells and Partial Cells of 586831, 324003, 262828 and 173938 respectively were gotten from discretization process and were used to analyse the simulation.

H. Running the flow simulation and check for convergence.

The simulation was run and the process of convergence began. Convergence is an iterative process. The discretization of the flow field imposes conditions on each parameter and each parameter cannot reach an absolutely stable value but will oscillate near this value from iteration to iteration. When SolidWorks Flow Simulation analyzes the goal's convergence, it calculates the goal's dispersion defined as the difference between the goal's maximum and minimum values over the analysis interval reckoned from the last iteration and compares this dispersion with the goal's convergence criterion dispersion, either specified by you or automatically determined by SolidWorks Flow Simulation. Once the oscillations are less than the convergence criterion the goal becomes converged (SOLIDWORKS Corporation, 2010).

I. Visualize the temperature flow field.

Once the calculation finished, the saved calculation results can be viewed in numerous ways and in a customized manner directly within the graphics area. The Result folder features functions were used to view results: Cut Plots (section views of parameter distribution), 3D-Profile Plots (section views in relief representation), Surface Plots (distribution of a parameter on a selected surface), Flow Trajectories, , XY Plots (diagrams of parameter behaviour along a curve or sketch), Point Parameters (getting parameters at specified points), Surface Parameters (getting parameters at specified surfaces), Goals (behaviour of the specified goals during the calculation), Reports (export of project report output into MS Word) and Animation of results. Figure 3-10 shows the summary of stages of the simulation process.

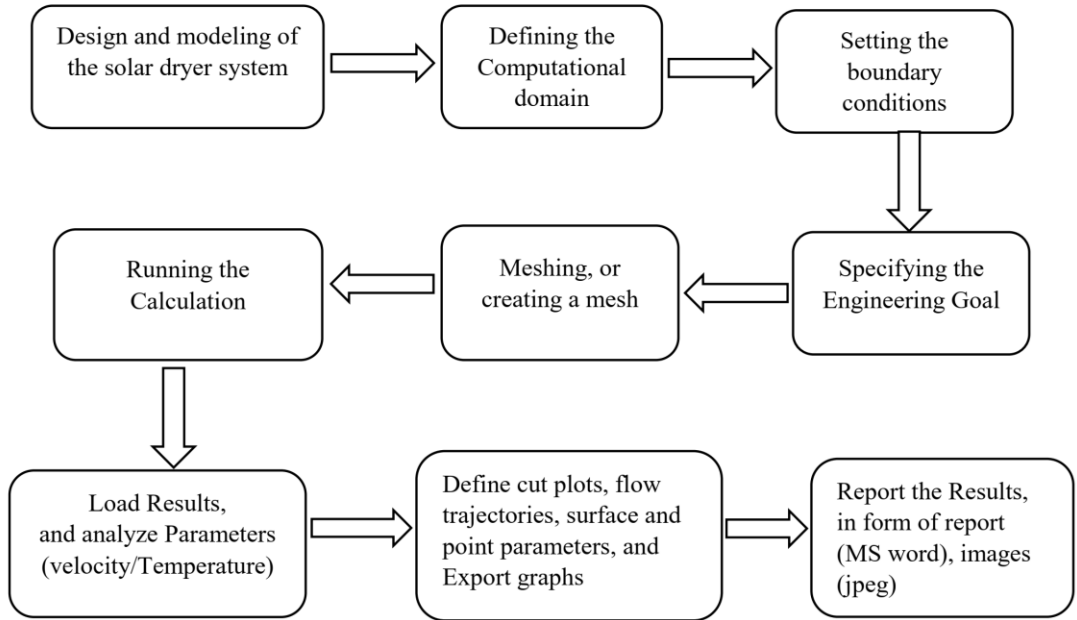


Figure 3-10: Flow chart of pre and post processing stages of simulation

3.5 Thin layer modelling of the drying curve

The drying behaviour of banana was investigated experimentally and statistically. The drying behaviour is governed by the evolution of moisture ratio during the drying process. Moisture ratio data of banana slices were fitted using eleven thin-layer drying models. The moisture ratio (MR) of banana slices during drying can be calculated using equations 3.4 and 3.5. However, for solar tunnel dryers, a simplified form described by Equation 3.5 was used to calculate the MR . The reason given for the simplification is that in solar tunnel dryers, the samples being dried are subjected to a varying temperature and relative humidity along the length of the tunnel (Cherotich, 2016).

$$MR = \frac{M - M_e}{M_o - M_e} \quad (3.4)$$

$$MR = \frac{M}{M_o} \quad (3.5)$$

Where; M and M_e are the moisture contents (w.b.) at time t during drying and at equilibrium moisture content respectively.

The *MR* results from experimental datasets using Equation (3.5) were fitted into 11 empirical thin layer models as shown in Table 3-3 using a statistical software Matlab R2018a which has a feature called curve fitting tool (*cftool*) to determine an appropriate thin layer model for the banana. The *cftool* requires a maximum of three input parameters and include the X data, Y data and Z data. The Matlab *cftool* was chosen because of its simplicity and also the robust capabilities of Matlab such as producing good quality graphics although other curve fitting tools exist.

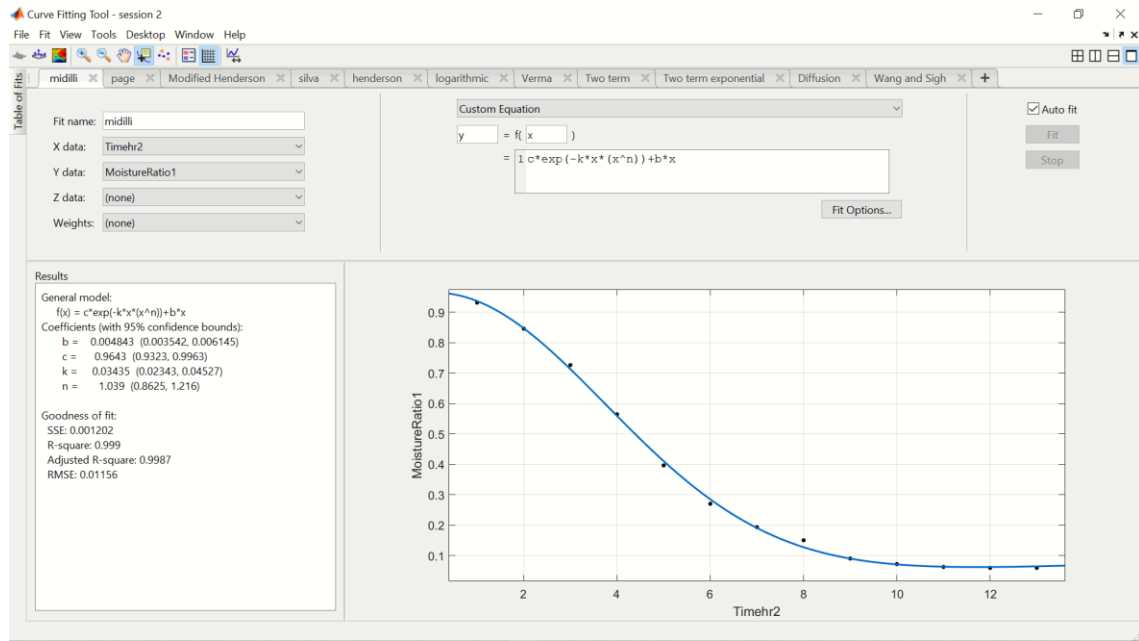


Figure 3.11 Matlab R2018a *cftool* interface and the data fitting process.

In Figure 3.11, the input parameters were the drying time on the X data field and MR on the Y data field. Then various model equations were entered for example the Midilli et al $MR = c \exp(-kt(t^n)) + bt$, the tool then determined the model coefficients b , c , k , and n . The correlation coefficient (R^2), was the primary criterion for selecting the best equation to describe the drying curve equation. In addition to (R^2), the reduced chi-square (X^2), as the mean square of the deviations between the experimental and calculated values for the models and the root mean square error analysis (*RMSE*) were used to determine the best model was established based on the criteria of three statistical parameters: Coefficient of determination (R^2), Sum of Square Error (SSE) and Root Mean Square Error (RMSE) which were calculated by the *cftool* according to Equations

(3.10), (3.11) and (3.12) respectively and subsequently plotted the predicted MR and experimental MR as depicted in Figure 3.11. This process was done for all the models shown in Table 3-3. After establishing the appropriate thin layer model, the model was used to predict the MR which was compared with the experimental MR in order to validate the model.

$$SSE = \sum_{i=1}^n w_i (MR_{Exp} - \overline{MR}_{Exp})^2 \quad (3.10)$$

$$R^2 = 1 - \frac{SSE}{\sum_{i=1}^n w_i (MR_{Exp} - \overline{MR}_{Exp})^2} \quad (3.11)$$

$$RMSE = \sqrt{\left(\frac{SSE}{v}\right)} \quad (3.12)$$

Table 3-3. Banana drying Models

Model	equation
Page	$MR = \exp(-kt^n)$
Henderson	$MR = a \exp(-kt)$
Modified Henderson	$MR = a \exp(-kt) + b \exp(-gt) + c \exp(-ft)$
Logarithmic	$MR = a \exp(-kt) + c$
Wang and Sigh	$MR = 1 + at + bt^n$
Diffussion	$MR = a \exp(-kt) + (1 - a) \exp(-kbt)$
Verma	$MR = a \exp(-kt) + (1 - a) \exp(-gt)$
Two term	$MR = 1 \exp(-kt) + u \exp(-gt)$
Two term exponential	$MR = a \exp(-kt) + (1 - a) \exp(-kat)$
Midilli <i>et al.</i>	$MR = c \exp(-kt(t^n)) + bt$
Silva <i>et al.</i>	$MR = e^{at+b\sqrt{t}}$

MR: moisture ratio; *a, b, c, k, g, h, l, u* and *n*: model constants; *t*: time

Source: (Omolola, et al., 2015)

3.6 Performance evaluation

3.6.1 The collector unit efficiency

The efficiency of flat plate collector is influenced by many factors such as the size of collector, geographical location, velocity, humidity, and the temperature of the surrounding air (Lingayat, et al., 2017). The collector unit was analysed for its performance by obtaining the collector efficiency which expresses the heat gained as a ratio of the solar insolation falling on its surface. The thermal efficiency for the solar collector can be determined by Equation 3.13

$$\eta_c = \frac{\dot{m}C_p(T_c - T_{am})}{I_s A_c} \quad (3.13)$$

Where; η_c is the collector efficiency, \dot{m} is the air mass flow rate in $\text{kg}/\text{m}^2\text{s}$, C_p is the specific heat capacity of the air in $\text{J}/\text{kg K}$, A_c is the area of the collector in m^2 and I_s is the solar insolation in W/m^2 .

3.6.2 The drying efficiency

The system drying efficiency is defined as the energy used to evaporate the moisture in the product divided by the energy input to the dryer (Chavan, et al., 2008). The drying efficiency was calculated using Equation (3.14) used for natural convection dryers (Chavan, et al., 2008).

$$\eta_{drying} = \frac{WL}{I_{ST} A_c} \quad (3.14)$$

Where η_{drying} is the drying efficiency, W is the total moisture removed in kg , L is the latent heat of vaporization of water at the dryer air temperature in kJ/kg and I_{ST} is the total solar insolation registered for the drying time.

3.6.3 The Chimney unit buoyancy pressure head

The chimney unit was evaluated for the developed buoyancy pressure head generated. The buoyancy pressure head generated by the chimney can be calculated according to Equation (3.15) (Brenndorfer, et al., 1987).

$$\Delta P_b = gH(\rho_{am} - \rho_{ch}) \quad (3.15)$$

Where; ΔP_b is the chimney buoyancy pressure head in Nm^{-2} , g is the acceleration due to gravity in ms^{-2} , H is the chimney height in m, ρ_{am} is the ambient air density in $kg m^{-3}$ and ρ_{ch} is the mean chimney air density in $kg m^{-3}$. Between air temperatures of 25°C and 90 °C, the density of dry air is related to the temperature by the following empirical expression.

$$\rho = 1.11363 - 0.00308 T \quad (3.16)$$

Equations (3.15) and (3.16) were manipulated to yield Equation (3.17) which uses the air temperatures as opposed to Equation (3.15) which uses air density to calculate buoyancy pressure.

$$\Delta P_b = 0.00308gH(T_{ch} - T_{am}) \quad (3.17)$$

By using Equation (3.17), the buoyancy pressure head was obtained using the temperature of the air leaving the chimney unit and ambient air temperature defined earlier as T_{ch} and T_{am} respectively.

3.6.4 Mean relative deviation

The model predicted results were validated with experiments using statistical analysis. The prediction ability of the model was tested by statistical measure: mean relative deviation. The mean relative deviation gives an idea of the mean departure of the measured data to the simulated data. The mean relative deviation should not exceed 10%. The mean relative deviation (MRD) as described by equation 3.18 was used to estimate the difference between the simulated results and from the model and measured results from the experiments.

$$MRD = \frac{1}{m} \sum_{i=1}^m \frac{|Simulated(i) - Measured(i)|}{Simulated(i)} \quad (3.18)$$

3.7 Energy and Exergy analysis

3.7.1 Energy analysis of Mixed-mode Solar Dryer

The solar air collector and the drying chamber were assumed to have steady air flow and were analyzed using steady flow mass and energy conservation principles. By mass conservation principle, the mass flow rate is constant which means the rate of air coming in is equal to the rate of air coming out of the system (Mugi & Chandramohan, 2020).

$$\sum \dot{m}_{ai} = \sum \dot{m}_{ao} \quad (3.19)$$

Where, \dot{m}_a represents the mass flow rate of air (kg/s). The subscripts i and o represent inlet and outlet, respectively. By energy conservation principle, the rate of energy transfer by work, heat and mass into the system is equal to the rate of energy transfer by work, heat and mass coming out of the system. Put a sentence here referring to Equation (3.20) and (3.21).

$$\sum \dot{E}_{in} = \sum \dot{E}_{out} \quad (3.20)$$

$$Q + \sum \dot{m}_{ai} \left(h_{ai} + \frac{v_{ai}^2}{2} + z_i g \right) = \sum \dot{m}_{ao} \left(h_{ao} + \frac{v_{ao}^2}{2} + z_o g \right) + W \quad (3.21)$$

Where, Q is the net heat transfer to the system, W is net work done by the system, h_a , v_a and z represent enthalpy, velocity and height, respectively from the datum of air. There is no work done by the dryer. The difference between kinetic and potential energies of the dryer is very small and it is neglected.

3.7.2 Energy analysis of solar air collector (SAC)

By applying steady flow mass and energy conservation principles to SAC, the following equations were obtained from Equations (3.21) and (3.22).

$$\sum \dot{m}_{ai} = \sum \dot{m}_{ao} = \sum \dot{m}_a \quad (3.21)$$

$$Q = Q_{u,SAC} = Q_{in,SAC} - Q_{is,SAC} = \dot{m}_a (h_{ao} - h_{ai}) \quad (3.22)$$

Where, $Q_{u,SAC}$ is the useful heat supplied by collector, $Q_{in,SAC}$ is the heat input to collector and $Q_{is,SAC}$ is the heat lost from collector. $Q_{in,SAC}$ is calculated using;

$$Q_{in,SAC} = I_s A_{SAC} \quad (3.23)$$

Where, I_s is instantaneous solar radiation flux (W/m^2) at a given time and A_{SAC} is the area of collector which is calculated as $0.75m^2$. $Q_{u,SAC}$ (Mugi & Chandramohan, 2020) is calculated using equation 3.24;

$$Q_{u,SAC} = \dot{m}_a C_{pa} (T_{co} - T_{ci}) \quad (3.24)$$

Where, C_{pa} is the specific heat of air in $\text{kJ}/(\text{kgK})$, T_{co} and T_{ci} are the temperatures of air at collector outlet and inlet, respectively. The efficiency of flat plate collector is influenced by many factors such as its size, geographical location, velocity, humidity, the temperature of the surrounding air, etc (Lingayat, et al., 2019). The collector efficiency or energy efficiency is the ratio of useful heat supplied by the collector to the heat input to collector and is given by equation (3.25),

$$\eta_{en,SAC} = \frac{Q_{u,SAC}}{Q_{in,SAC}} = \frac{\dot{m}_a C_{pa} (T_{co} - T_{ci})}{I_s A_{SAC}} \quad (3.25)$$

3.7.3 Exergy analysis using the second law of thermodynamics

The exergy values are calculated by using the characteristics of the working medium from a first law of thermodynamics. For this purpose, the general form of exergy equation (Chowdhury, et al., 2011; Ahern, 1980) is employed.

Exergy = internal energy + entropy + flow work + momentum + potential energy
+ chemical energy + radiation emission

$$\text{Exergy} = (u_0 - u_\infty) - T_\infty (s - s_\infty) + \frac{P_\infty}{j} (v_0 - v_\infty) + \frac{V^2}{2gj} + (z - z_\infty) \frac{g}{g_cj} + \sum_c (\mu_c - \mu_\infty) N_c + E_i A_i F_i (3T^4 - T_\infty^4 - 4T_\infty T^3) \quad (3.26)$$

Where, the subscript ∞ denotes the reference conditions. There are variations of this general exergy equation. In the analysis of many systems, some, but not all, of the terms shown in Equation (3.26) are used. Since exergy is energy available from many sources, the terms can be developed using electrical current flow, magnetic fields, and diffusion flow of materials. One common simplification is to substitute enthalpy for the internal energy and P_∞ terms that are applicable for steady flow systems. Equation (3.26) is often used under conditions where the gravitational and momentum terms are neglected. In addition to these, the pressure changes in the system are also neglected because of $v \cong v_\infty$ in this case, Equation (3.26) becomes:

$$\text{Exergy} = m_{da} C_{pa} \left[(T - T_\infty) - T_\infty \ln \frac{T}{T_\infty} \right] \quad (3.27)$$

Applying Equation (3.27), the exergy inlet, and outlet can be determined depending on the inlet and outlet temperature of the drying systems. However the exergy loss throughout the process is determined by Equation (3.28).

Exergy loss = Exergy inflow – Exergy outflow

$$\Sigma \dot{E}_{XL} = \Sigma \dot{E}_{x_i} - \Sigma \dot{E}_{x_o} \quad (3.28)$$

Exergy calculation for collector

The exergy inlet or inflow for the collector is stated as Equation (3.29).

$$Ex_{ci} = m_{cai} C_{pa} \left[(T_{ci} - T_{\infty}) - T_{\infty} \ln \frac{T_{ci}}{T_{\infty}} \right] \quad (3.29)$$

The exergy output for the collector is stated as Equation (3.30).

$$Ex_{co} = m_{cao} C_{pa} \left[(T_{co} - T_{\infty}) - T_{\infty} \ln \frac{T_{co}}{T_{\infty}} \right] \quad (3.30)$$

The exergy of solar radiation for collector can be expressed by Equation (3.31).

$$EX_{sol-in-col} = E_{net} \left[1 - \frac{4T_0}{3T} + \frac{1}{3} \left(\frac{T_0}{T} \right) \right] A_{cz} \quad (3.31)$$

The surface temperature of the sun is 5,500°C (NASA, 2022), and this is the value used in this analysis.

The exergy efficiency of the solar collector ($EX_{eff-col}$) is the ratio of the increase in air flow exergy to the exergy input into the collector from solar radiation ($EX_{sol-in-col}$) as given by Equation (3-32) (Simate, 2021).

$$EX_{eff-col} = \frac{Ex_{co} - Ex_{ci}}{EX_{sol-in-col}} \quad (3.32)$$

3.7.4 Exergy calculation for drying chamber

The exergy of air entering the drying chamber (Ex_{co}) is the same as that coming out of collector.

The exergy inflow and exergy outflow of the drying chamber are determined using: Exergy outflow for dryer can be expressed by equation (3.33) and (3.34):

$$Ex_{dci} = m_{dai} C_{pa} \left[(T_{di} - T_{\infty}) - T_{\infty} \ln \frac{T_{di}}{T_{\infty}} \right] \quad (3.33)$$

$$Ex_{dco} = m_{dao} C_{pa} \left[(T_{do} - T_{\infty}) - T_{\infty} \ln \frac{T_{do}}{T_{\infty}} \right] \quad (3.34)$$

The exergy losses can be determined using equation (3.35).

$$\Sigma \dot{E}_{XL} = \Sigma \dot{E}_{dci} - \Sigma \dot{E}_{dco} \quad (3.35)$$

The exergetic efficiency is defined as the ratio of the exergy outflow to the exergy inflow for the drying chamber (Karthikeyan & Murugavelh, 2018). Considering this, the exergetic efficiency of the drying chamber can be determined by equation (3.36)

$$\text{Exergetic efficiency} = 1 - \frac{\text{Exergyloss}}{\text{Exergy input}} \quad (3.36)$$

3.8 Closing remarks

In this chapter, the materials and methods specific to each objective were presented. The study area and the period in which the study was conducted have been indicated. A number of tools and softwares used to carry out the study have also been mentioned such as SolidWorks and Matlab *cftool*. Photographs have been used as much as possible to communicate the experimental procedures as they carry more clarity than words and finally, equations used for evaluating the energy and exergy have been described and presented.

CHAPTER FOUR: RESULTS AND DISCUSSIONS

4. Introduction

The solar tunnel dryer model used to simulate the temperature and airflow distributions was developed using the methodology described in the previous chapter. In this chapter, the simulation results of the model are presented then compared and validated against experimental results. The experimental results are used for subsequent energy and exergy parametric study. The results of the comparisons and the parametric study are presented in this chapter.

The chapter covers the following in detail; the load experiments results, the solar dryer model simulations, the dryer model modification in CFD and performance evaluation, energy and exergy evaluation then finally some closing remarks.

4.1 Heat transfer analysis

4.1.1 Temperature distribution

To determine the thermal behaviour of the collector and dryer various data were measured throughout the experiments. For the performance analysis, sliced fresh bananas were dried for 2 days.

A. Day 1

The variations of the air temperature and solar insolation under which the bananas were dried on the first day of the experiment are shown in Figure 4.1.

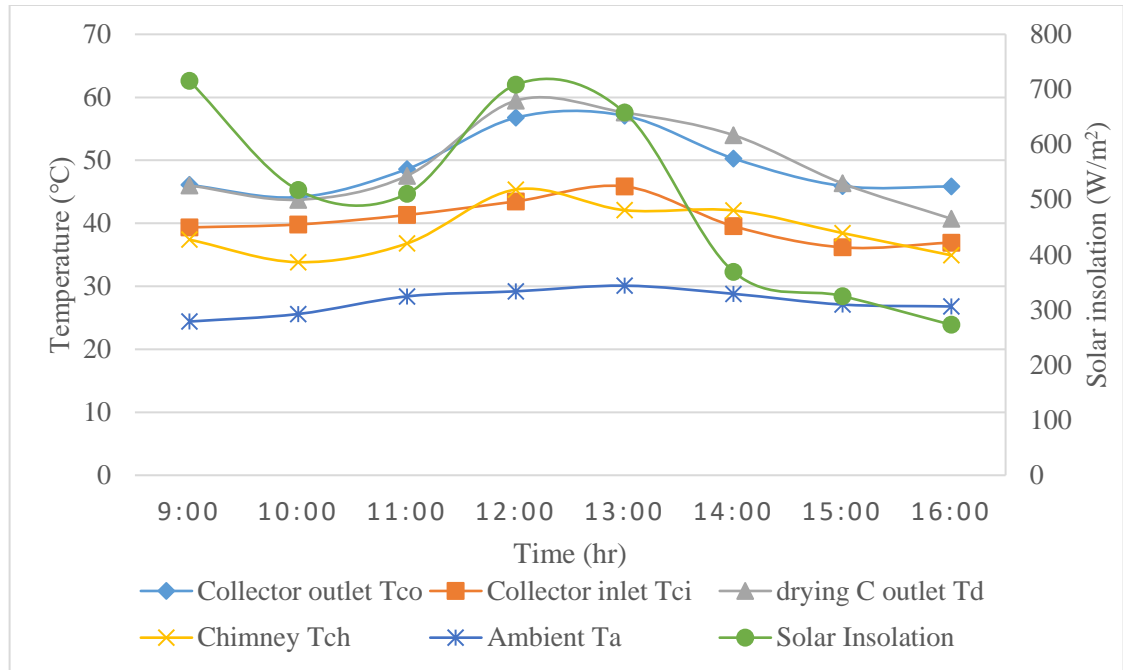


Figure 4-1: Air temperatures and solar radiation on the Day 1 of the drying Experiment

The pattern of the calculated average air temperature values at the beginning of the drying showed that T_{co} was greater than T_d , T_{ch} and T_{am} at start of the drying until after 12:00hrs when T_{co} is seen to decrease and the temperature in the drying chamber T_d is greater. This temperature difference observed between T_{co} and T_d was due to the heat mass transfer process during which the heated air from the collector outlet (T_{co}) picked up moisture from the product and resulted in heat loss from the air to the product and moisture from the product to the air (drying process). At about 10:30 hours all temperatures experienced a reduction due to a decrease in solar irradiation at this time. A maximum average air temperature of 57.01°C was recorded at the collector unit. The drying process showed minimal hourly drop in air temperature T_{co} to T_d of 1°C and below. The average temperature values for T_{am} , T_{co} , T_d , and T_{ch} , were obtained as 27.67°C, 49.3°C, 49.4°C and 38.8°C respectively. The heat losses in the dryer may have been due to imperfect insulation. Ambient temperature ranged between a low of 24.1 °C and a high of 30.1 °C before a slight reduction. The chimney was also painted with matt black paint to heat the exiting air even more and enhance the buoyant flow of air but it was observed that the temperature of the chimney dropped faster than that of the collector and drying unit, this was due to some ambient air entering through the exhaust vent of the

chimney. Additionally the back of the chimney which was not painted with matt black paint to absorb more heat or insulated could have also contributed to the faster drop in temperature. This would slow down the “chimney effect, thereby trapping warm air in dryer which could only escape slowly by transmission through the cover or by convection through the dryer walls. The product thus stayed longer in warm low humidity air and drying on Day 2 resumed with very little moisture gain. This observation was also reported by Berinyuy, et al., (2012).

B. Day 2

On the second day the resulting pattern of air temperatures shows that T_d was greater than T_{co} , T_{ch} and T_{am} throughout the drying process as shown in figure 4.2. This is expected since less energy is used for evaporation as the banana slices are in a period of lower drying rates. There is a slight drop in temperature from the drying chamber T_d to the chimney T_{ch} was recorded as the exhaust air then moved through the chimney after heat and moisture exchange with the drying product. The temperature of air at the chimney exit was lower than the temperature of the air exiting the drying chamber and entering the chimney by an average of 14.8 °C. The drop in air temperature was unexpected because the chimney, as a bare flat plate solar collector, was expected to continue heating the air from the drying unit to a higher temperature. This phenomenon of drop in temperature at the chimney unit could be explained by the high thermal heat losses associated with a bare-flat plate collectors (Ekechukwu & Norton, 1997). A maximum air temperature of 81.83°C was recorded in the drying chamber at a solar insolation of 934.45 W/m² around 12:00 hrs, while a mean collector temperature rise above ambient of 28.3°C was registered at a mean insolation of 626.97 W/m². After 12:00hrs solar insolation takes a downward trend, again with intermittent rises and falls.

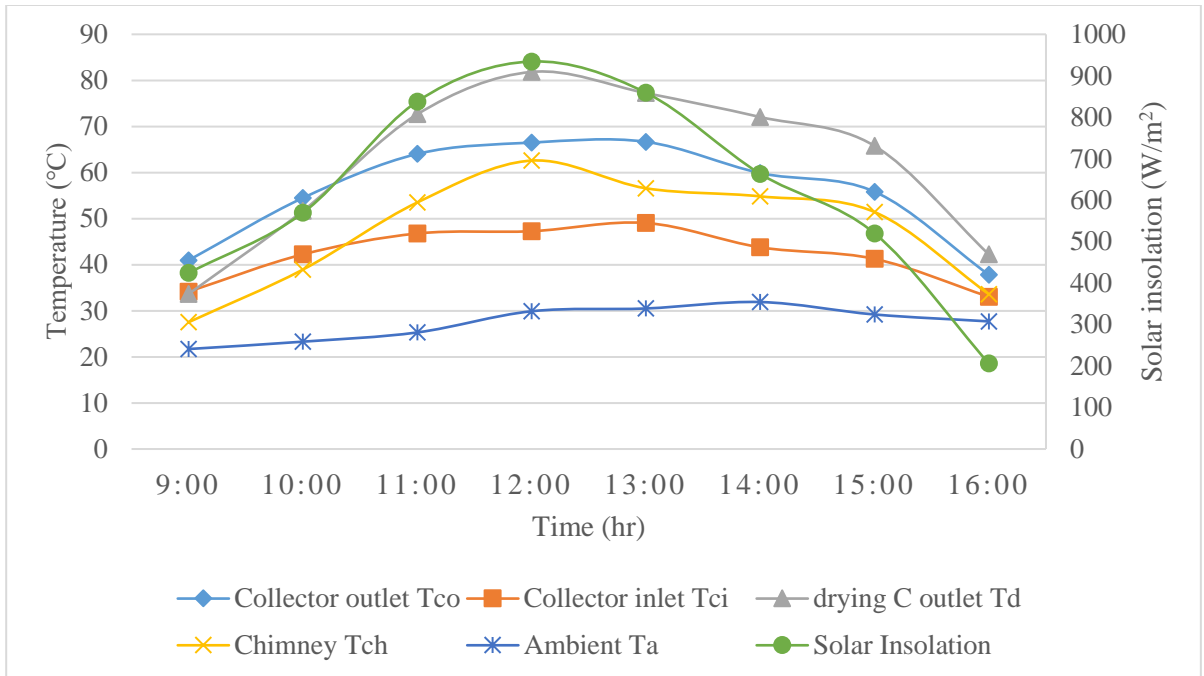


Figure 4-2: Air temperatures on the Day 2 of the drying Experiment

4.2 Relative humidity

The Relative Humidity of air changes as the air moves through the dryer from entry at the collector to the exit at the chimney as shown in figure 4-3. It can be seen that the relative humidity in the drying chamber (RH_d) is higher than that at collector exit (RH_c) because the air picks up moisture from the product in the drying chamber.

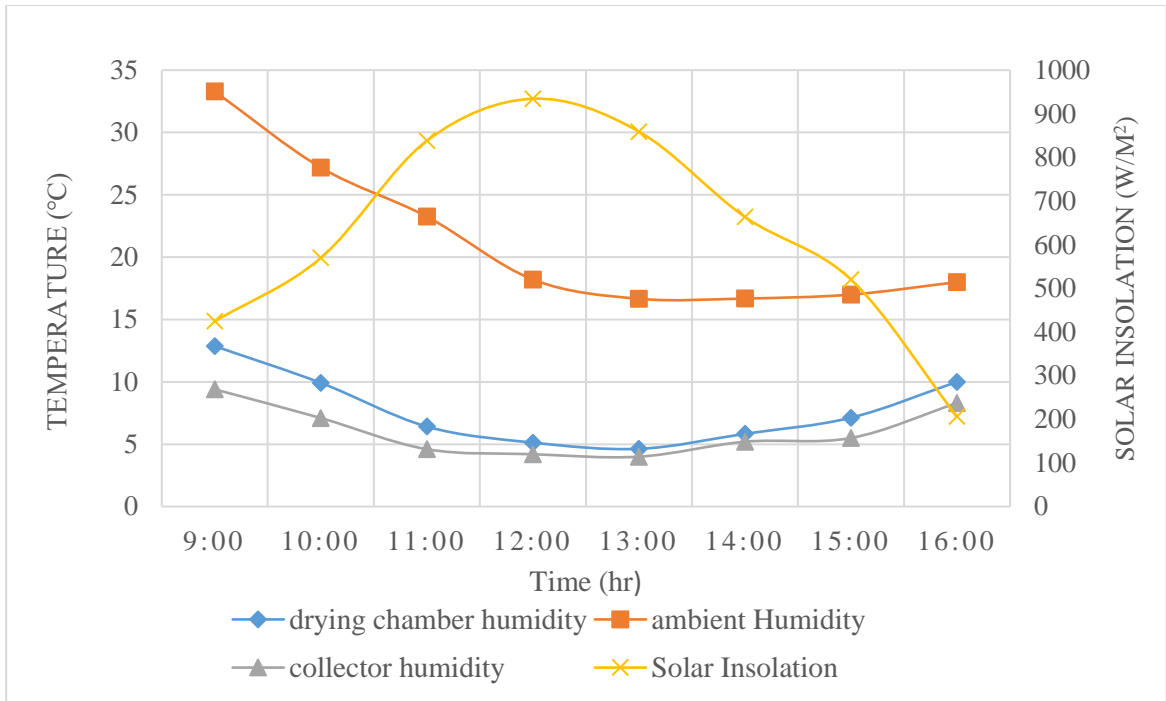


Figure 4-3: Variation of relative Humidity and Solar Insolation during the banana drying experiment

The increase in ambient temperature caused a decrease in ambient relative humidity accompanied by a sharp decrease in the collector and drying unit relative humidity. It was noticed that, the ambient RH was always higher than the collector and drying unit RH due to increased temperature inside the solar tunnel dryer. The ambient relative humidity varied between a minimum of 16% and a maximum of 33% while the drying unit RH varied between a minimum of 4.63% and a maximum of 12.86%. There was a significant difference of 13.55% in relative humidity inside the dryer compared to the ambient relative humidity. Mkhathini, et al., (2018) reported that the lowest relative humidity in the solar tunnel dryer occurred at mid-day. This can be compared to figure 4.3 which shows that the lowest relative humidity was at 12:00 hours. It was observed that as solar insolation decreased after 13:00 hours there was an increase relative humidity. The decrease in solar insolation led to a decrease in ambient temperature causing an increase in ambient relative humidity accompanied by a slight increase in the collector and drying unit relative humidity. The average drying unit relative humidity, was 7.74% which is good and sufficient for drying.

4.3 Moisture content changes with time

The detailed experimental setup and procedure used according to AOAC, (2005) for determining the initial moisture content have been explained in chapter 3. A thermostatically controlled hot air oven was used. The initial moisture content of the bananas was found to be 73.9% (w.b.) which is comparable to initial moisture content of 73% determined by Huselstein, (2016), Kamlesh & Nimesh, (2016) who determined ranges of about 72% to 77% (w.b.) and Abano & Sam-Amoah, (2011) of 75% to 77 % (w.b.). The initial moisture content was reduced to final moisture contents of between 4.39 % (w.b.) in 13 hours in the 2 days of drying the product as shown in Figure 4-4. After reaching the final moisture content of 4.39 % (w.b.), any further drying resulted in no further weight loss, hence moisture content of 4.39 % (w.b.) was considered as the equilibrium moisture content.

From Figure 4-4 it can be observed that the moisture content of the bananas decreased continuously. The total drying time was 13 hours to reach the final moisture content with 7 hours being the first day of drying because a typical experiment was done from 09:00 hours to 16:00 hours (7 hours period). The product was then kept in a polyethylene bag at the end of the first day of drying under room temperature to prevent any moisture loss or gain to the atmosphere, and then dried for the last 7 hours period on the second day.

The moisture removal in the first six hours of drying was higher due to availability of more free moisture on the surface of the bananas. Some of the heat energy was used to evaporate moisture from the surface while remaining increased the interior temperature of the sample. In the later hours the moisture removal was low due to less free water.

The final moisture content of the dried bananas in this study was compared well with what has been reported previously by Bowrey, et al., (1980) who reported that bananas were dried to less than 20 % final moisture content observed at slice thicknesses of 1 to 4 mm and selected banana slice thicknesses of 3 and 4 mm as optimal for enclosed solar drying. Huselstein, (2016) also dried bananas over a two day period to a final moisture content of 8% while Nguyen & Price, (2007) reported a final moisture content of 14%. At 4.39% final moisture content recorded in this experiment, the dried banana have a longer shelf life because of reduced microbial activity which spoils the product.

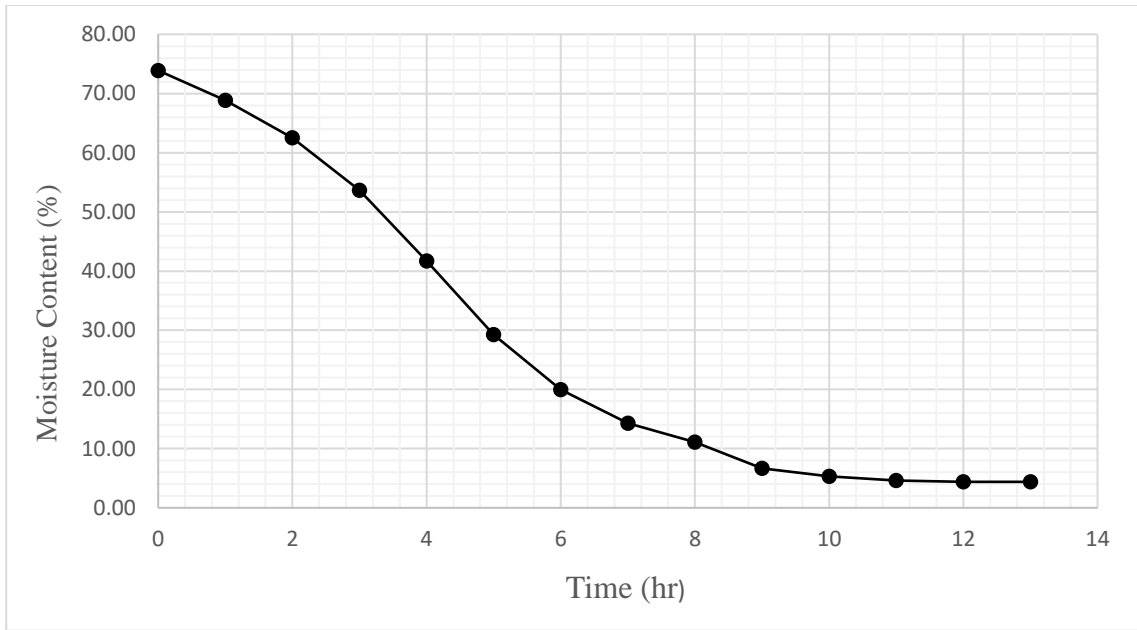


Figure 4-4 Banana drying curve

4.4 Airflow

The airflow through the chimney was measured at a specific point (mid-point) in the dryer chimney. As the air in the chimney expanded due to solar heating, it became relatively lighter. It rose out of the chimney outlet vent, drawing the cooler ambient air into the tunnel dryer through the inlet vent. This pull effect was further complemented by the push effect from the ambient wind. The ambient wind speed varied between 0.2 m/s and 6.4 m/s. The results of measurement indicated that airflow through the chimney varied throughout the drying period. The hourly velocity through the centre of the chimney varied from 0.06 m/s to 0.16 m/s which can be converted to give mass flow values of 0.0054 kg/s to 0.0129 kg/s during the drying experiment. The values were for a collector of 1m × 0.75 m and a chimney cross-section of 0.75 m × 0.75 m. It was estimated that the average airflow through the centre of the chimney was about 0.13 m/s during the drying experiment. Othieno, (1987) used a collector of 2 m × 1 m and measured the air velocity through the chimney cross-section of 0.2 m × 0.2 m. He obtained air speed of 0.05 to 0.3 m/s which can be converted to give mass flow values of 0.0021 to 0.0123 kg/s. The measured velocity through the centre of the chimney is shown in Figure 4-5.

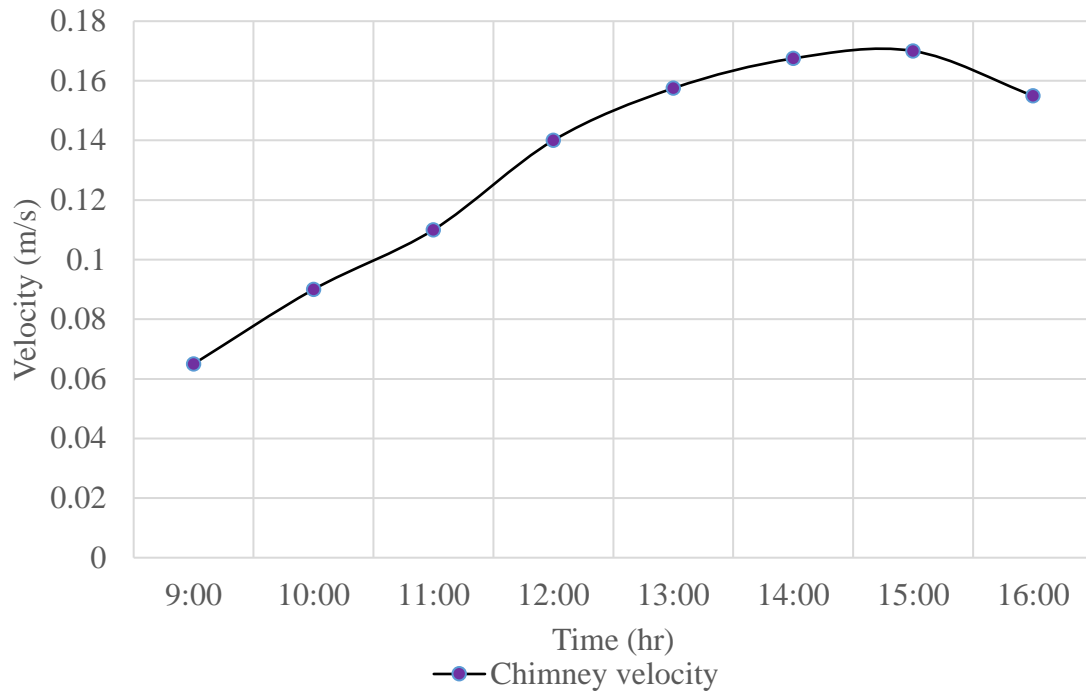


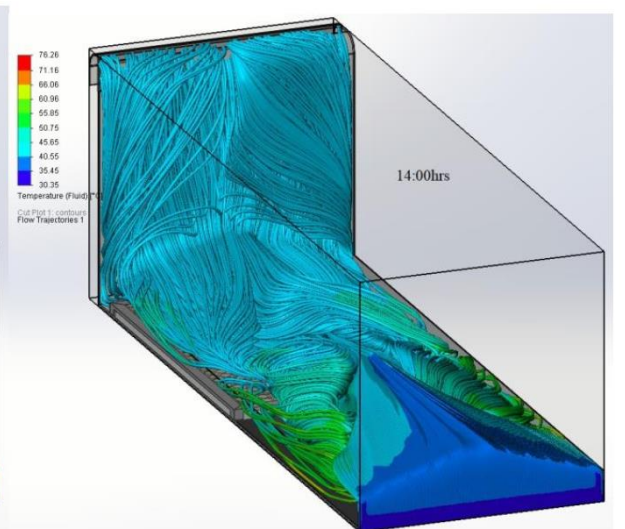
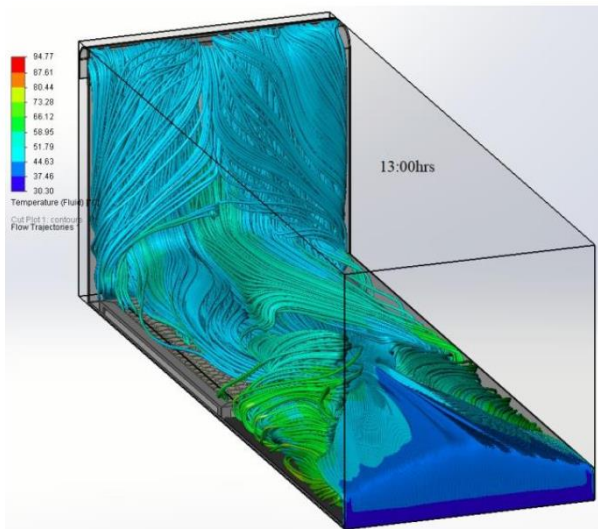
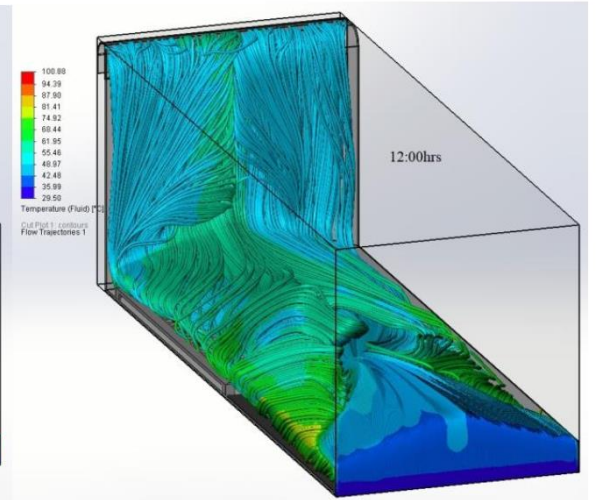
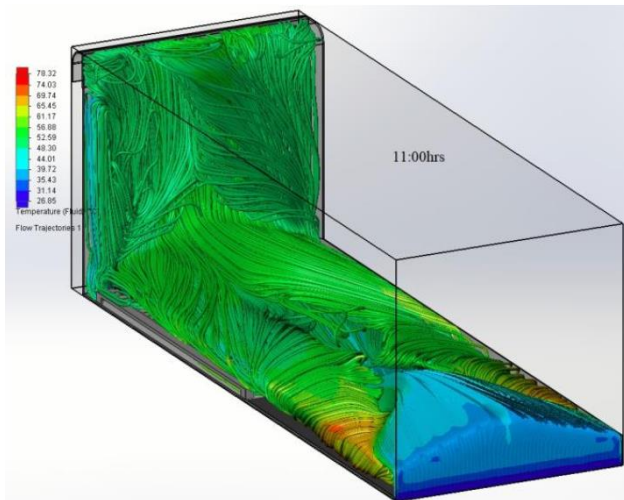
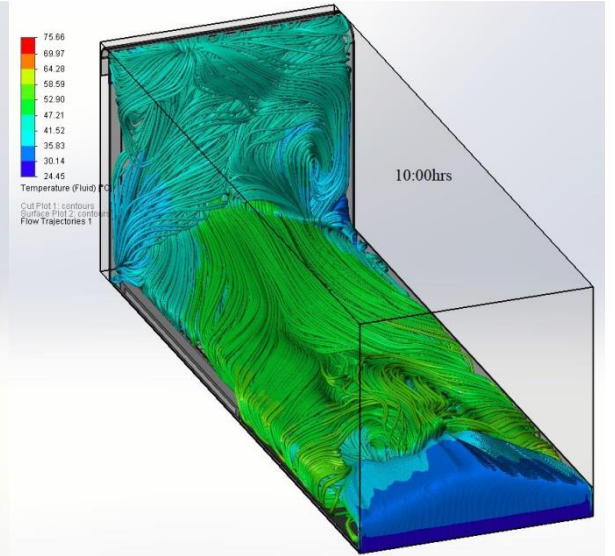
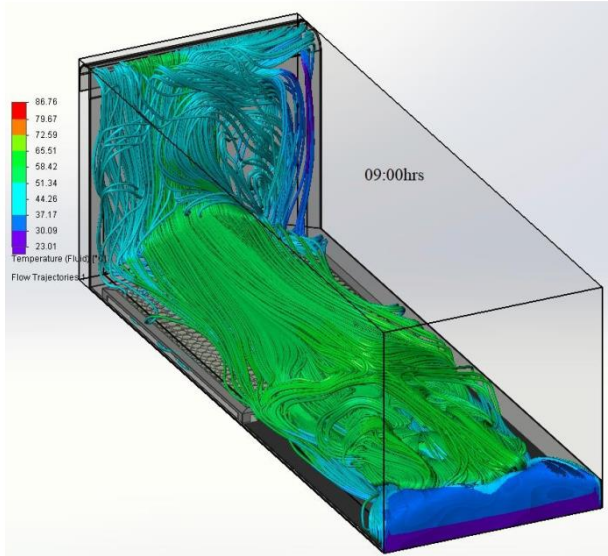
Figure 4-5 Velocity through the solar tunnel dryer chimney

4.5 Simulations

SOLIDWORKS flow simulation was used to simulate the temperature distribution inside the solar tunnel dryer based on solar insolation. The fluid temperature flow trajectories inside the solar dryer for hourly intervals of time is depicted in Figure 4-6. The simulations were done while considering the porous medium (bananas) and ambient temperature. This simulation was seeking to define the contours for the temperature and the velocity for the air inside the tunnel dryer.

4.5.1 Temperature

The variation of solar insolation from 09:00 hours to 16:00 hours significantly affects the tunnel temperature as because it is dependent on the solar insolation. The temperature of air adjacent to the collector plate increased as visualized from the figures. It can be also noted that the temperature at various locations of the dryer were different at any given time. The solar dryer temperature was increasing steadily with increase in solar insolation.



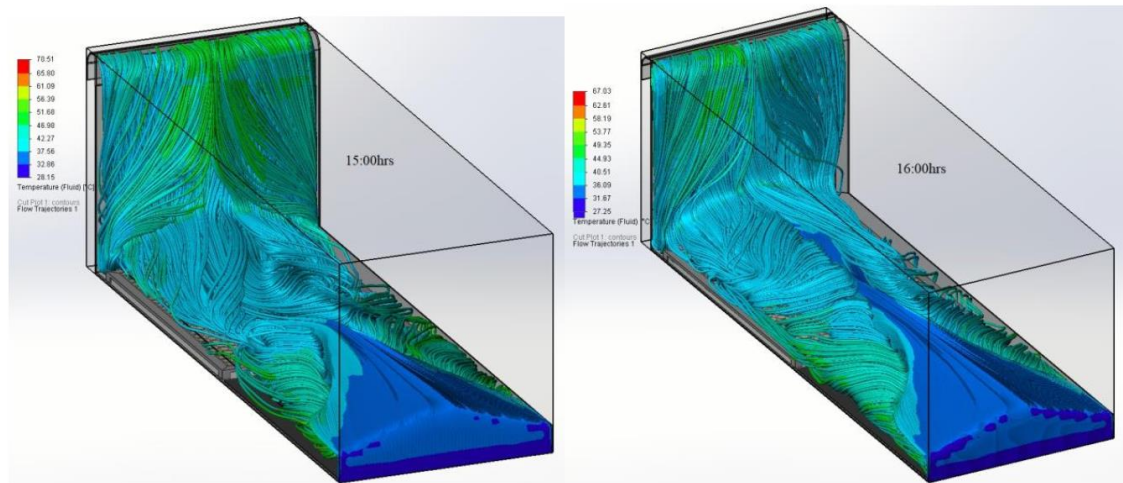
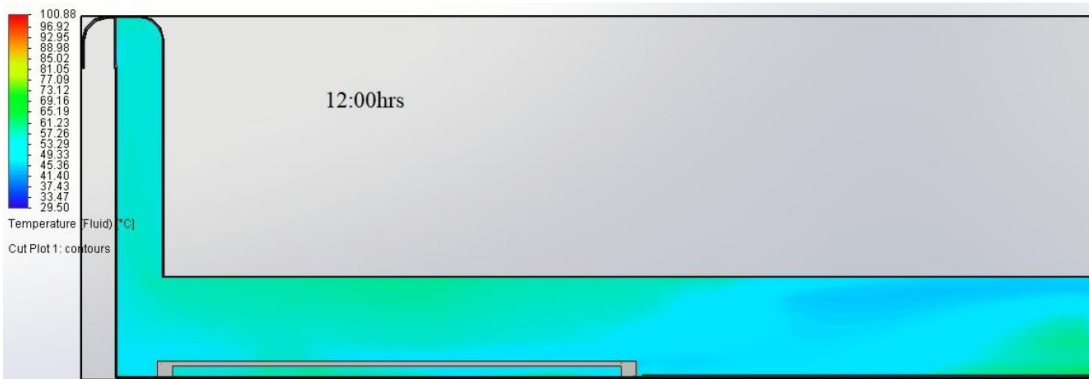
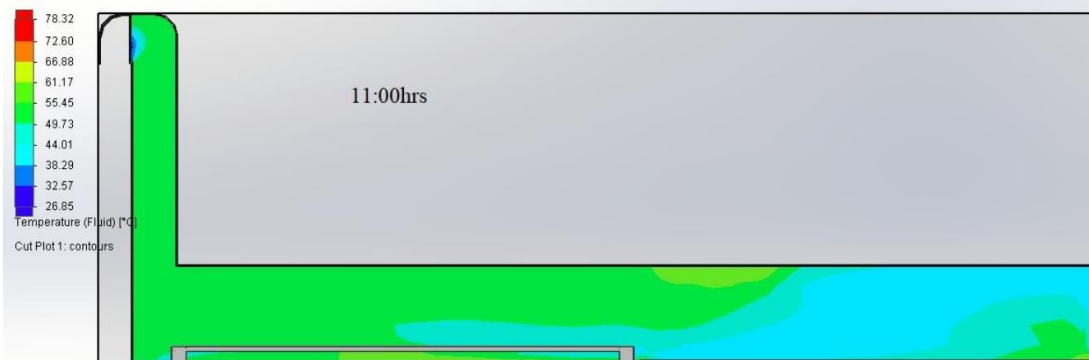
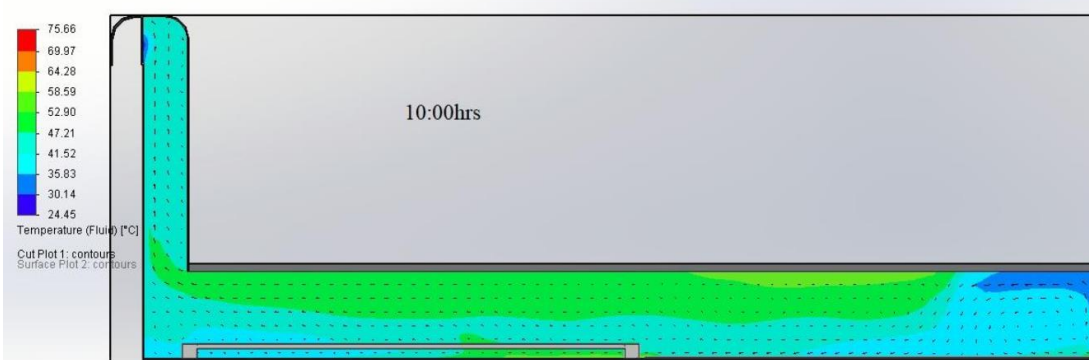


Figure 4-6 Simulated temperature flow trajectories

Figure 4.7 shows temperature cut plots. From the visualization of air temperature distribution across the collector and drying unit, it can be noticed that the maximum heat gain is at the collector and this is a similar trend as observed from the experiment. The air temperature near the wall is slightly lower compared to that at the centre of the drying chamber. It is due to the shortest path followed by air to exit of the dryer. It was observed that though the chimney was also receiving solar insolation there was some loss of heat from the air passing through the chimney which could have been due to the ambient air entering through the exhaust vent.

The results of simulation revealed that the average drying air temperature at collector and drying unit was to be 56.71°C and 62.9 °C, respectively, but the temperatures in the collector and drying unit could go as high as 66.83°C and 73.9°C, respectively.



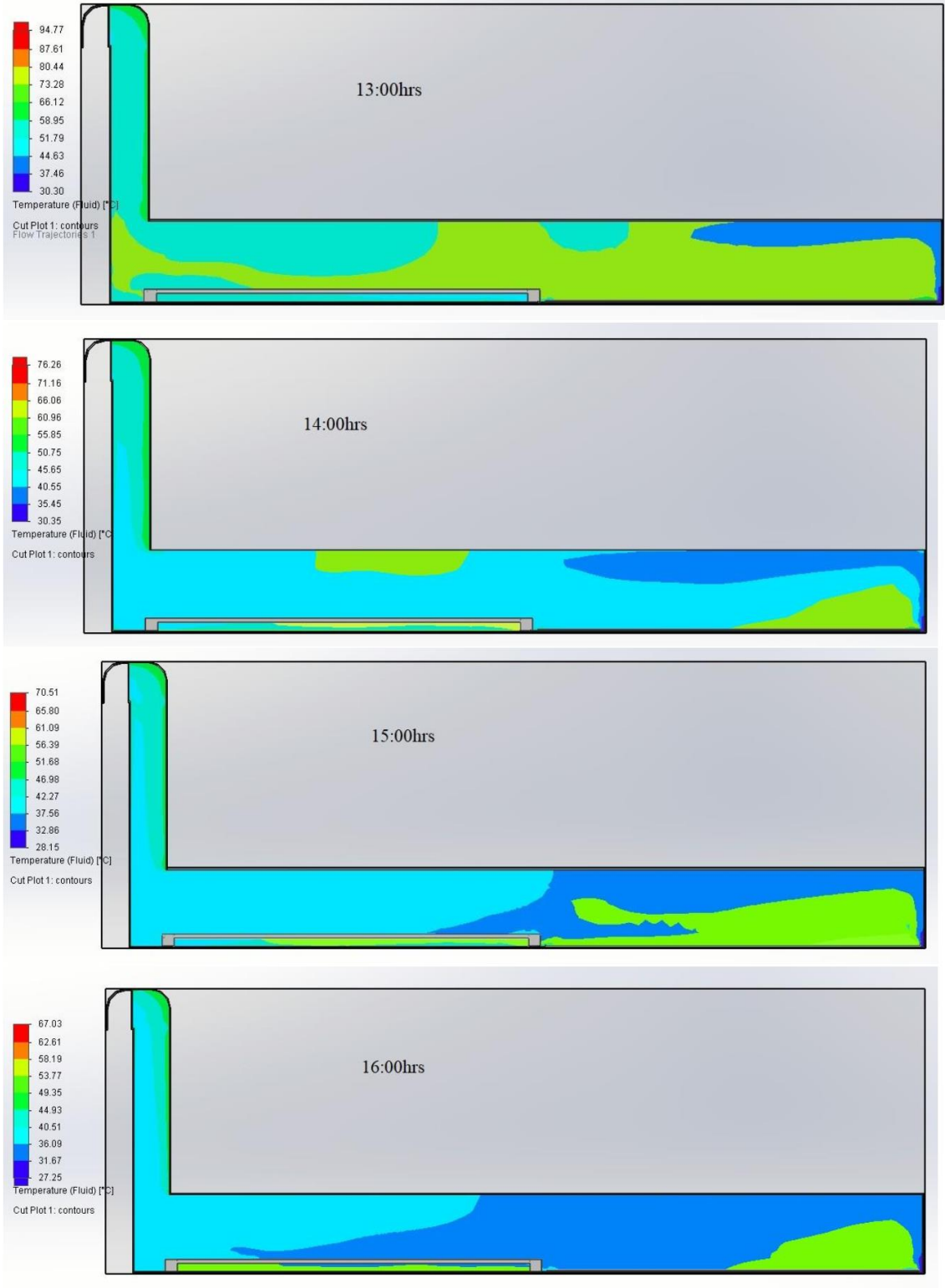


Figure 4-7 Temperature cut plots

Figure 4-8 shows that the surface temperature contours at the middle of the collector had the highest temperature and it reduced as the contours grew away from the middle of the collector. The red colour around the middle area indicates that there was little to no heat loss with temperature of 57.45°C around that region, as it moves towards the edge of the collector it shows a mixture of colours showing little heat loss at the edge. This demonstrates that, the energy impacting on the materials used in the dryer, is absorbed and this facilitates the increment of temperature inside the tunnel dryer.

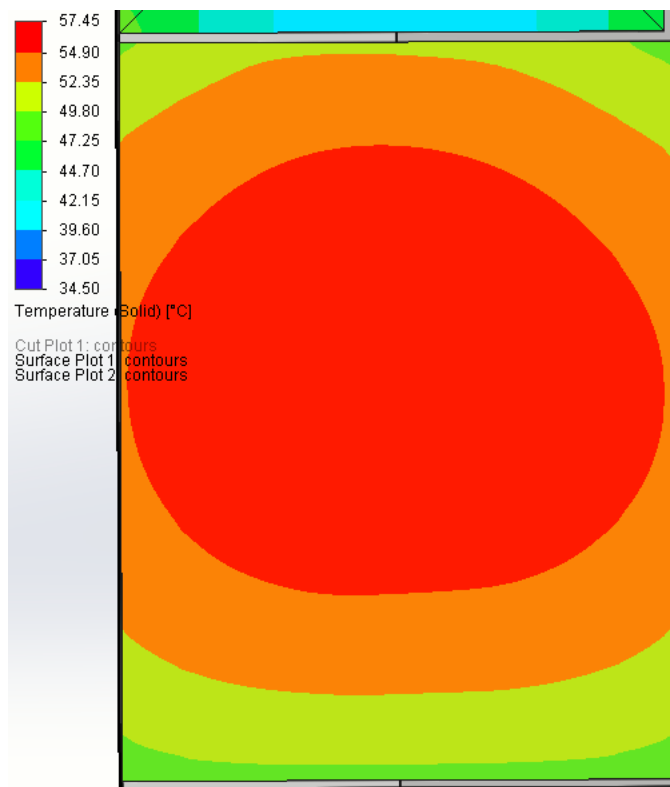
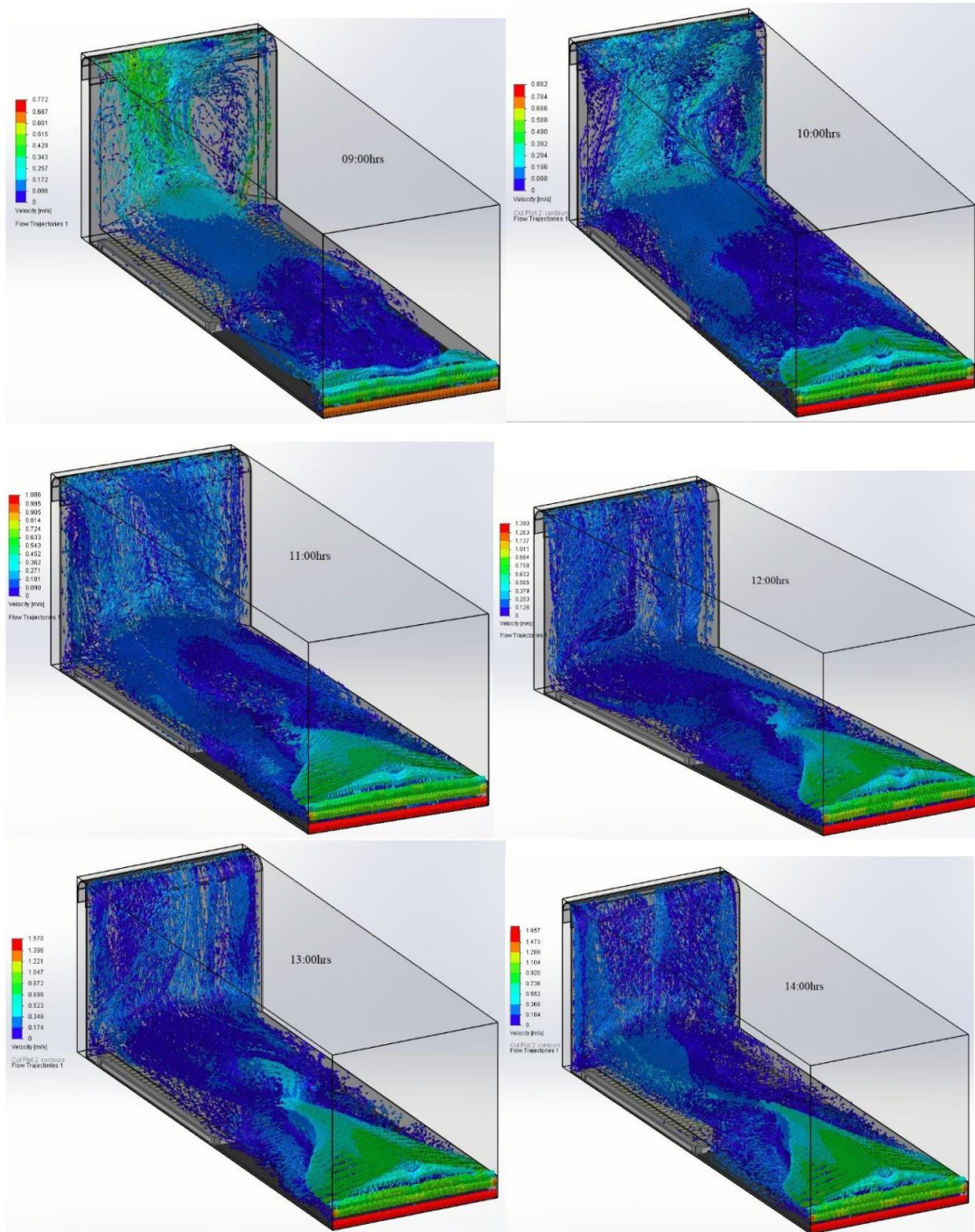


Figure 4-8 Surface temperature contours at collector

4.5.2 Airflow rate

The simulation results in Figure 4-9 show the velocity trajectories of the airflow in the solar dryer based on solar insolation. The velocity increases towards the exit (chimney exhaust vent). This behaviour was expected, since the flow cross-section decreases in this direction. The inlet and outlet regions depict the highest velocity and this is as a result of the openings at both ends. Also, it was observed that airflow velocity towards the drying

unit produced the lowest velocity profile, because the tray (wire mesh) and porous medium (banana slices) arrangement slightly obstructed airflow stream across the drying unit within the tunnel dryer as depicted by the contours in figure. The results showed air velocity flowing at an average of 0.034 m/s.



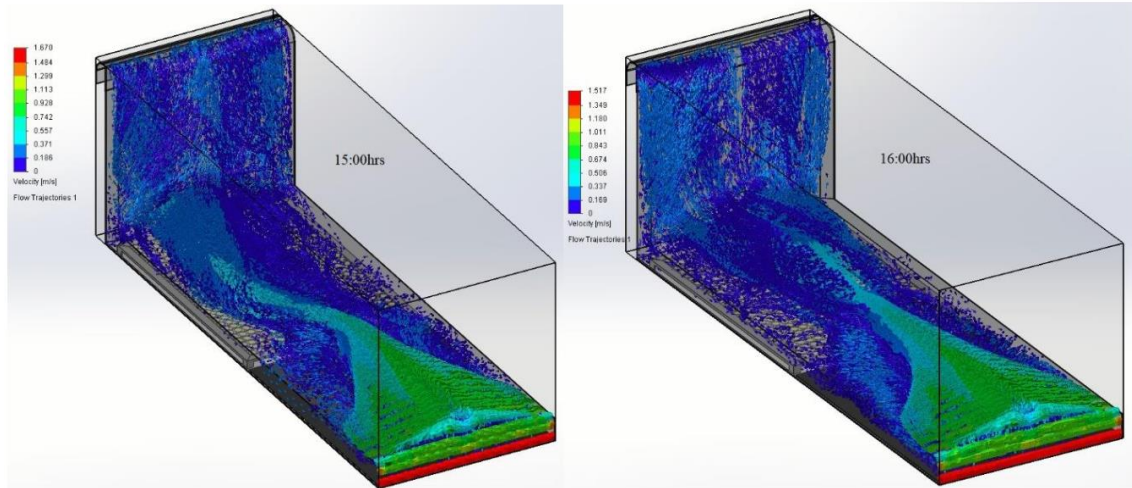
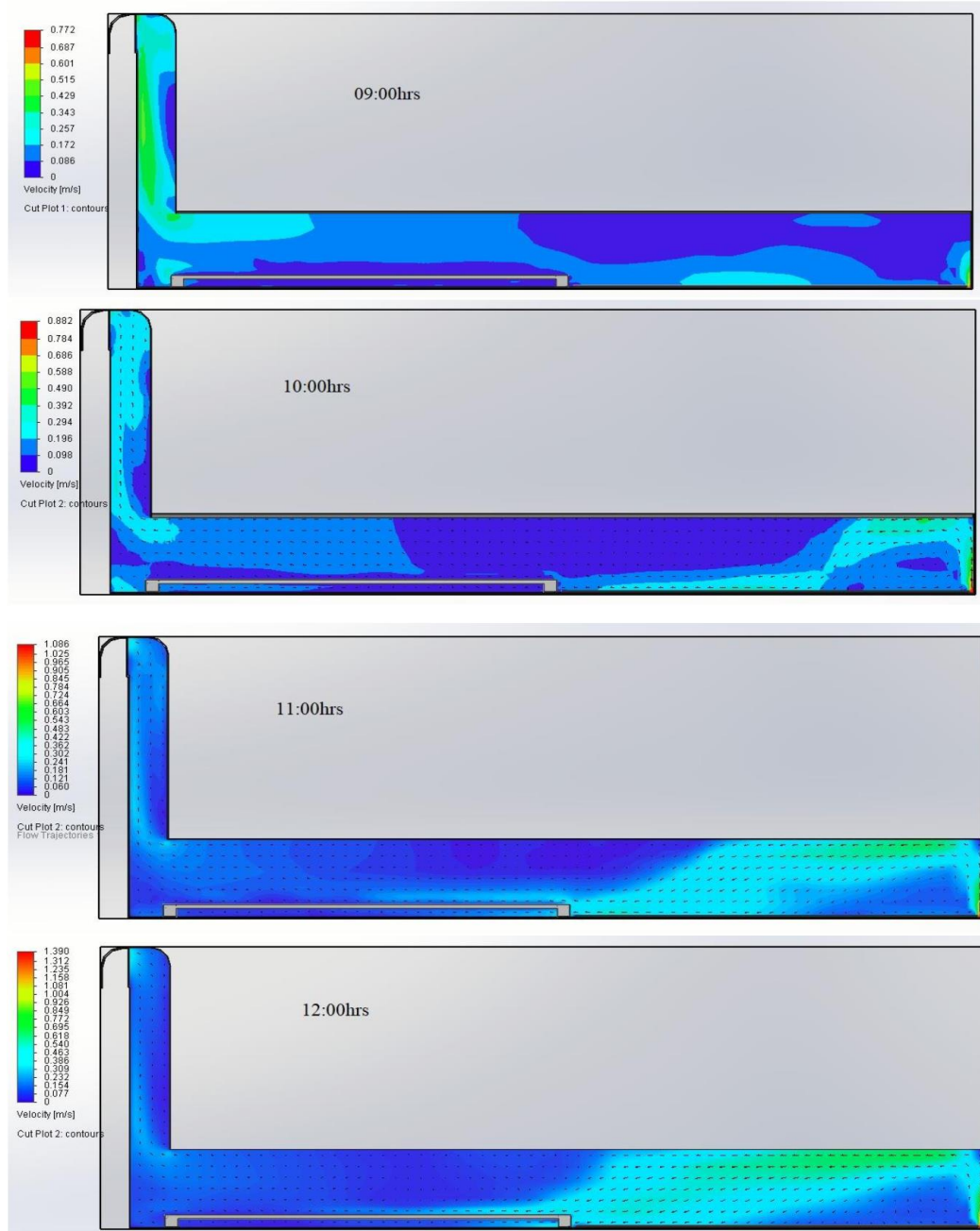


Figure 4-9 Velocity flow trajectories

Figure 4-10 shows velocity cut plots. The hottest air coming out of the collector forms a recirculation region before flowing to the drying unit. It was also observed that some ambient air was flowing into the chimney through the exhaust vent this resulted in decrease in temperature of the air flowing through the chimney. This flow pattern is in agreement with the cross-sectional temperature distribution plotted in Figures 4-6 and 4-7. The contours for the velocity are shown in the Figure 4-10; they make it possible to appreciate the homogeneity of the temperature through the solar dryer. However it was observed that there was a decrease of the velocity in some parts of the dryer. This was due to the loss in the velocity of the flux produced by the solids inside the chamber, which produced a uniform elevation of the heat.

With respect to the velocity, it was observed that the variation on the mesh of the drying unit, favours the velocity near the inlet. Hence, it was appreciated that the first pieces of fruit on the wire mesh, take the majority of the turbulence and backflows. However when it reached the first bananas at a distance of 1.25m from the inlet, its velocity dropped sharply to almost zero on the sides of the drying unit. This may have been due to the static resistance to its flow within the wire mesh and product. As the air left the drying unit, its velocity rose sharply, but did not reach its initial value, stabilizing at about an average of 0.055 m/s in the chimney. This could be attributed to the loss of some of its kinetic energy as it overcame the resistance to its flow through the wire mesh and product. Thus, air

velocity at the point on the wire mesh furthest from the air inlet is less than the point closer. This agrees with the observations by Misha *et al.* (2013) that air velocity decreases as distance from inlet increases.



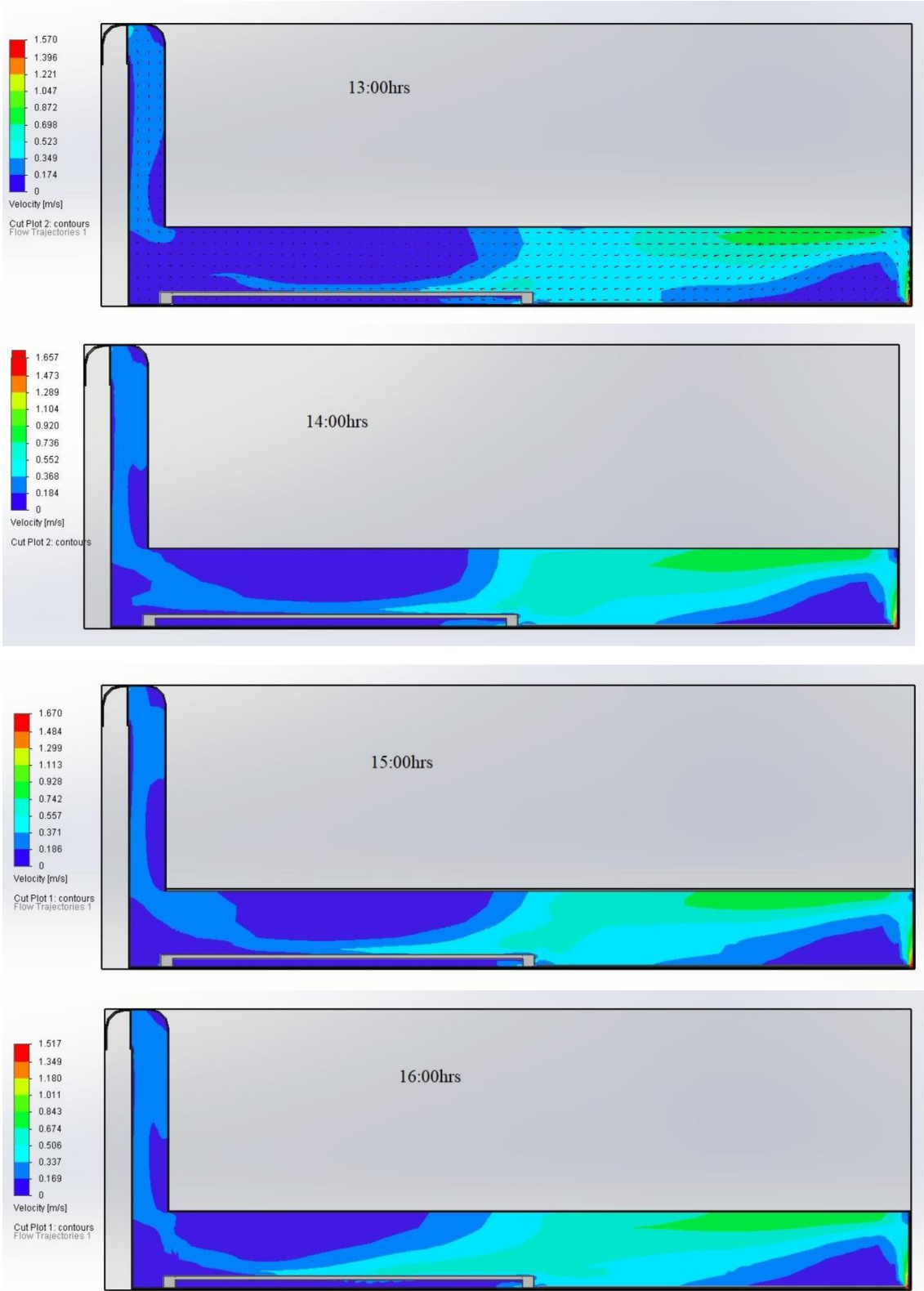
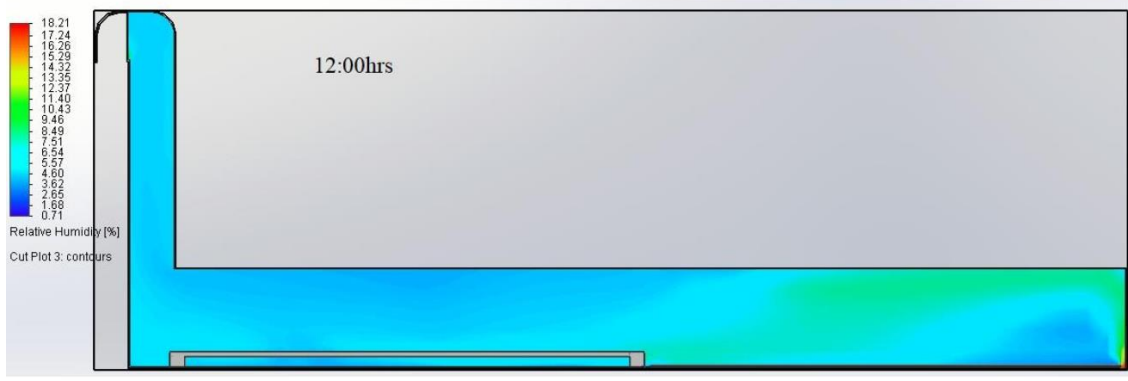
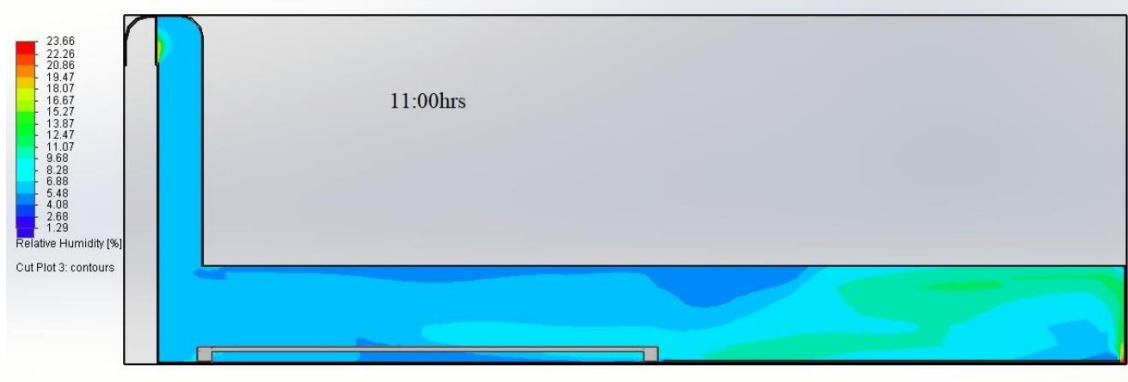
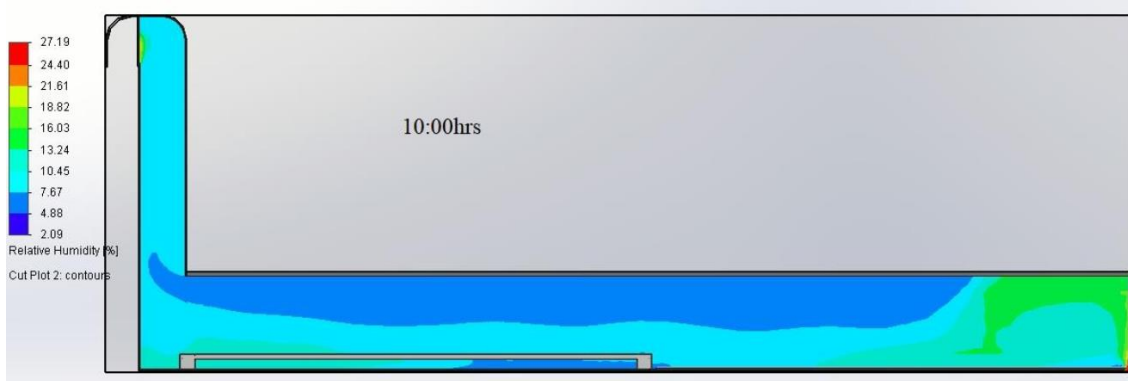
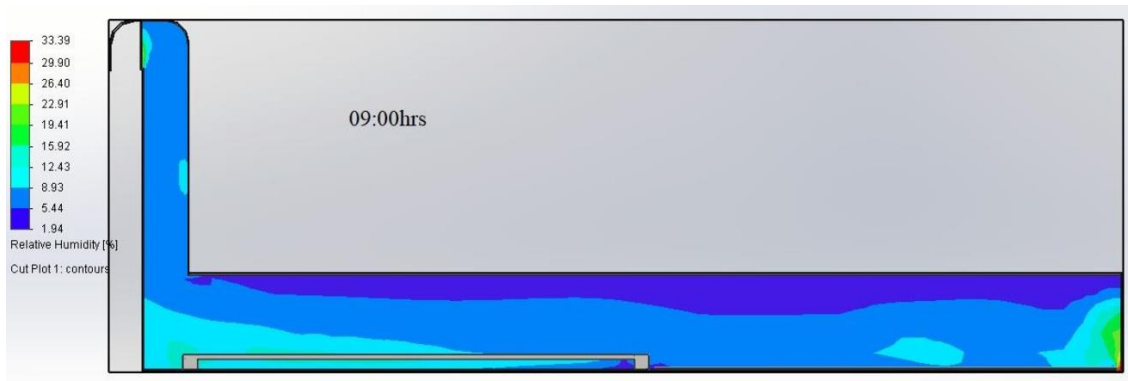


Figure 4-10 Velocity cut plots

4.5.3 Relative humidity

During the experiment relative humidity within the drying tunnel dryer was not controlled. It is therefore likely that the ambient relative humidity, which is what was measured, could have affected the drying rate in the drying unit. The hourly values ambient relative humidity measured from the experiment were used as initial input values of relative humidity of air entering the tunnel dryer. From the Figure 4-11 it can be observed that the relative humidity is dependent on solar insolation. As temperature increased inside the tunnel dryer there was a drop in the relative humidity. From the simulation, the lowest humidity was for the parameter conditions at 12:00 hours which agreed with the experimental results where the lowest humidity was found to be at the same particular time. Ondier, et al., (2010) reported that lower humidity had greater potential to increase drying rates than higher ones. They found that lowering relative humidity at a temperature of 26 °C increased the drying rate compared to doing the same at 30 and 34 °C. It would otherwise have been expected that drying rate should decrease as relative humidity increases.



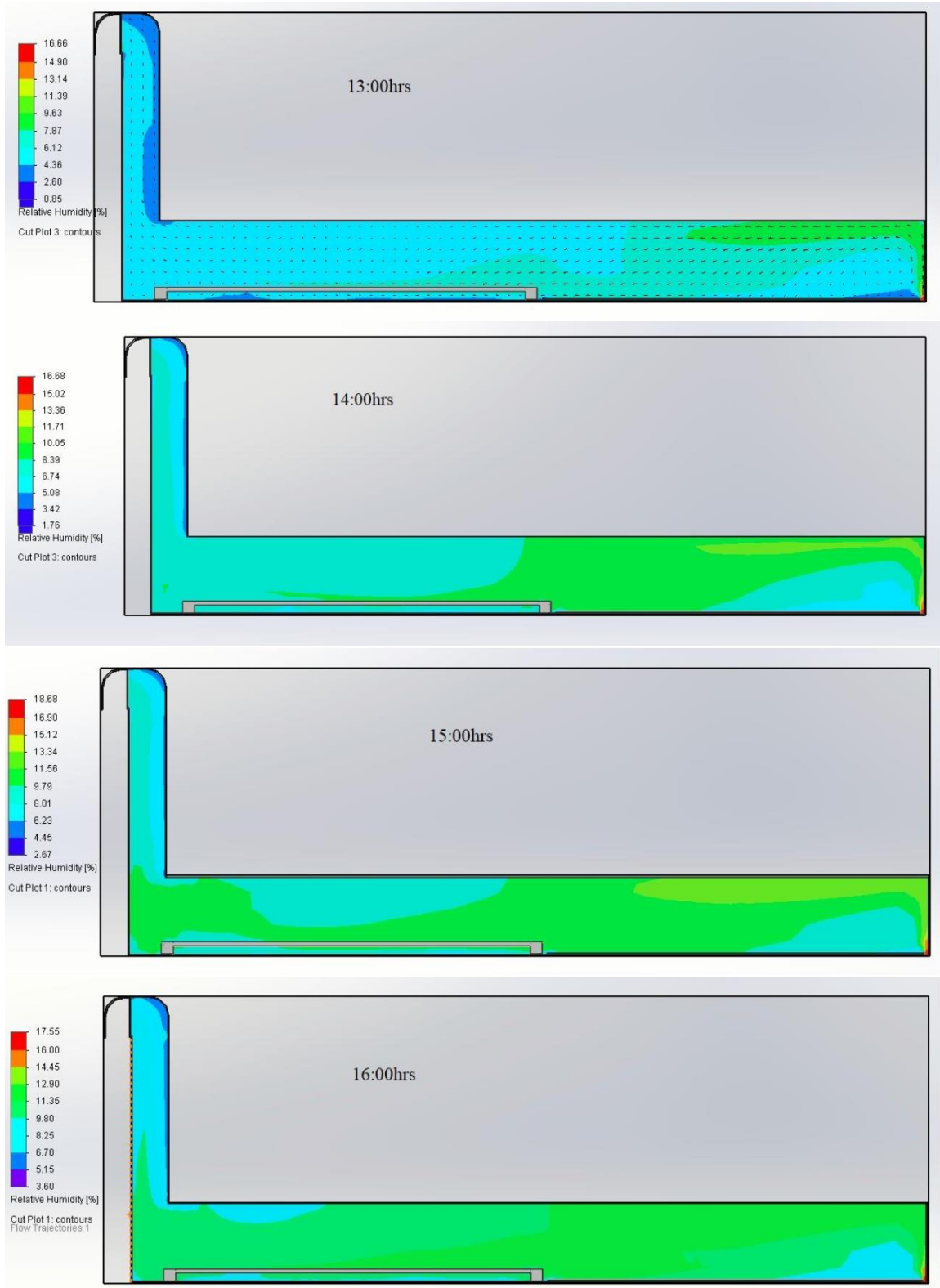


Figure 4-11 Relative Humidity

4.6 Comparison of experimental and simulation results

4.6.1 Drying unit

The comparison of experimental and simulation results in the drying chamber of the solar tunnel dryer are listed in Figure 4-12. The results indicate that the average temperature of drying air is in good agreement for the drying chamber, since the average temperature difference in the drying unit between the experimental and simulation was 5°C. Both the simulated and experimental results show a steady rise in temperature to a maximum of 73.96°C and 70.65°C respectively, followed by a steady decrease. The simulated results were consistently higher than the experimental results because the simulation was set to be adiabatic while the experimental setup had some heat losses through some parts that did not have insulation.

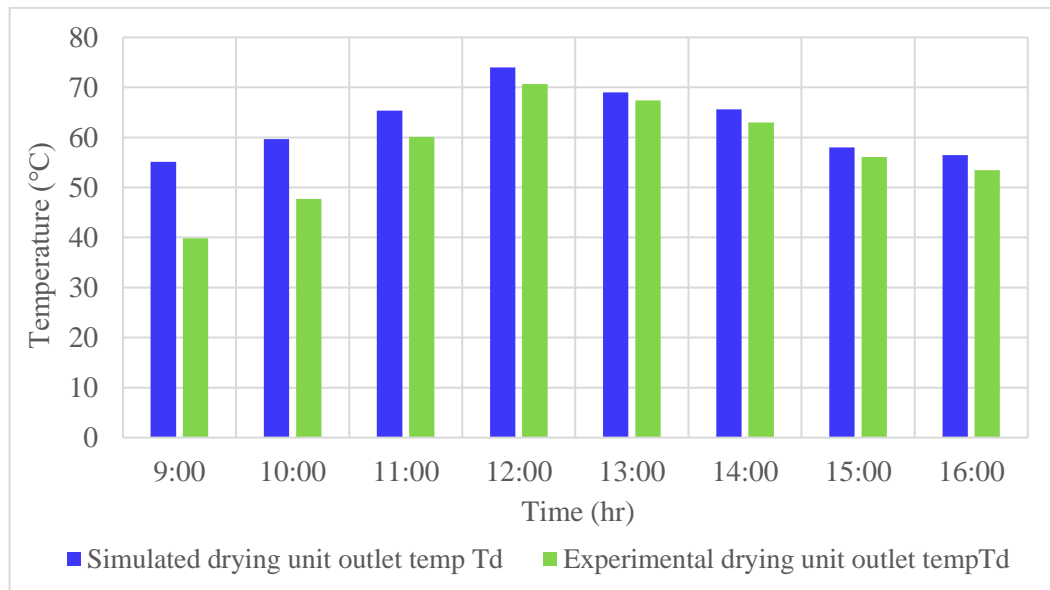


Figure 4-12 Average simulated and experimental temperatures in the drying unit

4.6.2 Collector

The simulated and experimental results of the solar collector outlet air temperatures as a function of global solar radiation that were obtained are shown in Figure 4-13. The simulated and experimental results of the solar collector system showed good agreement. During the experiment, the maximum temperature of the absorber plate was found to be 61.87°C. For the range of high solar radiation, the experimental results showed a lower temperature than that of the simulation which was 66.83°C. This was probably caused by

heat loss, which is affected by many factors of the surroundings, as the real conditions are lower than the predicted values. By contrast, with experiment, the maximum air temperature in the collector was found to be 66.83 °C. Thermal efficiency of the collector from the simulation was found to be 37.63% which was greater than the efficiency of 33.09% obtained from the experiment.

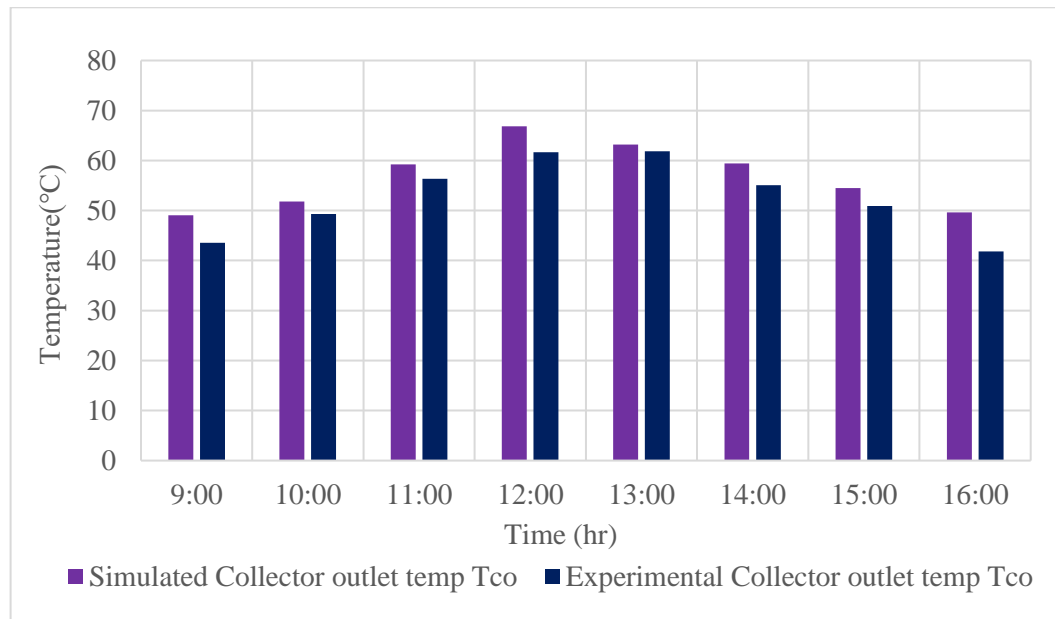


Figure 4-13 Average simulated and experimental temperatures at the collector outlet

4.7 Effects of varying the collector and drying chamber lengths through simulation

4.7.1 The collector length to 1.5m

A study to show the effects of varying the collector and drying chamber lengths on the temperature inside the solar dryer was done. The collector length was increased to 1.5m and 2m (twice the collector length) while maintaining the width of 0.75m then the collector temperature, drying chamber temperature and the relative humidity were obtained as shown in Table 4-1. The relative humidity of the drying air along the length of the dryer decreased rapidly on the solar collector, then increased in the first few meters along the length of the drying unit. The minimum value of relative humidity obtained at the drying unit was 6.4%. Increasing the collector length also increased the collector temperature because the area of solar radiation absorption was also increased. This in turn also increased the drying unit temperature. The maximum collector and drying unit

temperature obtained were 70.1°C and 59°C respectively. Collector efficiency is affected by the intensity of solar irradiance received by the collector and the temperature of the collector plate (Fatimah, et al., 2017). When the absorber plate's increased surface area was employed the thermal efficiency of the collector was found to be 41.2% which was much greater than the efficiency of a flat plate collector from the experiment.

Table 4-1 Increasing the Collector Length to 1.5m

Time [hours]	Solar collector Temp [°C]	Drying unit relative humidity and temperature		Chimney temperature [°C]	Solar Irradiance [W/m ²]
		RH [%]	Temp [°C]		
10:00	50.8	25.6	48.7	31.5	543.62
12:00	70.1	6.4	59	36.6	821.53
14:00	50.1	11.5	45.1	35.5	516.40
16:00	44.9	13.2	40	30.7	239.57

4.7.2 The collector length to 2m

Increasing the collector length from 1.5 to 2m showed a percentage increase of 8.98% in terms of temperature for the highest solar insolation of 821.53W/m². This increase in the collector area revealed a collector efficiency of 43.67%. The temperature and relative humidity showed an inverse proportion because if the collector temperature increased, the tunnel relative humidity decreases which agrees with what Mkhathini, et al., (2018) found. The increase in temperature of the collector led to increase in the drying unit temperature as well. The collector and drying unit temperatures maximum temperatures of obtained were 76.4°C and 64.6°C respectively. The Simulated results are as shown in table 4-2.

Table 4-2 Increasing the collector Length to 2m

Time [hours]	Solar collector Temp [°C]	Drying chamber relative humidity and temp		Chimney temperature [°C]	Solar Irradiance [W/m2]
		RH [%]	Temp [°C]		
10:00	55.6	11	50.2	37.3	543.62
12:00	76.4	4.4	64.6	39.3	821.53
14:00	65.7	7.7	57.7	39.6	516.40
16:00	48.5	10.2	45.2	35.3	239.57

4.7.3 The drying unit length to 2m

The length of the collector was maintained as 1m while increasing the drying unit length at 2m, low temperatures were observed in the drying unit, ranging from 32.4°C to 46.7°C which can lead to low drying rates. There was an observed increment of relative humidity at the drying unit with 26.9% as the maximum relative humidity obtained. The Simulated results are as shown in table 4-3.

Table 4-3 Increasing the drying chamber length to 2m

Time [hours]	Solar collector Temp [°C]	Drying chamber relative humidity and temp		Chimney temperature [°C]	Solar Irradiance [W/m2]
		RH [%]	Temp [°C]		
10:00	40.1	26.9	41.3	37.9	543.62
12:00	44.9	14.1	46.7	40.1	821.53
14:00	41.7	18.7	44.2	38.7	516.40
16:00	38.7	21.9	32.4	32.9	239.57

4.7.4 The Drying Chamber Length to 3m

The increment of the drying chamber from 1.5m to 3m (Table 4-4) showed a reduction in drying chamber temperature. The maximum temperature in the chamber was 38.7°C at 821.53W/m² with a temperature percentage decrease of 17.13% when the chamber was 1.5m. It was observed that the relative humidity was quite high with a maximum of 33.9%. The drying rate decreases as the relative humidity increases in the surrounding environment at a constant temperature and increases at an increasing temperature. The low temperatures could have attributed to the large length.

Table 4-4 Increasing the drying chamber length to 3m

Time [hours]	Solar collector Temp [°C]	Drying chamber relative humidity and temp		Chimney temperature [°C]	Solar Irradiance [W/m ²]
		RH [%]	Temp [°C]		
10:00	41.1	33.9	37.3	34.9	543.62
12:00	44.7	21.1	38.7	35.1	821.53
14:00	42.6	23.7	34.2	32.7	516.40
16:00	38.3	26.9	30.4	31.9	239.57

4.8 Evaluation of the dryer performance

The collector and drying unit efficiencies, the buoyancy pressure head and mean relative deviation were determined as described in the following sections. The equations described in chapter three were used to compute each of these parameters.

4.8.1 Calculation of the collector efficiency

The collector efficiency was calculated using Equation (3-8) as described in chapter. The collector efficiency of 33.09% obtained in this study was similar to collector efficiency of 31.5% reported by Lingayat, et al., (2017) using a natural convection solar dryer for drying banana. Other authors like Cherotich, (2016) reported a collector efficiency of 24.7% while evaluating a natural convection solar tunnel dryer. Schiavone, (2011)

reported a collector efficiency of 29.05% while evaluating a natural convection solar dryer. From these results we concur with what Cherotich, (2016) inferred, that natural convection systems are generally characterised by low efficiencies. The difference between ambient and air heater exit temperatures increased as the drying process continued, suggesting that the solar collector efficiency improved as temperature increased. This is in agreement with results of Aissa, et al., (2014), which showed that collector efficiency was greater at higher temperatures.

4.8.2 Calculation of the drying efficiency

The drying efficiency was calculated using Equation (3-9) described in chapter 3. Brenndorfer, et al., (1987) estimated the typical drying efficiency of natural convection dryers to be in the range of 10 and 15 %. Therefore, the drying efficiency of 13.5 % found in this study was marginally above the typical lower limit. Higher drying efficiency of the solar dryers are usually probably due to the higher mass transfer offered by the product in the initial stage and then it reduces the mass transfer after it is dried to a certain extent, implying that diffusion of moisture from inside the product to the surface of the product becomes difficult.

Moisture removal rate, however, increased with drying air temperature. Rahmatinejad, et al., (2016), showed that drying rate is proportional to drying air temperature. This conclusions were from investigations involving products such as thymus and mint. Drying efficiency decreased with increase in temperature possibly due to the imperfect insulation of the drying tunnel. Drying air temperature also affects the efficiency of the dryer. Matuam, et al., (2015) also reported that dryer efficiency decreases with increase in drying air temperature. This also appears to be confirmed according to results by Aissa, et al., (2014), who reported that dryer efficiency increased with increase in air flow rate, a phenomenon that results in reduced drying air temperature.

4.8.3 Buoyancy pressure head

The chimney is an integral part of the solar tunnel dryer and mounted vertically at end the drying unit. The chimney is a solar air heater. The chimney effect depends on the rise in temperature produced in the chimney. The driving force for air is due to the pressure difference produced by the heating of air. Figure 4-14 illustrates the pressure drop in the

chimney from the mathematical relationship of buoyancy pressure head and air temperature defined in Chapter 3 (Equation 3-17).

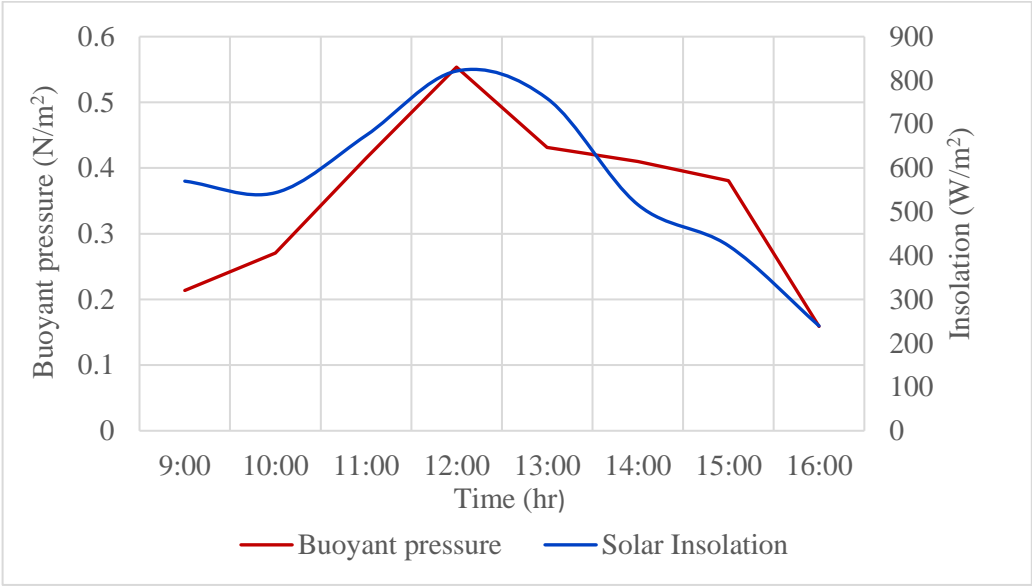


Figure 4-14 Buoyancy pressure head and solar insolation

With an average temperature rise of 15.62°C above ambient in the chimney, the buoyancy pressure head ranged between 0.1589 and 0.5536 N/m² m which was sufficient to drive the air in the tunnel dryer. For flow to take place in the tunnel dryer, the mean temperature inside the chimney has to be relatively higher than the ambient air temperature. In this case, there existed a pressure head which created an upward air flow. Therefore the relation among the buoyancy force that is the pressure drop that creates the air flow, density difference of the ambient air and the height of the chimney can be visualized as seen in figure 4-15 from the simulations.

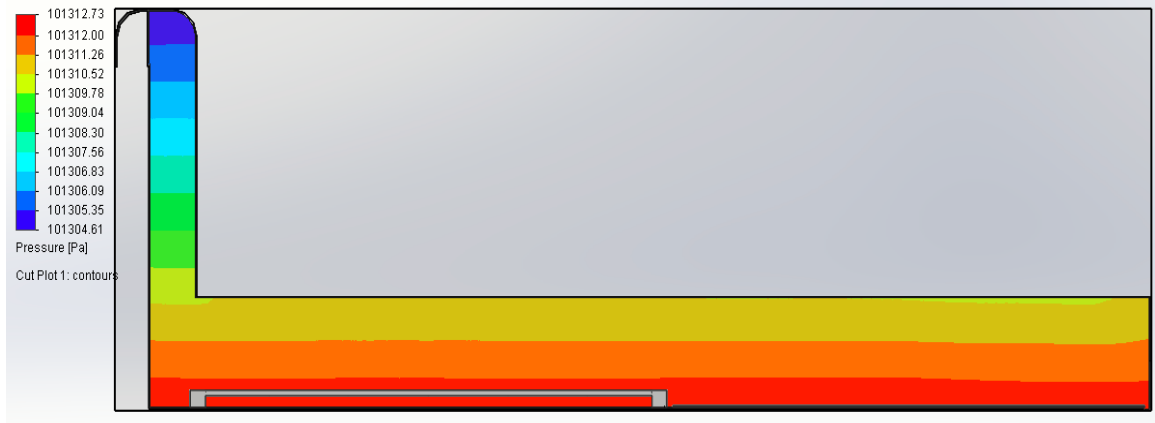


Figure 4-15 Pressure drop in the chimney

4.8.4 Mean relative deviation of collector temperature

A comparative study between our numerical results and experimental collector temperature results showed a good agreement, a mean relative error of 5.1% because maximum discrepancy between numerical and experimental results does not exceed 10%. Other authors such as Tagne, et al., (2020) found an error of 4.53% and which is close to what was found. From the low values of these errors, it can be inferred that the proposed model can predict the temperature profile inside the dryer satisfactorily.

4.9 Thin layer modelling

Eleven thin-layer drying models were used to fit the moisture ratio as a function of drying time (Table 3.2). Table 4-5 presents the results of non-linear regression analysis of fitting the proposed models to experimental data and comparison criteria used to evaluate goodness of fit namely, R^2 , SSE and $RMSE$.

Higher values of R^2 measured how successful the fit was in explaining the variation of the data and it shows the correlation between the experimental values and the model predicted values. The value of R^2 varies between 0 and 1, where a value closer to 1 indicates that a greater proportion of the variance has been accounted for by the model. For SSE and $RMSE$ values close to 0 indicated that the model fit was more useful for prediction. Therefore higher value of R^2 and the lower values of SSE and $RMSE$ indicate better goodness of fit model was selected to best describe the drying behaviour of Banana slices.

The Midilli et al and Page models provided excellent fits to the experimental data with a value of R^2 of **0.9990** and **0.9933** respectively, indicating a good fit. The values of SSE and $RMSE$ obtained from both models were both less than **0.008335** and **0.02753** respectively, which were within the acceptable range and better reflected drying mechanism of banana slices.

The results from the thin layer modelling are shown in Table 4-5. The model constants and the criteria values; R^2 and the lower values of SSE and $RMSE$ are indicated in the table.

Table 4-5 Thin layer model results

Model	Order of Best fit	Model coefficients	R ²	SSE	RSME
Midilli, <i>et al.</i>	1	b = 0.004843 c = 0.9643 k = 0.03435	0.9990	0.001202	0.01156
Page	2	n = 1.039 k = 0.05579 n = 1.708	0.9933	0.008335	0.02753
Two term exponential	3	a = 2.15 k = 0.3195 a = -72.55 b = 72.74	0.9919	0.01005	0.03023
Modified Henderson	4	c = 0.8946 f = 0.2436 g = 0.547 k = 0.5517	0.9870	0.01616	0.04805
Silva <i>et al</i>	5	a = -0.3484 b = 0.3611	0.9843	0.01944	0.04204
Logarithmic	6	a = 1.339 c = -0.09611 k = 0.1971	0.9784	0.02679	0.05176
Henderson	7	a = 1.31 k = 0.245 g = 0.2458	0.9717	0.03509	0.05648
Two term	8	k = 0.2452 u = 0.3117	0.9717	0.03509	0.05924
Wang and Sigh	9	a = -0.1439 b = 0.005285 a = -11.47	0.9635	0.04528	0.06416
Diffusion	10	b = 1.102 k = 0.0656	0.9516	0.05998	0.07745
Verma	11	a = -7.299 g = 0.07323 k = 0.06287	0.9349	0.06003	0.07748

Key: 1. Highest r₂, and lowest SSE and RMSE –Most accurate model

11. Lowest r₂, and highest SSE and RMSE – Least accurate model

To show the goodness of fit by the best model which was the Midilli *et al* model, a plot of experimental MR and Midilli *et al* model predicted MR against drying time was made and is presented in Figure 4-16.

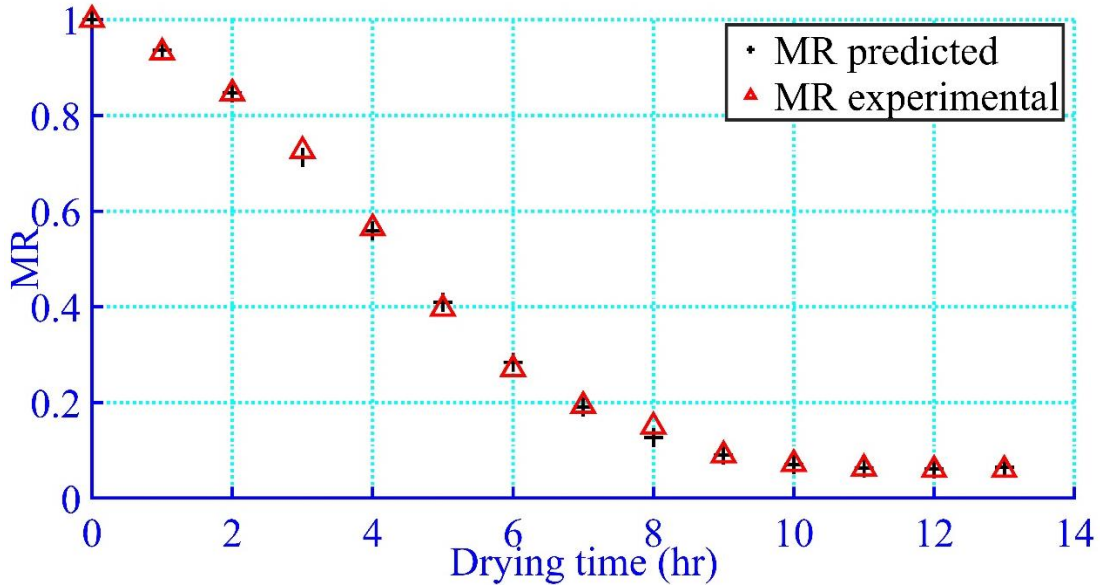


Figure 4-16 Experimental and predicted MR model

It can be observed from figure 4-16 that the results showed smooth and good scatter of the data points showing that the predicted and experimental MR compare well. This implied that the Midilli *et al* model can predict with a high degree of accuracy the MR of banana slices as drying progresses under similar conditions shown earlier in Figures 4-1 and 4-2. Nasri, (2020), results show that the Midilli model was the most appropriate model for banana drying though there was a disparity in the dryers used. Doymaz, (2010) on the other hand found the Page and Logarithmic models were found to satisfactorily describe the thin-layer drying kinetics of banana slices in a hot air dryer. In another research Madamba, *et al.*, (1996), the Page model gave the second best find, nonetheless the models in all cases, gave the value of R^2 which was greater than 0.90 indicating a good fit. The high correlation between the experimental and predicted moistures ratios of the Midilli *et al* model as compared to the other models ascertains the suitability of usefulness for this study.

4.10 Energy and exergy analysis

4.10.1 Energy analysis

The energy analysis of solar drying process of banana was accomplished by using data obtained from the experimentation. Figure 4-17 shows the variation of energy efficiency as a function of drying time. The energy efficiency of the flat plate collector varied from 8.7 to 54.9%. The low energy efficiency values seen in the early stages of drying could be attributed to more energy being used in sensible heating of the collector to bring it to its operating temperature (Simate, 2021). The energy efficiency was observed to be increasing even after the solar insolation started decreasing around 13:00 hours. This implied that the solar collector absorbed most of the incident radiation and stored the energy for raising the collector temperature. The average collector efficiency obtained during the experiment was 33.09 % which was not significantly different from the average collector efficiency of 38.14% reported during Energy and exergy analyses of natural convection solar dryer for banana drying by Lingayat, et al.,(2019). Mugi & Chandramohan, (2020) obtained an average collector efficiency of 61.49% in natural convection mode during the drying of Okra. The efficiency was found to be dependent on the absorbed radiations and collector outlet temperatures.

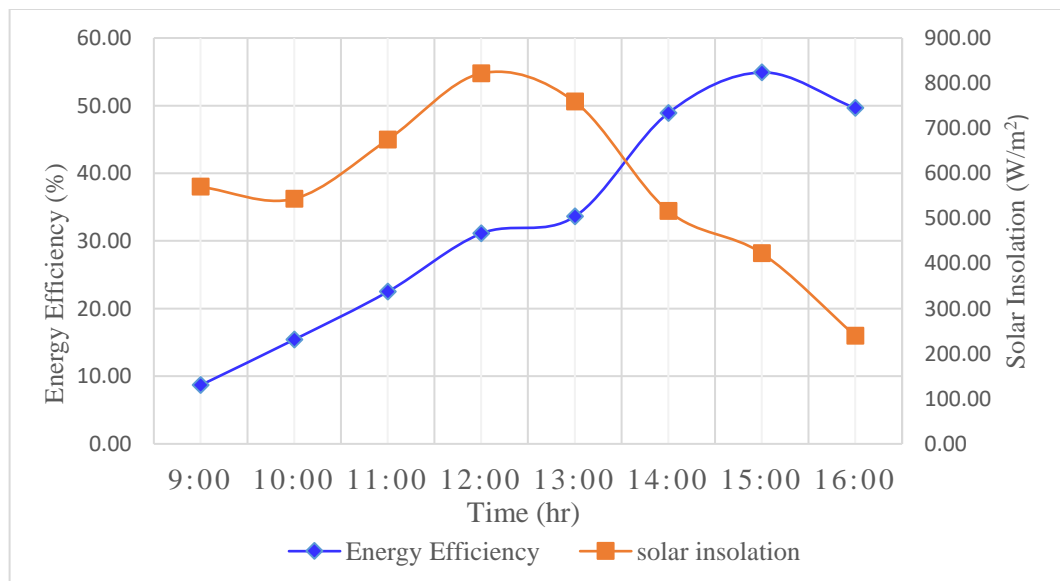


Figure 4-17 Energy efficiency

4.10.2 Collector exergy analysis

Variations in collector exergy input, exergy output and exergy loss with drying time are shown in Figure 4-18. The exergy output patterns followed the exergy input patterns of the collector which solely depends on the solar radiation which varies with the time of the day. The exergy inflow, and exergy loss of the collector varied from 1.28J/s to 6.20J/s. The maximum value of exergy inflow was recorded around 13:00hours. Exergy outflow gradually increases from the morning to midday due to high solar radiation and then started decreasing in the afternoon. Exergy outflow varied from 3.71 J/s to 20.39 J/s. Exergy loss as a function of drying time increased till mid-day and started decreasing in the afternoon. It varied from 2.02J/s to 14.19J/s. The average values of exergy inflow, exergy outflow and exergy loss were 3.39 J/s, 15.57 J/s and 8.18 J/s respectively.

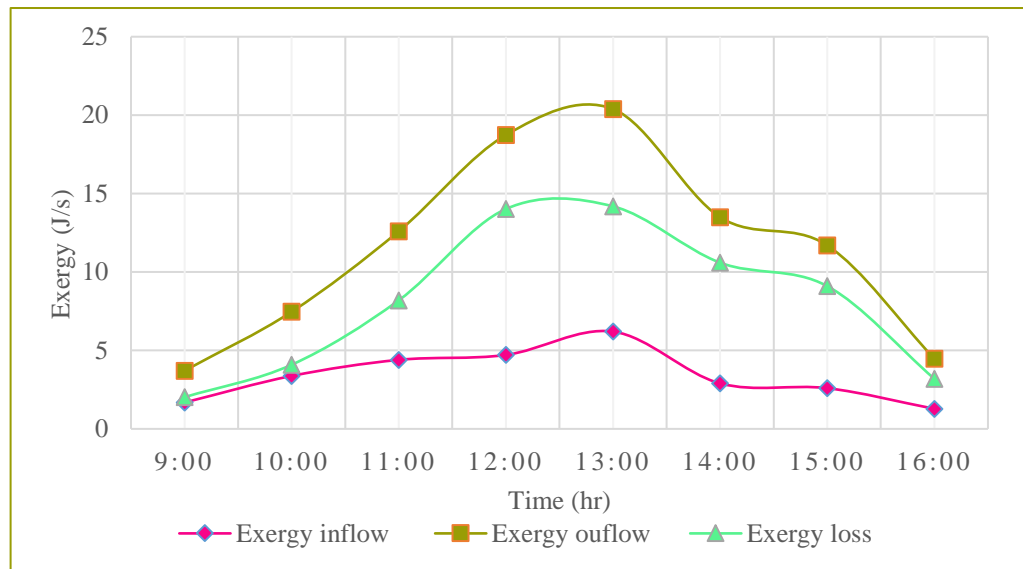


Figure 4-18 Collector exergy input, exergy output and exergy loss

Figure 4-19 shows the collector exergy efficiency plotted against drying time. The collector exergy efficiency varied between 0.48% and 2.89% with an average collector exergy efficiency of 1.91 % which was lower than the energy efficiencies. Simate, (2021) reported the collector exergy efficiencies of 2.4% and 2.6% for the 10 kg and 5 kg loads, respectively in an Indirect-Mode Natural Convection Solar Dryer for Maize. Mugi & Chandramohan, (2020) reported average collector exergy efficiencies of 2.44% in natural

convection indirect solar dryer and 2.03% in a forced convection indirect solar dryer respectively.

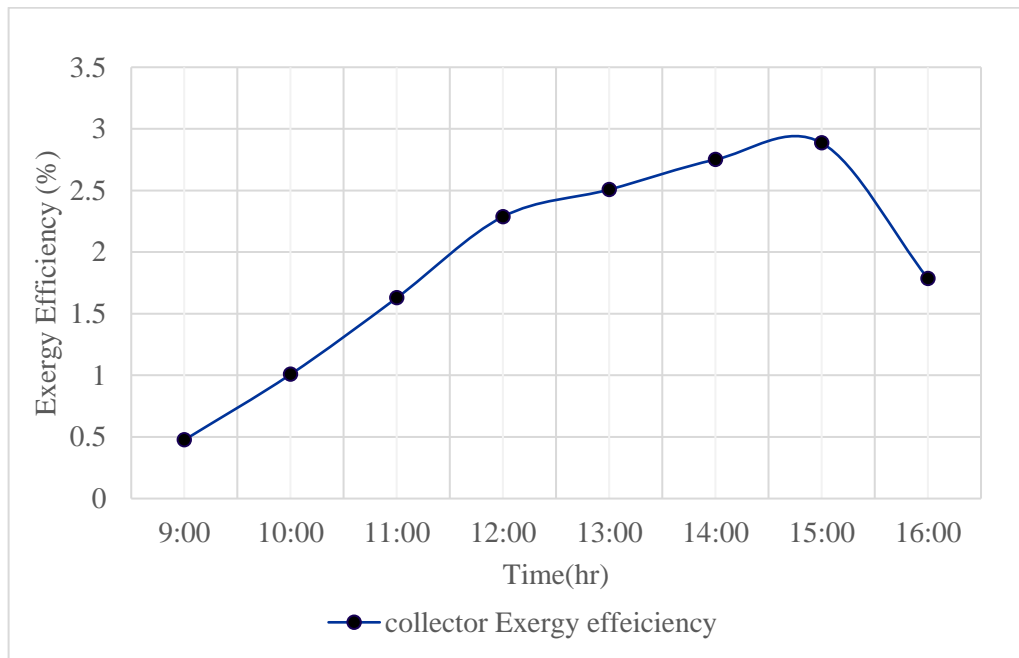


Figure 4-19 Collector efficiency

4.10.3 Drying chamber exergy analysis

The variations in drying chamber exergy inflow, exergy loss and exergy outflow from the dryer with drying time are shown in Figure 4-20. It is observed that exergy outflow and exergy loss in the drying chamber increased during the first 5 hours (until 13.00 hours), and after that, it decreases. These changes are dependent on solar insolation. The average values of the exergy inflow and exergy outflow were 11.57 J/kg and 5.23 J/kg respectively. Exergy inflow and outflow varied from 3.71 to 20.39 J/kg and 2.51 to 30.23 J/kg, respectively. Exergy losses in the drying chamber varied between 0.19 J/kg to 11.50 J/kg with an average loss of 5.01 J/kg.

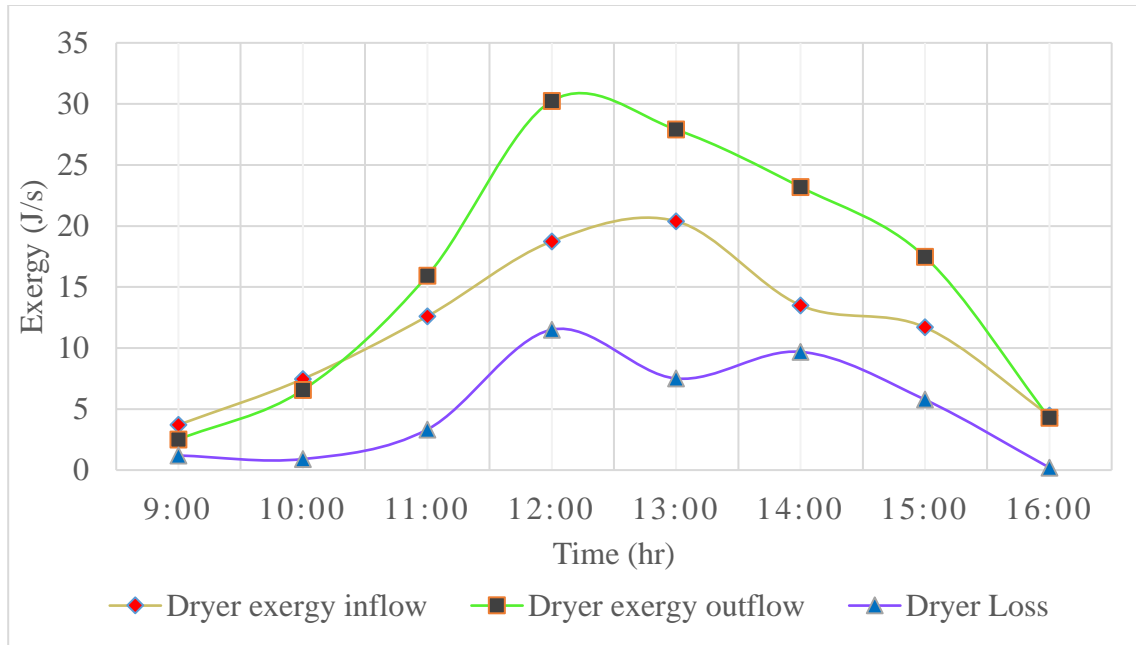


Figure 4-20 Drying chamber exergy inflow, exergy loss and exergy outflow

The drying chamber exergy efficiency varied from 28.21% to 95.60% with an average of 63.20%. Karthikeyan & Murugavelh, (2018) reported that exergetic efficiency varied between 23.25 and 73.31% with a mean value of 49.12% in a mixed mode forced convection solar tunnel in drying turmeric. Rabha, et al., (2017) dried ghost chilli and found the exergy efficiency of the drying chamber to be in the range of 21% to 98% with an average of 63% while for ginger it was 4% to 96% with an average of 47%. Murugavelh, et al., (2019) using a forced convection mixed mode dryer in drying tomato waste and reported that exergetic efficiency of the dryer varied from 38.53% to 67.58% with an average of 52.21%. Exergy efficiency of the dryer decreased with an increase in the drying temperature. Other researchers reported that exergy efficiency decreases with increasing drying air temperature (Midilli, et al., 2002; Ahern, 1980; Murugavelh, et al., 2019).

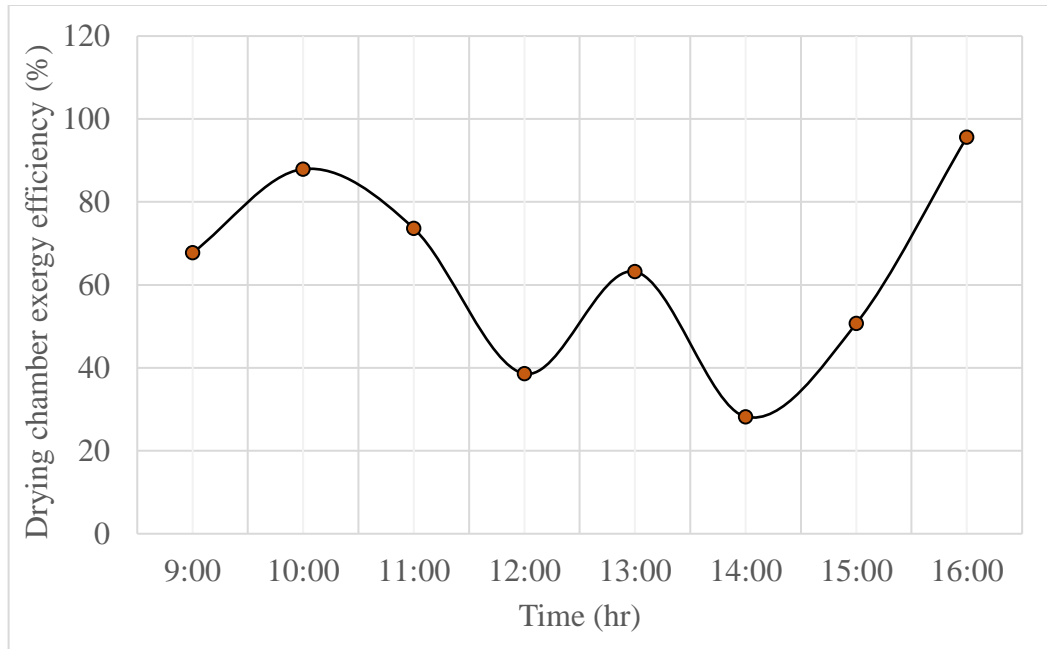


Figure 4-21 Drying chamber exergy efficiency

4.11 Closing remarks

The results and discussions of the study were covered in this chapter. Relevant literature to back up the findings of the study have been provided as much possible. In general, the specific objectives were met as the banana slices were dried and CFD simulations done, also evaluation based on the parameters that were defined in the study.

CHAPTER FIVE: CONCLUSIONS AND RECOMMENDATIONS

5. Introduction

This chapter presents the conclusions and recommendations drawn from the study. The conclusions have been presented to reflect the achievement of each specific objective and for clarity purposes.

5.1 Conclusions

- **To perform simulations for the evaluation of temperature and airflow distribution in the natural convection solar tunnel dryer**
 - Simulations were performed in a designed mixed mode natural convection solar tunnel dryer using Solidworks2016 flow simulation. The mean drying air temperatures at collector and drying unit obtained were 60.2°C and 56.71°C respectively. A comparative study between the numerical and experimental results shows a good agreement with a mean relative error of 5.1%. It was observed from the simulations that the increase in the collector length from 1.5 to 2m showed a percentage increase of 8.98% in the collector temperature also a rise on the drying unit.
- **To evaluate the collector efficiency, drying efficiency and buoyancy pressure by the chimney**
 - The performance evaluation parameters for the solar tunnel dryer, the collector and drying efficiencies were calculated and found to be 33.09% and 13.5% respectively. With an average temperature rise of 15.62°C above ambient in the chimney the buoyancy pressure head ranged between 0.1589 and 0.5536 N/m² as the chimney air was heated to higher values above ambient to cause enough buoyancy pressure for air flow, which was sufficient to drive the air in the tunnel dryer.
- **To determine an appropriate mathematical thin layer model to predict the drying characteristic of the banana slices and validate it against experimental results**
 - After analysis, the system dried 0.943kg of banana slices per square meter with an average mass flow rate of around 0.011kg/s. Bananas were dried from an

average moisture content of 73.89% to 4.39% on a wet basis in 13 hours as temperature reached as high as 70°C in the drying unit.

- Thin layer mathematical models were established to help predict the drying of banana slices and validated against experimental results. Midilli et al and Page models provided excellent fits to the experimental data with a value of R^2 of **0.9990** and **0.9933** respectively. The values of *SSE* and *RMSE* obtained from both models were both less than **0.008335** and **0.02753** respectively.
- **To carryout Energy and Exergy studies of the solar dryer.**
 - From the energy and exergy analysis the average collector efficiency during the experiment was 33.09%. The average collector exergy and drying chamber exergy efficiencies were 1.91% and 63.20% respectively.
 - In view of this, the findings of this study conclusively confirm that the natural convection solar tunnel dryer is well suited for drying of banana slices and CFD is an efficient tool that can be used in the drying process.

5.2 Recommendations

The following are recommended for further study

1. The solar collector can also be modified to evaluate more effective designs. For instance, fins can be incorporated to absorb additional heat or different material compositions can be explored to achieve improved solar collection.
2. In view of the fact that this dryer may be used to dry other product other than banana slices i.e. pineapple, tomato etc experimentation of the dryer using these products is imperative in order to find the drying time to equilibrium.
3. Another potential study area in this constructed dryer is comparison of the dryer performance for different slice thicknesses of the same product.
4. Another area of study can be cost based optimization of the dryer.

5.3 Closing remarks

This chapter provides the conclusions and the recommendations from the study. The recommendations section has attempted to point out some gaps that need to be investigated by subsequent researches.

REFERENCES

- Abano, E. & Sam-Amoah, L., 2011. Effects of different pretreatments on drying characteristics of banana slices. *ARN Journal of Engineering and Applied Sciences*, 6(3), pp. 121-129.
- Abdel-Galil, H. S., 2007. 'Solar System With Energy Storage for Drying Poultry Manure'. *Misr J. Ag. Eng*, 24(4), p. pp. 978–1002.
- Abdulmajid, A., 2015. An alternative to Open-Sun Drying of Silver Cyprinid (*Rastrineobola argentea*) Fish Under Varying Climatic Condition in Kenya. *International Scholars Journals*, 3(3), p. pp. 298–312.
- Agarry, S., Ajani, A. & Aremu,, M., 2013. Thin Layer Drying Kinetics of Pineapple : Effect of Blanching Temperature-Time Combination. *igerian Journal of Basic and Applied Science*, 21(1), p. pp. 1–10..
- Ahern, J., 1980. *The exergy method of energy system analysis..* New York, USA: John Wiley.
- Aissa, W., El-Sallak, M. & Elhakem, A., 2014. Performance of Solar dryer Chamber used for Convective Drying of Sponge-cotton. *Thermal Science*, 18(2), pp. 45 - 462.
- Akpinar,, E. K., 2006. Determination of suitable thin layer drying curve model for some vegetables and fruits. *Journal of food engineering*, Issue 73, pp. 75-84.
- Al-Neama, M. A. & Farkas, I., 2016. Influencing of Solar drying performance by chimney. *Hungarian Agricultural Engineering*, Volume DOI:10.17676/HAE.2016.30.11, pp. 11- 16.
- Ambesange, A. & Kusekar, S., 2017. Analysis of Flow Through Solar Dryer Duct Using CFD. *International Journal of Engineering Development and Research*, 5(1).
- Angula, J. P. & Inambao, F., 2019. Computational Fluid Dynamics in Solar Drying. *International Journal of Mechanical Engineering and Technology*, 10(11), pp. pp. 259-274.

- ANSYS,, 2012. *ANSYS FLUENT Manual. ANSYS FLUENT Adjoint Solver*. s.l.:ANSYS, Inc.
- AOAC, 2005. Official method of Analysis. *18th Edition, Association of Officiating Analytical Chemists, Washington DC, Method 935.14 and 992.24*. .
- Aregbesola, O., Ogunsina, B., Sofolahan, A. & Chime, N., 2015. Mathematical modeling of thin layer drying characteristics of dika (*Irvingia gabonensis*) nuts and kernels. *Nigerian Food Journal*, p. <http://dx.doi.org/10.1016/j.nifoj.2015.04.012>.
- Bala, B. & Wood, J., 1995. Optimization of natural convection solar drying systems. *Energy*, 20(4), pp. 285-294.
- Bayrak, M., Midilli, A. & Nurveren, K., 2003. Energy and exergy analyses of sugar production stages. *International Journal of Energy Research*, 27(11), pp. 989-1001.
- Belessiotis, V. & Delyannis, E., 2011. Solar drying. *Solar Energy*, 85(8), p. 1665–1691.
- Bolaji , O. & Olalusi, A., 2008. Performance Evaluation of a Mixed-Mode Solar Dryer. *AU Journal of Technology*, pp. 225-231.
- Bolaji, B., 2005. Development and performance evaluation of box-type absorber solar air collector for crop drying. *Journal of Food Technology*, 3(4), p. 515–600.
- Borges, S. V., Mancini, M. C., Corrêa, J. L. G. & Leite, J., 2010. Secagem de bananas prata e d'água por convecç~ ao forçada. *Ciência e Tecnologia de Alimentos*, 30(3), p. 605–612 <https://doi.org/10.1590/S010120612010000300006>.
- Bowrey, R., Buckle, K. A., Hamey, I. & Pavenayotin, P., 1980. Use of solar energy for banana drying. *Food Technology in Australia*, 32(6), pp. 290-291.
- Brenndorfer, B., Kennedy, L. & Mrema, G., 1987. *Solar dryers: their role in posharvest processing*. s.l., Commonwealth Secretariat.
- Chavan, A., Vitankar, V., Mujumdar, A. & Thorat, B., 2020. Natural convection and direct type (NCDT) solar dryers: a review. *Drying Technology*, Issue DOI:10.1080/07373937.2020.1753065.

Chavan, B., Yakupitiyage, A. & Kumar, S., 2008. Mathematical Modeling of Drying Characteristics of Indian Mackerel (*Rastrilliger kangurta*) in Solar-Biomass Hybrid Cabinet Dryer. *Drying Technology*, Volume 26, pp. 1552-1562. DOI:10.1080/07373930802466872.

Cherotich, S., 2016. Experimental investigation and mathematical modelling of a natural convection solar tunnel fruit dryer. *Master of Engineering dissertation*.

Chowdhury, M., Bala, B. & Haque, M., 2011. Energy and exergy analysis of the solar drying of jackfruit leather. *Biosystems Engineering* 110, pp. 222 -229 doi:10.1016/j.biosystemseng.2011.08.011.

Coleman, N., 2010. A Derivation of the Navier-Stokes Equations. *B.S. Undergraduate Mathematics Exchange*, 7(1).

Dandamrongrak, R., Young, G. & Mason, R., 2002. Evaluation of various pre-treatments for the dehydration of banana and selection of suitable drying models. *J. Food Eng*, Issue 55, pp. 139-146.

Daud, L. E. I. & Simate, I. N., 2017. Drying Kinetics of Sliced Pineapples in a Solar Conduction Dryer. *Energy and Environment Research*, 7(2), pp. 14-26.

Dhanushkodi, S., Wilson, V. H. & Sudhakar, K., 2014. Thermal Performance Evaluation of Indirect Forced Cabinet Solar Dryer for Cashew Drying. *American-Eurasian Journal Agriculture & Environmental Science*, 14(11), p. 1248–1254.

Diamante, L. M., Ihns, R., Savage, G. P. & Vanhanen, L., 2010. A new mathematical model for thin layer drying of fruits. *Int. J. Food Sci. Technol*, Volume 45, pp. 1956-1962.

Dincer, I., 2011. Exergy as a potential tool for sustainable drying systems. *Sustainable Cities and Society*, 1(2), p. 91–96.

Dincer, I. & Sahin, A., 2004. A new model for thermodynamic analysis of a drying process. *International Journal of Heat and Mass Transfer*, 47(4), p. 645–52.

- Doymaz, İ., 2010. Evaluation of Mathematical Models for Prediction of Thin-Layer Drying of Banana Slices. *International Journal of Food Properties*, 13(3), pp. 486-497, DOI:10.1080/10942910802650424.
- Ekechukwua, O. & Norton, B., 1999. Review of solar-energy drying systems II: an overview of solar drying technology. *Energy Conversion & Management*, Volume 40, pp. 615-655.
- Ekechukwu, O. & Norton, B., 1997. Design and measured performance of a solar chimney for natural-circulation solar-energy dryers. *Renewable energy*, Volume 10, pp. 81-90.
- El-Sebaili, A. & Shalaby, S., 2012. Solar drying of agricultural products: A review. *Renewable and Sustainable Energy Reviews*, Issue 16, p. 37– 43.
- Erek, A. & Dincer, I., 2009. A new approach to energy and exergy analyses of latent heat storage unit. *Heat Transfer Engineering*, 30(6), p. 506–515.
- Fatimah, B. et al., 2017. *Effect of openings collectors and solar irradiance on the thermal efficiency of flat plate finned collector for indirect-type passive solar dryer*. Indonesia, American Institute of Physics <https://doi.org/10.1063/1.4985528>.
- Fudholi, A. et al., 2010. Review of solar dryers for agricultural and marine products. *Renewable and Sustainable Energy Reviews*, Volume 14, pp. 1-30.
- Fuller, F., 1995. A comparison between solar tunnel dryers and conventional fuel dehydrators for on-farm drying. *Drying Technology*, Volume 13, pp. 1489-1502.
- Ganesapillai, M., Regupathi, I. & Murugesan, T., 2011. Modelling of thin layer drying of banana (Nendran spp.) under microwave, convective and combined microwave-convective processes. *Chem. Prod. Proc. Modell*, Volume 6, pp. 1-10.
- Gatea, A. A., 2011. Design and construction of a solar drying system, a cylindrical section, and an analysis of the performance of the thermal drying system. *African Journal of Agricultural Research*, Volume 6, pp. 343-351.

- Gupta, M., Sehgal, V. & Arora, S., 2011. Optimization of drying process parameters for cauliflower drying. *Journal of Food Science and Technology*, Volume 6, pp. 62-69.
- Haseli, Y., Dincer, I. & Naterer, G. F., 2010. Exergy efficiency of two-phase flow in a shell and tube condenser. *Heat Transfer Engineering*, 31(1), p. 17–24.
- Hedge, V. N., Hosur, V., Rathod, S. & Harsoor, P., 2015. Design , Fabrication and Performance Evaluation of Solar Dryer for Banana. *Energy, Sustainability and Society*, 5(23), p. pp. 1–12.
- Hosain, M. L. & Fdhila, R. B., 2015. Literature Review of accelerated CFD Simulation Methods. *Energy Procedia* 75, p. 3307 – 3314.
- Hossain, M. & Bala, B., 2007. Drying of hot chilli using solar tunnel drier. *Solar Energy*, Volume 81, p. 85–92.
- Hughes, B. R. & Oates, M., 2011. Performance investigation of a passive solar-assisted kiln in the United Kingdom. *Solar Energy*, Volume 85, pp. 1488-1498.
- Huselstein, S., 2016. *Development of a System Model for an Indirect Passive Solar Dryer with Experimental Validation*, s.l.: Thesis. Rochester Institute of Technology.
- Ingle, P. W., Pawar, A. A., Deshmukh, B. D. & Bhosale, K. C., 2013. CFD Analysis of Solar Flat Plate Collector. *International Journal of Emerging Technology and Advanced Engineering*, 3(4).
- Jain, A. et al., 2018. Computational fluid dynamics simulation and energy analysis of domestic direct-type multi-shelf solar dryer. *Journal of Thermal Analysis and Calorimetry*, 136(1), pp. 173-184.
- Jain, D. & Tiwari, G. N., 2003. Thermal aspects of open sun drying of various crops. *Energy* , Volume 28, p. pp. 37–54.
- Kachru,, R., Kotwaliwale, N. & Balasubramanian, D., 1995. Physical and Mechanical Properties of Green Banana (Muss paradisiaca) Fruit. *Journal of Food Engineering*, Volume 26, pp. 369.-378.

- Kamlesh, J. & Nimesh, C., 2016. Drying Characteristics of Banana Powder. *Indian Journal of Science*, Volume 23, pp. 75-88.
- Kant, K. et al., 2016. Thermal Energy storage based solar drying systems: A review. *Innovative Food Science and Emerging Technologies*, Issue doi: 10.1016/j.ifset.2016.01.007.
- Karthikeyan, A. & Murugavelh, S., 2018. Thin layer drying kinetics and exergy analysis of turmeric (*Curcuma longa*) in a mixed mode forced convection solar tunnel dryer. *Renewable Energy*, Volume 128, pp. 305-312.
- Kaushal, P. & Sharma, H., 2012. Concept of Computational Fluid Dynamics (CFD) and its Applications in Food Processing Equipment Design. *J Food Process Technol*, 3(138).
- Kayne, Alexander, 2012. Computational Fluid Dynamics (CFD) Modeling of Mixed Convection Flows in Building Enclosures. *All Theses and Dissertations (ETDs)*. 740.
- Kelley, T. R., 2010. Optimization, an important stage of engineering design. *The Technology Teacher*, 69(5), pp. 18-23.
- Khoozani, A. A., Birch, J. & Bekhit, A. E.-D. A., 2019. Production, application and health effects of banana pulp and peel flour in the food industry. *Journal of Food Science and Technology*, 56(2 <https://doi.org/10.1007/s13197-018-03562-z>), p. 548–559.
- Krokida, , M. K. & Maroulis, Z. B., 1999. Effect of microwave drying on some quality properties of dehydrated products. *Drying Technology*, 17(3), pp. 449-466.
- Kumar, A. et al., 2019. Experimental Investigation on Performance of Solar Air Heaters With Thermal Storage. *International Journal of Renewable Energy and Its Commercialization*, 5(1), p. 37–46.
- Lahsani, S. et al., 2004. Thin layer convective solar drying and mathematical modeling of prickly pear peel (*Opuntia ficus indica*). *Energy*, Issue 29, pp. 211-224.
- Leon, M., Kumar, S. & Bhattacharya, S., 2002. A comprehensive procedure for performance evaluation of solar food dryers. *Renewable and Sustainable Energy Reviews*, Volume 6, pp. 367-393.

- Leon, M., Kumar, S. & Bhattacharya, S., 2002. A comprehensive procedure for performance evaluation of solar food dryers. *Renewable and Sustainable Energy Reviews*, Volume 6, pp. 367-393.
- Lingayat, A., Chandramohan, V. & Raju, V., 2017. Design, Development and Performance of Indirect Type Solar Dryer for Banana Drying. *Energy Procedia*, Volume 109, p. 409 – 416.
- Lingayat, A., Chandramohan, V. & Raju, V., 2019. Energy and Exergy Analysis on Drying of Banana Using Indirect Type Natural Convection Solar Dryer. *Heat Transfer Engineering*, pp. 1-12.
- Lockhart, S. & Johnson, C., 1996. *Engineering design communication*. Reading, MA: Addison-Wesley.
- Macedo, L. L. et al., 2020. Effect of drying air temperature on drying kinetics and physicochemical characteristics of dried banana. *Journal of Food Processing Engineering*, Issue e13451. <https://doi.org/10.1111/jfpe.13451>.
- Madamba, P., Driscoll, R. & Buckle, K., 1996. The thin-layer drying characteristics of garlic slices. *Journal of food engineering*, Volume 29, pp. 75-97.
- Madhlopa, A., Jones, S. & Saka, J., 2002. A solar air heater with composite-absorber systems for food dehydration. *Renewable Energy*, Volume 27, p. 27–37.
- Maia, C. B. et al., 2012. Simulation of the Airflow Inside a Hybrid Dryer. *IJRRAS*, 10(3).
- Mathioulakis, E., Karathanos, V. & Belessiotis, V., 1998. Simulation of air movement in a dryer by computational fluid dynamics: application for the drying of fruits.. *Journal of Food Engineering*, 36(2), p. 183–200.
- Matuam, B., Edoun, M., Kuitche, A. & Zeghmami, B., 2015. Experimental Evaluation of the Thermal Performance of Dryer Airflow Configuration. *International Journal of Energy Engineering*, 5(4), pp. 80-86. doi: 10.5923/j.ijee.20150504.03.

- Michael, E. R., 2014. *Unit 03: Glazing - Greenhouse Management Online*. [Online] Available at: https://greenhouse.hosted.uark.edu/Unit03/Printer_Friendly.html [Accessed 23 May 2022].
- Midilli, A., Kucuk, H. & Yapar, Z., 2002. A new model for single layer drying. *Dry. Technol*, Volume 20, pp. 1503-1513.
- Minka, C., 1986. *Potential improvement to traditional solar crop drying in Cameroon: research and development solar drying in Africa*. Proceedings of a Workshop held in Dakar, s.n., p. 11–22.
- Mkhathini, K. & Zulu, S., 2015. *Postharvest food drying technique using a solar tunnel dryer*, s.l.: Kwazulu-Natal Department of Agriculture & Rural Development Crop Production, Horticulture, Cedara.
- Mkhathini, K., Magwaza, L., Workneh, T. & Mwithiga, G., 2018. Effects of relative humidity and temperature on small scale peach fruit drying using a tunnel solar dryer: a case study of peach fruit produced by small scale farmers in the midlands of KwaZulu-Natal, South Africa. *S. Afr. J. Agric. Ext*, 46(2), pp. 1-13.
- Mowlah, G., Takano, K., Kamoi, I. & Obara, T., 1983. Water transport mechanism and some aspects of quality changes during air dehydration of bananas. *Lebensmittel Wissenschaft-und-Technologie*, Volume 16, pp. 103-107.
- Mugi, V. & Chandramohan, V., 2020. Energy end exergy analysis of forced and natural convection indirect solar dryers: Estimation of exergy inflow, outflow, losses, exergy efficiencies and sustainability indicators from drying experiments. *Journal of Cleaner Production*.
- Mundada, M., Hathan, B. S. & Maske, S., 2011. Mass transfer kinetics during osmotic dehydration of pomegranate arils. *J. Food Sci*, Volume 76, pp. 31-39.
- Murugavelh, S. et al., 2019. Exergy analysis and kinetic study of tomato waste drying in a mixed mode solar tunnel dryer. *Energy Sources, Part A: Recovery, Utilization, and Environmental Effects*, Volume <https://doi.org/10.1080/15567036.2019.1679289>.

- Murugavelh, S. et al., 2019. Exergy analysis and kinetic study of tomato waste drying in a mixed mode solar tunnel dryer. *Energy Sources, Part A: Recovery, Utilization, and Environmental Effects*, pp. 1-17 DOI:10.1080/15567036.2019.1679289.
- Mustayen, A. G. M. B., Mekhilef, S. & Saidur, R., 2014. Performance Study of Different Solar Dryers : A Review. *Renewable and Sustainable Energy Reviews*, Volume 34, p. 463–470.
- Nakasone, Y., Yoshimoto, S. & Stolarski, T., 2006. Chapter 2 - Overview of ANSYS Structure and Visual Capabilities. In: S. Y. T. S. Y. Nakasone, ed. *Engineering Analysis with ANSYS Software*. s.l.:Butterworth-Heinemann, pp. 37-50 <https://doi.org/10.1016/B978-075066875-0/50032-6>.
- NASA, 2022. *Overview | Sun – NASA Solar System Exploration*. [Online] Available at: <https://solarsystem.nasa.gov/solar-system/sun/overview/> [Accessed 17 May 2022].
- Nasri, F., 2020. Solar thermal drying performance analysis of banana and peach in the region of Gafsa (Tunisia). *Case Studies in Thermal Engineering*, Volume 20, pp. 1-12 <https://doi.org/10.1016/j.csite.2020.100771>.
- Nguyen, M.-H. & Price, W. E., 2007. Air-drying of banana: Influence of experimental parameters, slab thickness, banana maturity and harvesting season. *Journal of Food Engineering*, 79(1), pp. 200-207.
- Ni, H., 1997. *Multiphase Moisture Transport in Porous Media under Intensive Microwave Heating. Ph.D Dissertation*, , NY, USA: Cornell University, Ithaca.
- Nimesh, C. & Jethva, K., 2016. Drying Characteristics of Banana Powder. *Indian Journal of Science*, 23(77), pp. 75-88.
- Norton, T. & Sun, D. W., 2010. CFD: An Innovative and Effective Design Tool for the Food Industry. In: Aguilera J., Simpson R., Welti-Chanes J., Bermudez-Aguirre D., Barbosa-Canovas G. (eds) *Food Engineering Interfaces*. In: *Food Engineering Series*. New York: NY: Springer, pp. pp. 55-68.

- Olawoye, B., Kadiri, O. & Babalola, T., 2017. Modelling of Thin-Layer Drying Characteristic of Unripe Cardaba Banana (Musa ABB) Slices. *Cogent Food & Agriculture*, 3(1), pp. 1-12.
- Omolola, A. O., Jideani, A. I. O. & Kapila, P. F., 2015. DRYING KINETICS OF BANANA (Musa spp.). *Interciencia*, 40(6), pp. 374 - 380.
- Ondier, G., Siebenmorgen, T. & Mauromoustakos, A., 2010. Technical Note: Equilibrium Moisture Contents of Rough Rice Dried Using High-Temperature, Fluidized-Bed Conditions. *Transactions of the ASABE*, Volume 53, pp. 1667-1672 DOI:10.13031/2013.34885.
- Othieno, H., 1987. *Circulation of Air in Natural-Convection Solar Dryers*. roceedings of a Workshop held in Dakar, Senegal, IDRC, Canada, Retrieved from <https://idl-bnc-idrc.dspacedirect.org/bitstream/handle/10625/17684/IDL-17684.pdf?sequence=1>.
- Pangavhane, D. & Sawhney, R., 2002. Review of research and development work on solar dryers for grape drying. *Energy Conversion and Management*.
- Patil, R. & Gawande, R., 2016. A review on solar tunnel greenhouse drying system. *Renewable and Sustainable Energy Reviews*, p. 196–214.
- Rabha, D., Muthukumar, P. & Somayaji, C., 2017. Energy and exergy analyses of the solar drying processes of ghost chilli pepper and ginger. *Renewable Energy*, Volume 105, pp. 764-773 <http://dx.doi.org/10.1016/j.renene.2017.01.007>.
- Radhika, G., Satyanarayana, S., Rao, D. & Raju, B., 2011. Mathematical model on thin layer drying of finger millet (Eluesine coracana). *Advance Journal of Food Science and Technology*, Volume 3, pp. 127-131.
- Rahmatinejad, B., Hosseinzadeh, H., Sharifi, O. & Rezazadeh, A., 2016. The Effect of Temperature and Speed of Wind on the Drying Time of Basil Leaves in a Solar-Photovoltaic Dryer. *International Journal of Advanced Biotechnology and Research*, Volume 7, pp. 432-437.
- Rajput, R., 2012. *Heat and Mass Transfer*. Fifth Revised Edition ed. New Delhi: S. Chand and Company Limited.

- Reuther, J., Jameson, A., Farmer, J. & Martinelli, L., 1996. *erodynamic shape optimization of complex aircraft configurations via an adjoint formulation*, NASA Ames Research Center: Research Institute for Advanced Computer Science,.
- Rigit, A. R. & Patrick, T. L., 2010. Heat and Mass Transfer in a Solar Dryer with Biomass Backup Burner. *International Journal of Environmental, Ecological, Geological and Geophysical Engineering*, 4(2).
- Román, R. N.-I. et al., 2019. Computational fluid dynamics analysis of heat transfer in a greenhouse solar dryer “chapel-type” coupled to an air solar heating system.. *Energy Sci Eng*, Volume 7, p. 1123–1139 <https://doi.org/10.1002/ese3.333>.
- Romero , V., Cerezo, E., Garcia, M. & Sanchez, M., 2014. Simulation and validation of vanilla drying process in an indirect solar dryer prototype using CFD Fluent program. *Energy Procedia*, Volume 57, p. 1651 – 1658.
- Sacilik, K., Keskin, R. & Elicin, A. K., 2006. Mathematical modelling of solar tunnel drying of thin layer organic tomato. *Journal of Food Engineering*, 73(3), pp. 1-2.
- Sahdev, R. K., 2004. Open Sun and Greenhouse Drying of Agricultural. *International Journal of Engineering Research & Technology (IJERT)*, 3(3), p. pp. 1053–1067.
- Sangpradit, K., 2014. Study of the Solar Transmissivity of Plastic Cladding Materials and Influence of Dust and Dirt on Greenhouse Cultivations. *Energy Procedia*, Volume 56, pp. 566-573.
- Sankat, C. K., Castaigne, F. & Maharaj, R., 1996. The air drying behaviour of freshly and osmotically dehydrated banana slices. *International Journal of Food Science and Technology*, Volume 31, pp. 123-135.
- Schiavone, F., 2011. *Development and Evaluation of a Natural Convection Solar Dryer For Mango in Rural Haitian Communities*, s.l.: Msc. Thesis, Univeristy of Florida.
- Schirmer, P. et al., 1996. Experimental investigation of the performance of the solar tunnel dryer for drying bananas. *Renewable Energy*, 7(2), p. 119–129.
- Sharafani, A., 2015. CFD simulation of the agitated batch. *Master thesis*.

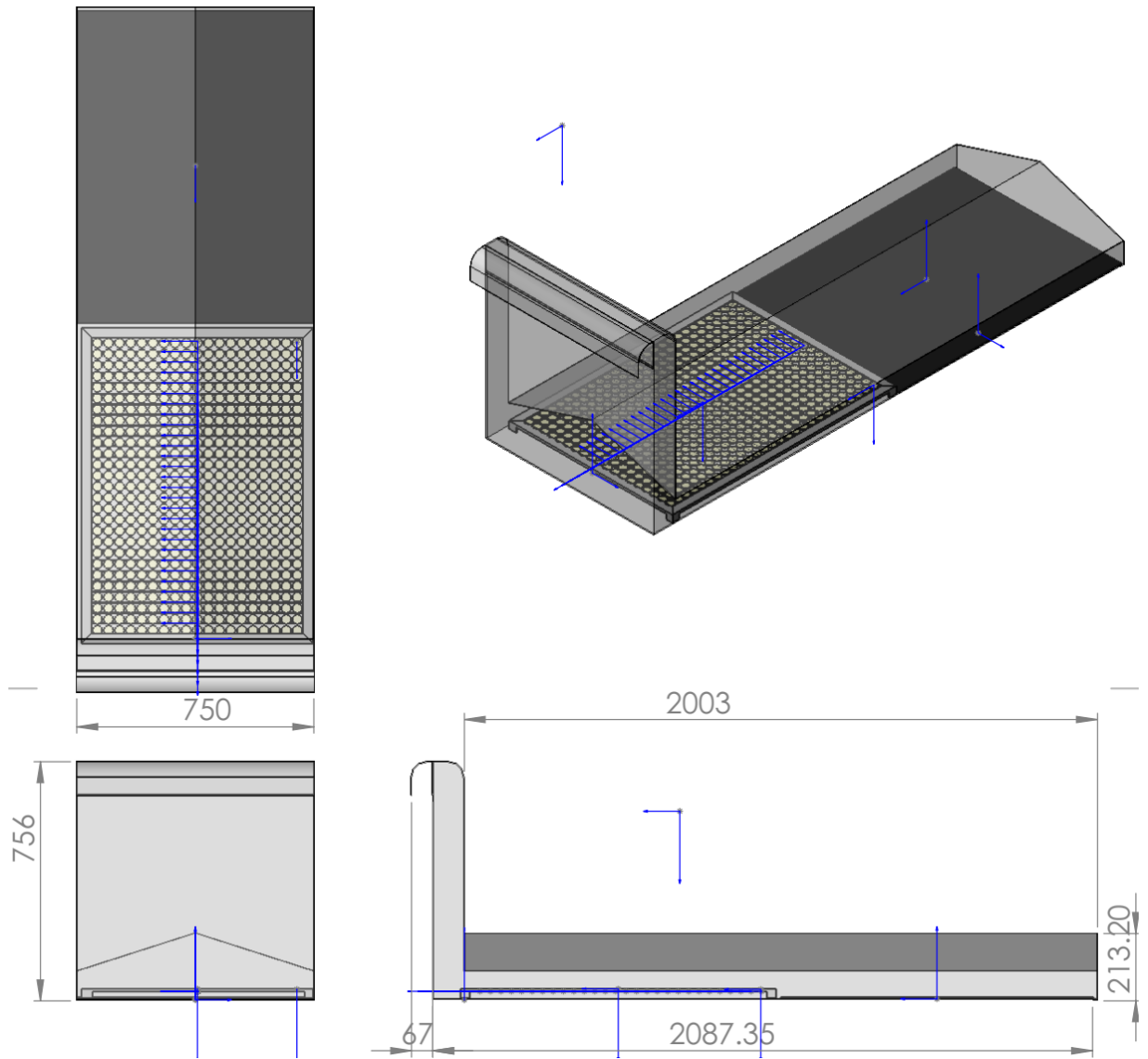
- Sharma , S. ..., Sharma, V., Ranjana, J. & Ray, R., 1990. Evaluation of the performance of a cabinet type solar dryer. *Energy Conversion & Management*, 30(2), p. 75–80.
- Sharma, A., Chen, C. & Lan, N. V., 2009. Solar-energy drying systems: A review, *Renewable and Sustainable Energy Reviews*. Volume 13, pp. 1185-1210.
- Sidhu, . J. S. & Zafar, T. A., 2018. Bioactive compounds in banana fruits and their health benefits. *Food Quality and Safety*, 2(4), p. 183–188
<https://doi.org/10.1093/fqsafe/fyy019>.
- Silva, W., Silva, C., Gama, F. & Gomes, J., 2014a. Mathematical models to describe thin-layer drying and to determine drying rate of whole bananas. *J. Saudi Soc. Agric Sci*, Volume 13, pp. 67-74.
- Silva, W., Silva, C., Sousa, J. & Farias , V., 2013. Empirical and diffusion models to describe water transport into chickpea (*Cicerarietinum L.*). *Int. J. Food Sci. Technol*, Volume 48, pp. 267-273.
- Simate, I. N., 2003. Optimization of mixed mode and indirect mode natural convection solar dryers. *Renewable Energy*, Volume 28, pp. 435-453.
- Simate, I. N., 2021. Energy and Exergy Analysis of an Indirect-Mode Natural Convection Solar Dryer for Maize. *Energy and Environment Research*, 11(2), pp. 19-30.
[doi:10.5539/eer.v11n2p19](https://doi.org/10.5539/eer.v11n2p19).
- Smitabhindu, R., Janjai, S. & Chankong, V., 2008. Optimization of a solar-assisted drying system for drying bananas. *Renewable Energy*, Volume 33, p. 1523–1531.
- SOLIDWORKS Corporation, 2010. *Engineering Design and Technology Series: An Introduction to Flow Analysis Applications with SolidWorks Flow Simulation, Instructor Guide*. Concord, Massachusetts USA: Dassault Systèmes - SolidWorks Corporation.
- Tagne, M. S., Ndukwu, C. M. & Azese, . N. M., 2020. Experimental Modelling of a Solar Dryer for Wood Fuel in Epinal (France). *Modelling*, Volume 1, p. 39–52
[doi:10.3390/modelling1010003](https://doi.org/10.3390/modelling1010003).

- The Engineering Toolbox, 2003. "Emissivity Coefficients Materials," *Engineering Toolbox*. [Online] Available at: https://www.engineeringtoolbox.com/emissivity-coefficients-d_447.html [Accessed November 2021].
- Thirunavukkarasu, V. & Thamaraikannan, B., 2014. Design Optimization of Mechanical Components Using an Enhanced Teaching-Learning Based Optimization Algorithm with Differential Operator. *Mathematical Problems in Engineering*, Issue Article ID 309327, 10 pages, 2014. <https://doi.org/10.1155/2014/309327>.
- Thuwapanichayanam, R., Prachayawarakorn, S. & Kunwisawa, J., 2011. Determination of effective moisture diffusivity and assessment of quality attributes of banana slices during drying. *Food Sci. & Tech*, Volume 44, pp. 1502-1510.
- Tiwari, G., 2002. *Solar Energy: Fundamentals, Design, Modeling and Applications*, s.l.: Parybourne: Alpha Science International Limited.
- Tzanakis, A., 2014. *Duct optimization using CFD software 'ANSYS Fluent Adjoint Solver Master's thesis in Automotive Engineering*, Goteborg, Sweden: Chalmers University of Technology.
- Udomdejwatana, S., 1994. *Thermal properties of Musa suerier and Musa sapientum Linn, Master's Thesis*, Bangkok, Thailand: Chulalongkorn University.
- Vallverdú1, J., 2014. What are Simulations? An Epistemological Approach. *Procedia Technology*, Volume 13, pp. 6-15. doi: 10.1016/j.protcy.2014.02.003.
- Visavale, G., 2012. *Principles, Classification and Selection of Solar Dryers. In Solar drying: Fundamentals, Applications and Innovations*,. Published in Singapore: s.n.
- Wisara, T. & Kittichai, B., 2019. Investigation of Heat and Moisture Transport in Bananas during Microwave Heating Process. *Processes*, Volume 7, p. doi:7. 545. 10.3390/pr7080545..
- Xia, B. & Sun, D.-W., 2002. Applications of computational fluid dynamics (CFD) in the food industry: a review. *Computers and Electronics in Agriculture*, Volume 34, pp. 5-24.

Zooba, A. F. & Bansal, R., 2011. *Handbook of Renewable Energy Technology*. singapore: World Scientific Publishing Co. Pte. Ltd.

Zoukit, A. et al., 2019. Simulation, design and experimental performance evaluation of an innovative hybrid solar-gas dryer. *Energy*, Issue
<https://doi.org/10.1016/j.energy.2019.116279>.

Appendix I: Solar dryer



All dimensions in mm

Appendix II: The banana slices after drying

Photograph of solar dried bananas



Appendix III: Sample calculation of the heat transfer rate

Assumptions:

- Radiation heat losses from the plate are negligible.
- Heat losses through the edges of the plate are negligible.
- The back of the plate is perfectly insulated. Thus, at steady-state, the temperature of the plate is uniform.
- The incident radiation, the convection heat transfer coefficient and the absorptivity of the surface are all uniform over the surface of the plate.

At steady-state, the rate at which heat is transferred into the plate from the sun by radiation must be equal to the rate at which heat is lost from the plate to the surrounding air by convection.

$$\dot{q}_{\text{radiation}} = \dot{q}_{\text{convection}}$$

a is the fraction of the incident radiation that is absorbed by a surface. Therefore:

$$\dot{q}_{\text{radiation}} = a \dot{q}_{\text{convection}}$$

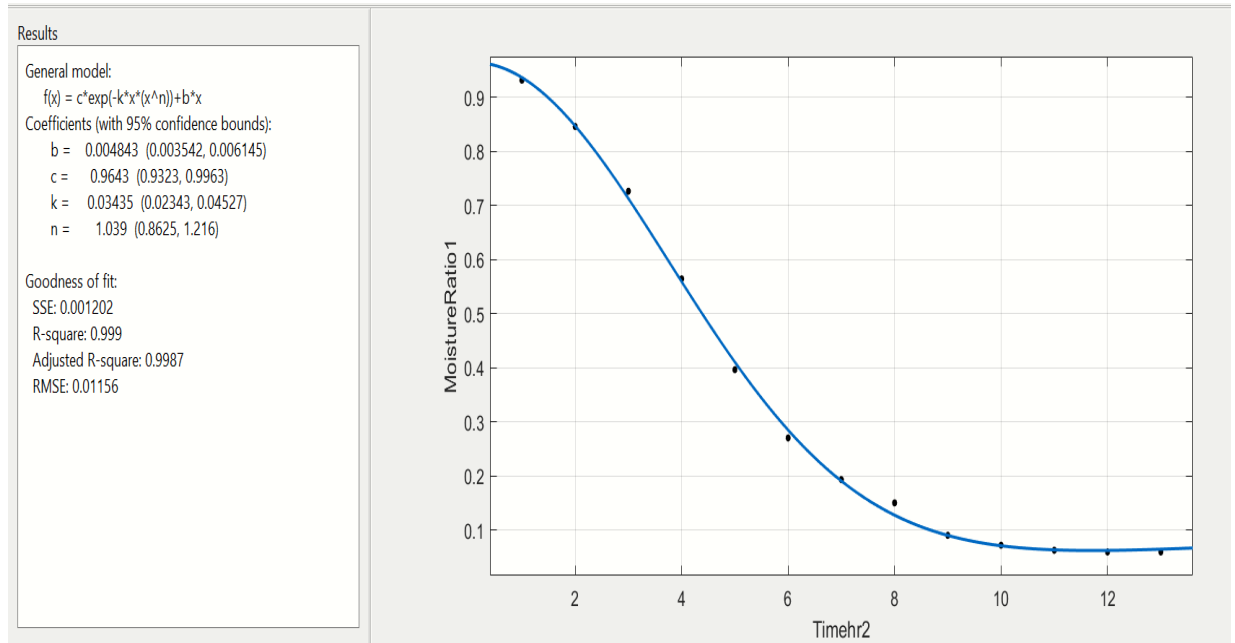
Newton's Law of Cooling gives us the convection heat transfer rate at the surface of the plate.

Hence

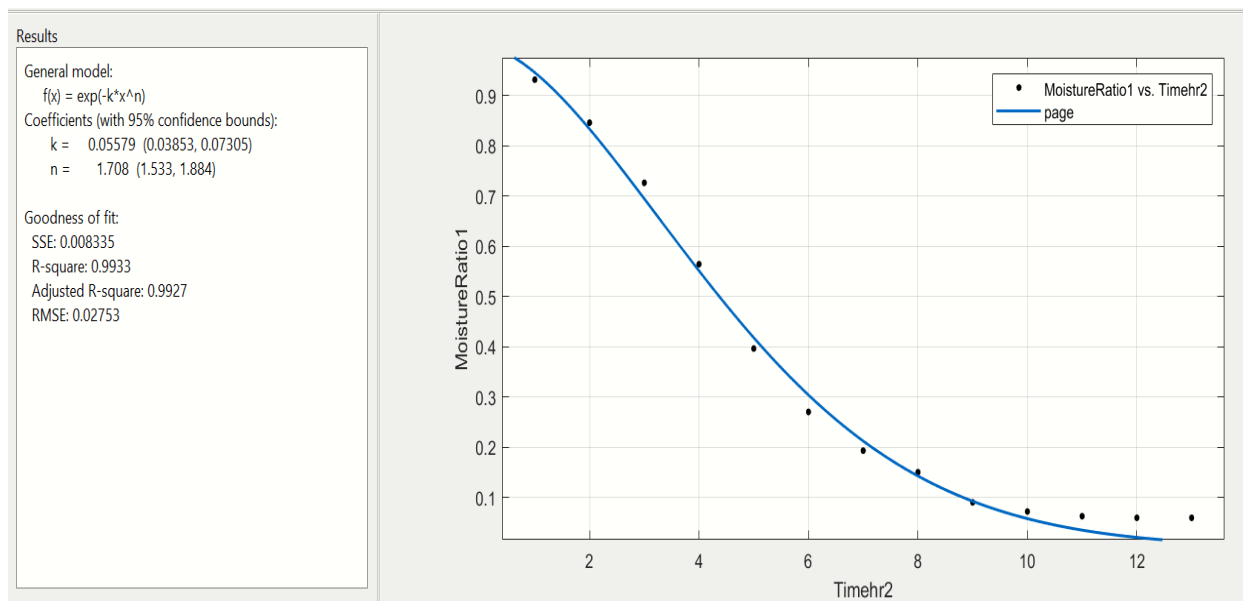
$$\begin{aligned}\dot{q}_{\text{convection}} &= \frac{\dot{q}_{\text{radiation}}}{a} = \frac{h(T_s - T_f)}{a} \\ &= \frac{821.53}{0.65} \\ &= 1263.89 \text{ W/m}^2\end{aligned}$$

Appendix IV: The best fitting thin layer models midilli et al and page models.

1. Midilli et al model



2. Page model



Appendix V: Simulation input and output variables

An average mass flow of 0.014 kg/s was used in the simulation.

	Input variables							
	9:00	10:00	11:00	12:00	13:00	14:00	15:00	16:00
Ambient temperature (°C)	23.45	25.53	28.40	30.85	32.33	31.95	31.53	31.20
Solar insolation (W/m ²)	569.97	543.62	674.37	821.53	758.66	516.40	422.63	239.57
	Output variables							
Collector temperature (°C)	49.03	51.79	59.26	66.83	63.20	59.44	54.52	49.62
Drying unit temperature (°C)	55.12	59.70	65.34	74.97	69.03	65.61	58.04	56.46
Chimney temperature (°C)	38.78	45.53	56.66	58.85	59.99	55.26	51.85	44.15

Appendix VI: Approval of Study



THE UNIVERSITY OF ZAMBIA DIRECTORATE OF RESEARCH AND GRADUATE STUDIES

Great East Road Campus | P.O. Box 32379 | Lusaka10101 | Tel: +260-211-290 258/291 777
Fax: (+260)-211-290 258/253 952 | E-mail: director.drgs@unza.zm | Website: www.unza.zm

APPROVAL OF STUDY

IORG No. 0005376
NASRECREC IRB No. 00006465

7th March, 2023

REF NO. NASREC-2023- FEB - 003

Mr. Maona Mukanema,
The University of Zambia,
School of Engineering,
P.O. Box 32379,
LUSAKA.

Dear Mr. Mukanema,

RE: “PERFORMANCE ASSESSMENT OF A NATURAL CONVECTION SOLAR TUNNEL DRYER THROUGH EXPERIMENTATION AND CFD SIMULATION OF TEMPERATURE AND AIRFLOW”

Reference is made to your protocol dated as captioned above. NASREC resolved to approve this study and your participation as Principal Investigator for a period of one year.

REVIEW TYPE	ORDINARY REVIEW	APPROVAL NO. NASREC-2023-FEB. 003
Approval and Expiry Date	Approval Date: 7 th March, 2023	Expiry Date: 7 th March, 2024
Protocol Version and Date	Version - Nil.	7 th March, 2024
Information Sheet, Consent Forms and Dates	<ul style="list-style-type: none">English.	To be provided
Consent form ID and Date	Version - Nil	To be provided
Recruitment Materials	Nil	Nil
Other Study Documents	Questionnaire.	

Specific conditions will apply to this approval. As Principal Investigator it is your responsibility to ensure that the contents of this letter are adhered to. If these are not adhered to, the approval may be suspended. Should the study be suspended, study sponsors and other regulatory authorities will be informed.

CONDITIONS OF APPROVAL

- No participant may be involved in any study procedure prior to the study approval or after the expiration date.
- All unanticipated or Serious Adverse Events (SAEs) must be reported to NASREC within 5 days.
- All protocol modifications must be approved by NASREC prior to implementation unless they are intended to reduce risk (but must still be reported for approval). Modifications will include any change of investigator/s or site address.
- All protocol deviations must be reported to NASREC within 5 working days.
- All recruitment materials must be approved by NASREC prior to being used.
- Principal investigators are responsible for initiating Continuing Review proceedings. NASREC will only approve a study for a period of 12 months.
- It is the responsibility of the PI to renew his/her ethics approval through a renewal application to NASREC.
- Where the PI desires to extend the study after expiry of the study period, documents for study extension must be received by NASREC at least 30 days before the expiry date. This is for the purpose of facilitating the review process. Documents received within 30 days after expiry will be labelled “late submissions” and will incur a penalty fee of K500.00. No study shall be renewed whose documents are submitted for renewal 30 days after expiry of the certificate.
- Every 6 (six) months a progress report form supplied by The University of Zambia Natural and Applied Sciences Research Ethics Committee as an IRB must be filled in and submitted to us. There is a penalty of K500.00 for failure to submit the report.
- When closing a project, the PI is responsible for notifying, in writing or using the Research Ethics and Management Online (REMO), both NASREC
- and the National Health Research Authority (NHRA) when ethics certification is no longer required for a project.
- In order to close an approved study, a Closing Report must be submitted in writing or through the REMO system. A Closing Report should be filed when data collection has ended and the study team will no longer be using human participants or animals or secondary data or have any direct or indirect contact with the research participants or animals for the study.
- Filing a closing report (rather than just letting your approval lapse) is important as it assists NASREC in efficiently tracking and reporting on projects. Note that some funding agencies and sponsors require a notice of closure from the IRB which had approved the study and can only be generated after the Closing Report has been filed.

- A reprint of this letter shall be done at a fee.
- All protocol modifications must be approved by NASREC by way of an application for an amendment prior to implementation unless they are intended to reduce risk (but must still be reported for approval). Modifications will include any change of investigator/s or site address or methodology and methods. Many modifications entail minimal risk adjustments to a protocol and/or consent form and can be made on an Expedited basis (via the IRB Chair). Some examples are: format changes, correcting spelling errors, adding key personnel, minor changes to questionnaires, recruiting and changes, and so forth. Other, more substantive changes, especially those that may alter the risk-benefit ratio, may require Full Board review. In all cases, except where noted above regarding subject safety, any changes to any protocol document or procedure must first be approved by NASREC before they can be implemented.

Should you have any questions regarding anything indicated in this letter, please do not hesitate to get in touch with us at the above indicated address.

On behalf of NASREC, we would like to wish you all the success as you carry out your study.

Yours faithfully,



Dr. Mususu Kaonda

**VICE-CHAIRPERSON
THE UNIVERSITY OF ZAMBIA NATURAL AND APPLIED SCIENCES RESEARCH
ETHICS COMMITTEE - IRB**

CC: Director, Directorate of Research and Graduate Studies
Assistant Director (Research), Directorate of Research and Graduate Studies
Assistant Registrar (Research), Directorate of Research and Graduate Studies

Appendix VII: Article

Energy and Environment Research; Vol. 13, No. 1; 2023
ISSN 1927-0569 E-ISSN 1927-0577
Published by Canadian Center of Science and Education

CFD Simulation of Temperature and Air Flow in a Natural Convection Solar Tunnel Dryer with a Bare Flat-Plate Chimney

Maona Mukanema¹ & Isaac N. Simate²

¹ Department of Mechanical Engineering, School of Engineering, University of Zambia, Lusaka, Zambia

² Department of Agricultural Engineering, School of Engineering, University of Zambia, Lusaka, Zambia

Correspondence: Maona Mukanema, Department of Mechanical Engineering, School of Engineering, University of Zambia, Lusaka, Zambia. E-mail: maonamukanema@gmail.com

Received: January 30, 2023

Accepted: February 26, 2023

Online Published: February 27, 2023

doi:10.5539/eer.v13n1p1

URL: <https://doi.org/10.5539/eer.v13n1p1>

Abstract

Computational Fluid Dynamics simulation of a natural convection solar tunnel dryer with a bare flat-plate chimney is presented. The chimney's function is to create airflow in the dryer through the buoyancy effect by re-heating the air coming from the drying unit and is therefore a major factor in the drying rate. CFD simulation was therefore employed to study the temperature and airflow in the dryer and determine the areas that could be improved upon. The design of the solar tunnel dryer geometry used in this simulation was done in SOLIDWORKS 2016 whereas the simulation of temperature distribution of airflow inside the dryer was performed using SOLIDWORKS 2016 flow simulation program in a steady-state regime. The boundary conditions were set using the obtained experimental data. The simulation results showed that the chimney losses heat, that there is air recirculation in the collector, that the airflow experiences some pressure loss as it moves from the drying chamber to the chimney, and that there is some reduction of the velocity in some parts of the dryer. The simulated and experimental collector efficiencies were found to be 33.09 and 37.63%, respectively, giving a mean relative deviation of collector temperature of 5.1%. To improve the performance of the dryer, insulating and glazing of the chimney is suggested as well as using a curved joint between the chimney and the drying chamber.

Keywords: CFD simulation, temperature and airflow, natural convection, solar tunnel dryer, chimney

1. Introduction

Natural convection solar dryers do not use fans and therefore have advantages over forced convection solar dryers in terms of operations in rural or remote settings where there is no electricity grid and where installed solar PV panels are prone to theft (Simate & Cherotich, 2017). In both natural and forced convection solar dryers, heated air is key to the performance of the dryer as it supplies all/some of the heat to the food to evaporate the moisture, as well as take away the evaporated moisture (Bala & Wood, 1994). A study of the airflow behaviour in the dryer can help develop better performance solar dryers (Simate, 2020). The drying rate is a strong function of airflow and it is of great importance to know the areas of adequate air velocities for proper drying (Xia & Sun, 2002). Mathioulakis et al. (1998) showed, using CFD that the degree of fruit dryness depended on its position within the dryer. Kaushal and Sharma (2012) determined the pressure profiles and air velocities using CFD and showed that the main cause of the variations in drying rates and moisture contents was the lack of spatial homogeneity of air velocities within the dryer. For a natural convection solar dryer, Al-Neama & Farkas (2016) showed that the velocity of air in the chimney was a function of temperature change across the chimney. Vintilă et al. (2014) used CFD in natural convection solar dryers to simulate the temperature distribution and velocity field in the collector and drying chamber. Omolola et al. (2015) conducted a CFD analysis of a solar dryer using SolidWorks Flow Simulation. They investigated the effect of airflow distribution, flow velocity, and pressure field on transient moisture within the dryer. Some of the simulation parameters such as air temperature were accurately predicted resulting in small deviations of about 0.02%. Their simulation of the drying process for the green bell pepper was conducted using the standard turbulence model under steady-state conditions. Zoukit et al. (2019) used SolidWorks and presented a numerical simulation of a hybrid solar-gas dryer operated under forced convection with an air mass flow rate of 0.025kg/s. Jheresson et al. (2018) also used SolidWorks to simulate velocity and temperature in a food dryer in order to define the contours with the aim of evaluating the operating

conditions of the chamber and found that the design having outlets on both sides with horizontally inclined trays gave the best performance. According to Misha et al. (2013), CFD can be a valuable tool for engineering design and analysis of complex fluid flow situations, addressing heat and mass transfer phenomena, aiding in the better design of tray dryers, and production of high-quality dried products. One type of natural convection solar dryer, the natural convection solar tunnel dryer, has shown great potential in drying fruits such as mango and banana. This type of dryer has a distinct collector unit that heats the air, a drying unit where the product is located and, a bare flat-plate chimney that creates buoyancy by re-heating the air coming from the drying unit. However, one drawback with this dryer is the temperature of the air in the chimney being lower than that of air coming from the drying unit, implying that the chimney losses heat to the environment, consequently reducing the air flow rate and, ultimately, the drying rate (Cherotich & Simate, 2016). Since the airflow through a natural convection solar dryer is initiated by the buoyancy-induced pressure head that is created above the atmospheric pressure, any changes in the chimney air temperature affect the air flow and temperature in the collector and drying chamber. It was therefore the objective of this study to use CFD to model the temperatures and airflow in the dryer and identify factors contributing to air temperature and flow and, areas that could be improved upon.

2. Materials and Methods

2.1 Description of the Dryer and its Components

The natural convection solar tunnel dryer designed by Cherotich, (2016) and presented by Cherotich and Simate (2016) was modeled and simulated using SolidWorks Flow simulation developed by Dassault systems. Figure 1 shows the modeled natural convection solar tunnel dryer. The dryer consists of a collector unit, a drying unit, and a bare flat-plate chimney unit. The solar collector unit is a flat-plate type. The absorber plate is made from a 0.3 mm thick flat Galvanized Iron (GI) sheet and its top side is painted matt black (absorptivity = 0.95, emissivity = 0.8). The collector is covered with a transparent 200 μm polythene sheet (transmissivity = 0.857) which allowed the solar radiation to heat the absorber, consequently heating the ambient air entering the collector and moving to the drying unit. The drying unit, also covered with the same polythene sheet, and the collector unit, were made in one subassembly and from the same materials, and are configured in series. The drying unit contains a removable wire mesh tray to hold the product during drying. Then the drying unit is linked to a chimney. The chimney is a bare flat-plate type collector also constructed from a 0.3 mm thick flat GI sheet and painted matt black to absorb most of the incident solar radiation falling on it so as to reheat the air exiting the drying unit.

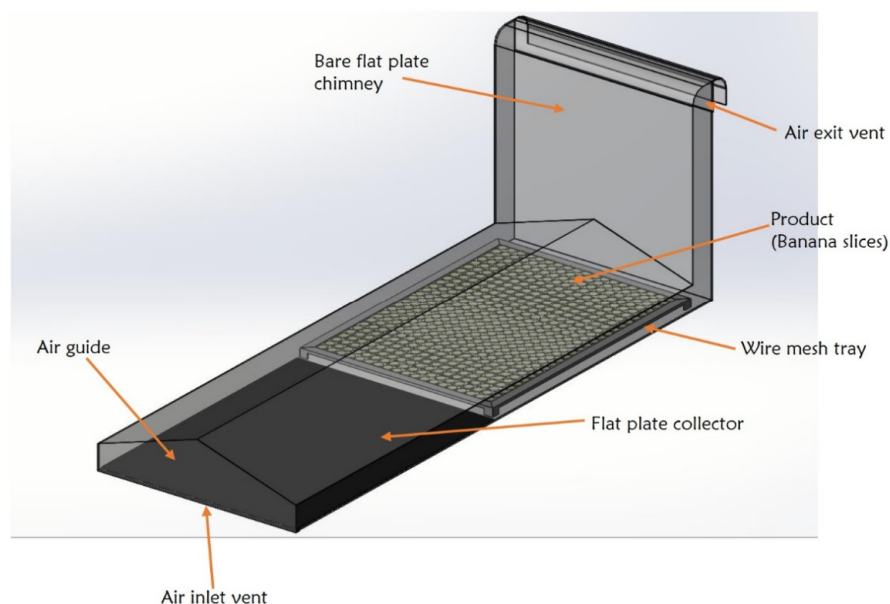


Figure 1. Modelled natural convection solar tunnel dryer

2.2 Experimentation

The experiments were conducted on the solar tunnel dryer at the field station of the Department of Agricultural Engineering, University Zambia, Lusaka Zambia (Latitude 15.3°S; Longitude 28.3°E). Drying experiments using fresh banana slices were conducted in April 2022. The simulation was performed with banana slices in the drying unit. The results of the load condition were used to illustrate the velocity and temperature contours. Simulating the inception conditions of the experiment was done to validate the result.

2.3 Simulation Procedure

SOLIDWORKS 2016 was utilized to produce a 3 Dimensional (3D) geometry of the solar tunnel dryer. CPU Type: Intel(R) Core(TM) i5-5300U CPU @ 2.30GHz, CPU Speed: 2295 MHz, RAM: 3970 MB, Flow Simulation 2016 SP0.0. Build: 3259 helps provide valuable data to pinpoint the system's low temperature points and this knowledge will be helpful for optimizing and advancing solar tunnel dryer design. The boundary conditions for pressure (environmental pressure) and mass flow rate were set at the inlet and outlet of the geometric model. To perform the computation, the k- ϵ turbulence model was chosen because it yielded precise and acceptable results. After the creation of a 3D geometric model of the solar tunnel dryer shown in Figure 2, the configuration of the Flow simulation project was done.

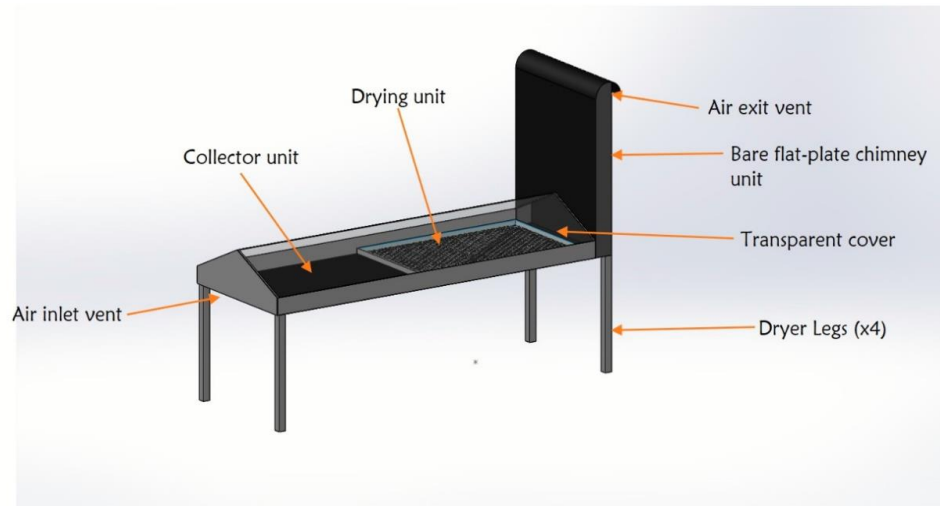


Figure 2. Solar tunnel dryer geometric model

2.3.1 Flow Simulation Project Configuration

For the internal flow analysis, specific information about the decline in pressure as a function of the flow of mass is provided. The goal of the project is to produce a simulation for fluid dynamics using computational fluid dynamics (CFD) where the following are defined: Unit system, Analysis type (internal analysis and excluding the cavities without conditions of flow), Fluid (Air, flow type: Laminar) and Initial conditions. This study employed the following simulation procedure.

2.4 Setting up a 3D Flow Condition

2.4.1 Computational Domain

The area around the 3D model, which defines the flow simulation in the restricted area, is known as the Computational Domain. This defines the boundary under which the flow simulation will take place. It is within the Computational Domain where flow and heat transfer calculations are carried out. The Computational Domain is a rectangular prism for the 3D analyses. The Computational Domain boundaries are parallel to the global coordinate system planes. The icon Computational Domain is used to modify the dimensions of the volume that it is being analysed and it allows visualizing the limits of the Computational Domain (SOLIDWORKS Corporation, 2010). Table 1 shows the coordinates of the Computational Domain size, and Figure 3 shows the visualization of the Computational Domain.

Table 1. Computational Domain size

Axis	size
X min	0.345 m
X max	1.091 m
Y min	1.037 m
Y max	1.789 m
Z min	0.442 m
Z max	2.546 m

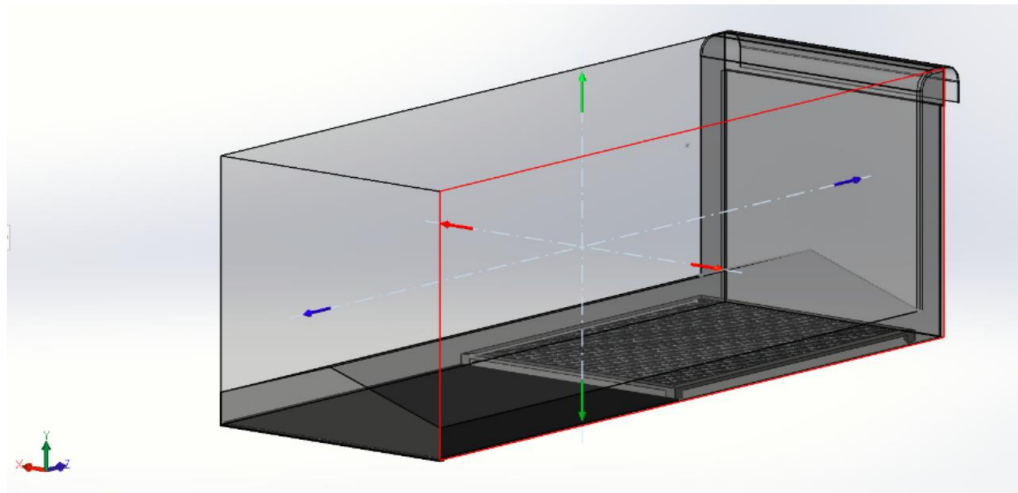


Figure 3. Visualization of Computational Domain

2.4.2 Material Properties

The properties of materials used in the simulation study are shown in Table 2.

Table 2. Material properties

Parameter	Value	Units	Source
Banana dimension (D × h)	30 × 3	mm	In this study
Initial moisture content - Ripe banana	73.8	%w.b.	In this study
Initial Equivalent porosity - Ripe banana	0.83	-	(Ni, 1997)
Thermal conductivity - Ripe banana	0.97	W/m K	(Udomdejwatana, 1994)
Density - Ripe banana	870	Kg/m ³	
Specific heat capacity (Cp) - Ripe banana	3,430	J/kg K	
Ambient pressure	10,1325	Pa	In this study
Polyethylene Cover			
-Density	915	Kg/m ³	(Roman, Lopez, Garcia, Pilatosky, & Ituna, 2019)
-Thermal conductivity	0.33	W/m K	
-Emissivity	0.9	-	
-Specific heat capacity (Cp)	1,900	J/kg K	
Single-layer polyethylene sheet			
-Transmittance	85.7	%	(Michael, 2014)
Galvanized iron sheet			
-Density	7,870	Kg/m ³	(Kumar, Sreenivaslu, P S Raghavendra, Kumar, & Pattanaik, 2019)
-Thermal Diffusivity	84.18x10 ⁶	m ³ /s	
-Specific Heat (Cp)	896	J/kg K	
-Thermal Conductivity (k)	204.2	W/m K	

2.4.3 Applying Boundary Conditions

In this study, the boundary conditions in regard to pressure and mass flow, and the dryer's surfaces (top cover, floor, and sides) were considered to be no-slip walls for the purpose of fluid flow analysis. These surfaces also had adiabatic considerations. The top cover had a boundary condition to simulate incident sunlight upon the dryer. The collector was modeled with radiation and a characteristic of rough galvanized iron. The plastic cover making up the dryer's roof was modeled to have a transmissivity of 0.86, the average light transmissivity for polyethylene plastic film (Sangpradit, 2014). The model geometry was characterized by a laminar flow regime.

2.4.4 Porous Medium

The porous medium icon allows the selection of components to be treated as such, using information from the engineering database (SOLIDWORKS Corporation, 2010). The banana was considered as porous media in the solar tunnel dryer. Figure 4 shows the arrangement of banana slices on the mesh. The porous media is modelled by the addition of a momentum source term to the standard fluid flow equations such as conservation of energy, momentum, and moisture transport equation. For this simulation study, the banana porosity was assumed to be constant.

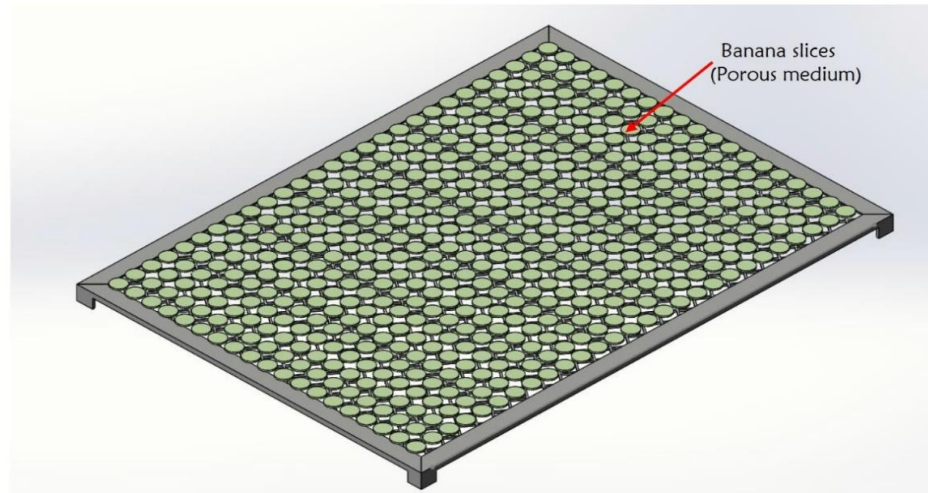


Figure 4. Arrangement of the bananas on the mesh

2.4.5 Initializing the Mesh

When the model is meshed, computational cells are created within the model and Computational Domain. Therefore, subdividing a model into a continuous set of nodes and elements, i.e., meshing a model, is a necessary prerequisite in the solution process. Fortunately, within SOLIDWORKS, simulation meshing occurs automatically. The operation can also be used to define the motion of the system and the analyses of simulation. The discretization process produced Total cell count, Fluid cells, Solid cells, and Partial cells equal to 760769, 324003, 262828, and 173938 respectively, these were used in the simulation analysis. Figure 5 shows the generated mesh of the solar dryer model.

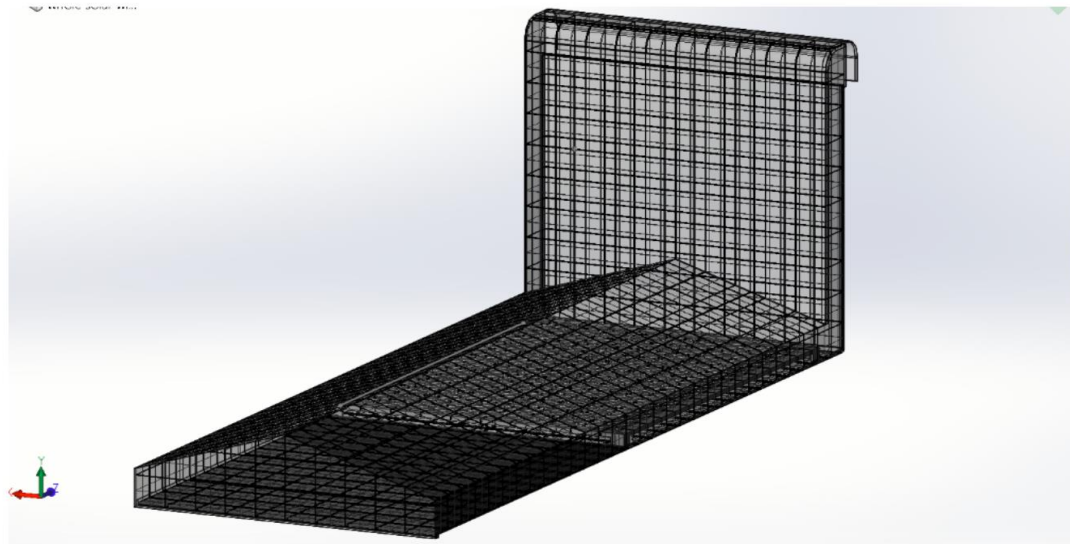


Figure 5. Generated Mesh

2.5 Running the Calculation

The simulation was run, and the process of convergence which is iterative, began. Due to the restrictions imposed on each parameter by the discretization of the flow field, no parameter can acquire a perfectly stable value, but will instead oscillate near it from iteration to iteration.

2.6 Visualization of the Temperature Flow Field

Once the calculation is done, the results of the saved computations can be modified and seen in a variety of ways right in the graphics area. The following features were used to view the results: cut plots, surface plots, flow trajectories, point parameters, surface parameters, goals, reports, and result animations.

2.7 Mean Relative Deviation

The model-predicted results were validated with experimental results using statistical analysis. The prediction ability of the model was tested by a statistical measure known as mean relative deviation (MRD) described by Equation (1). The mean relative deviation gives an idea of the mean departure of the measured data from the simulated data. The acceptable mean relative deviation should not exceed 10%.

$$MRD = \frac{1}{m} \sum_{i=1}^m \frac{|Simulated(i) - Measured(i)|}{Simulated(i)} \quad (1)$$

2.8 Calculation of the Collector Efficiency

Collector efficiency (η_c) is a measure of the efficacy of transfer of the solar insolation incident upon the collector to the air flowing through the collector (Tiris, Tiris, & Dincer, 1995). It was used to evaluate the performance of a flat-plate collector and is described by Equation (2).

$$\eta_c = \frac{\dot{m} C_p (T_c - T_{am})}{I_s A_c} \quad (2)$$

Where A_c = collector area, m²

I_s = mean solar insolation, W/m²

T_c = mean collector air temperature, °C

T_{am} = mean ambient air temperature, °C

C_p = specific heat capacity of air, J/kg °C

\dot{m} = air mass flow rate, kg/s

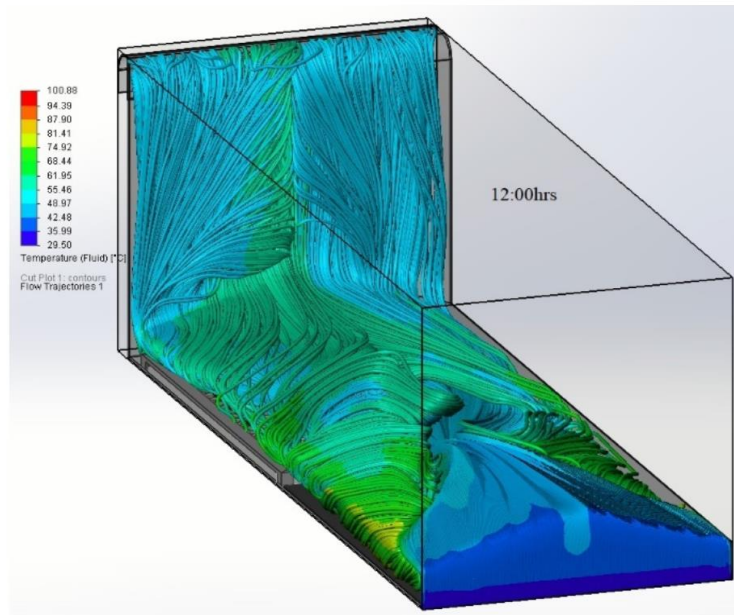
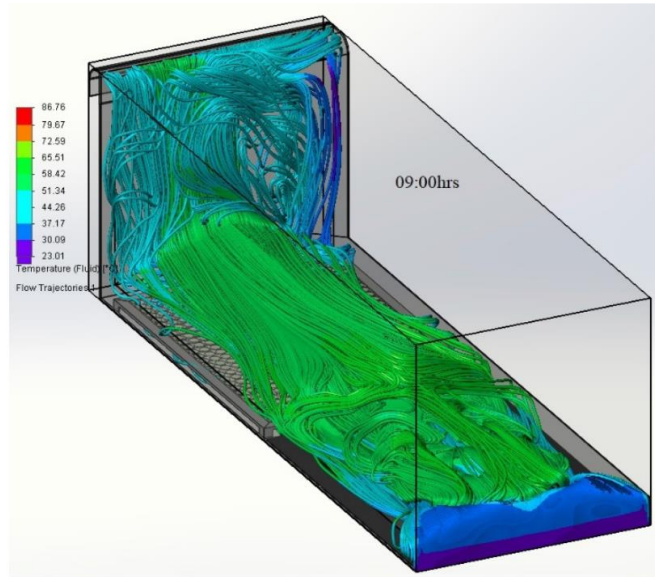
3. Results and Discussion

3.1 Simulation of the Natural Convection Solar Tunnel Dryer

The temperature distribution inside the solar tunnel dryer was determined through simulation. The simulations were carried out while taking into account the porous nature of bananas. This simulation was seeking to define the working fluid's (air) temperature and velocity contours inside the tunnel dryer.

3.1.1 Temperature

The fluid temperature flow trajectories inside the solar dryer at 09:00, 12:00 and 15:00 hours are depicted in Figure 6. It is evident from Figure 6 that air at the flat plate collector entry is at ambient temperature and increases towards the top of the collector as it enters the drying unit. The temperature of air adjacent to the collector plate increased as visualized in the figure. The tunnel temperature remains higher than the ambient temperature. It can also be noted that the temperature at various locations of the dryer varies with time. The solar dryer temperature is increasing steadily with the increase in solar insolation. The temperature of the air at the collector outlet ranged between 49.03 and 66.82°C. The heated air moved from the solar collector to the drying unit. The air was observed to have increased in temperature at the drying unit due to the mixed mode design of the dryer. The temperatures inside the drying unit ranged between 55.12 and 73.97 °C. The difference in temperature between the middle and the edge of the removable wire mesh tray located in the drying unit was deemed insignificant, and it can be assumed that the current design was successful in achieving a suitable uniform air temperature. The results of the simulation revealed that the average drying air temperature at the collector and drying unit were 56.71 and 62.9 °C, respectively, but the maximum hourly simulated maximum temperatures in the collector and drying unit were 66.83 and 73.9°C, respectively. The lowest temperatures were observed in the chimney and ranged from 38.78 to 59.9°C with an average of 51.38°C. These results are comparable to the simulation of a hybrid solar-gas dryer in solar mode done by Zoukit et al. (2019) who obtained temperature and relative humidity inside the drying chamber in the range of 50 to 60°C and 10 to 6.2%, respectively.



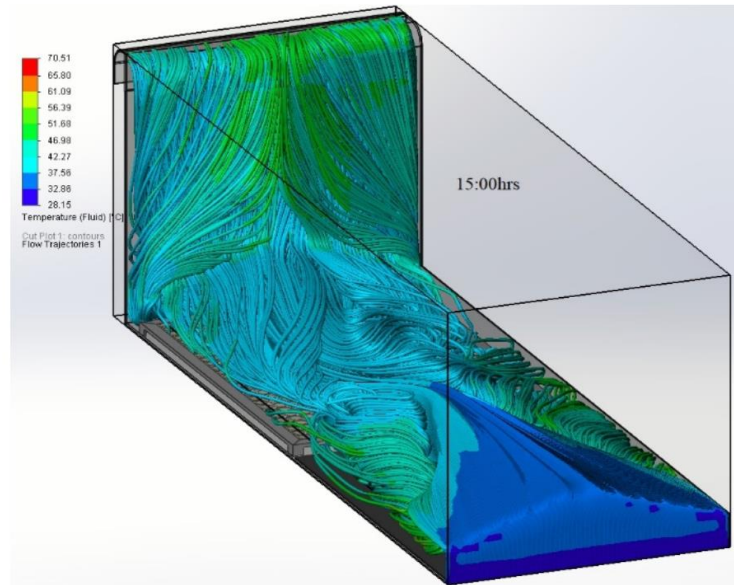


Figure 6. Temperature flow trajectories

Figure 7 shows temperature cut plot at 14:00 hours. From the visualization of air temperature distribution across the collector and drying unit, it can be noticed that the maximum heat gain is at the collector and this is a similar trend observed from the experiment. The air temperature near the wall is slightly lower compared to that at the centre of the drying chamber. It is due to the shortest path followed by air to exit the dryer (which can also be observed from the flow trajectories in Figure 6). It was observed that although the chimney was receiving solar insolation through its absorber (the side facing the drying chamber), the air in the chimney did not seem to have benefited from this heating as its temperature remained at the same level as that it came with from the drying chamber. This is an indication that there was some loss of heat from the air passing through the chimney. One way of reducing the heat loss from the chimney is to insulate the back and sides of the chimney and add glazing on the front side.

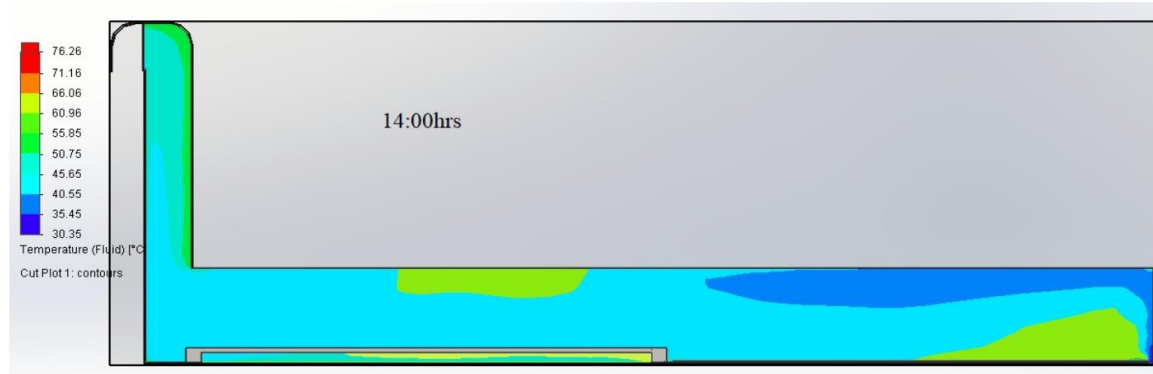
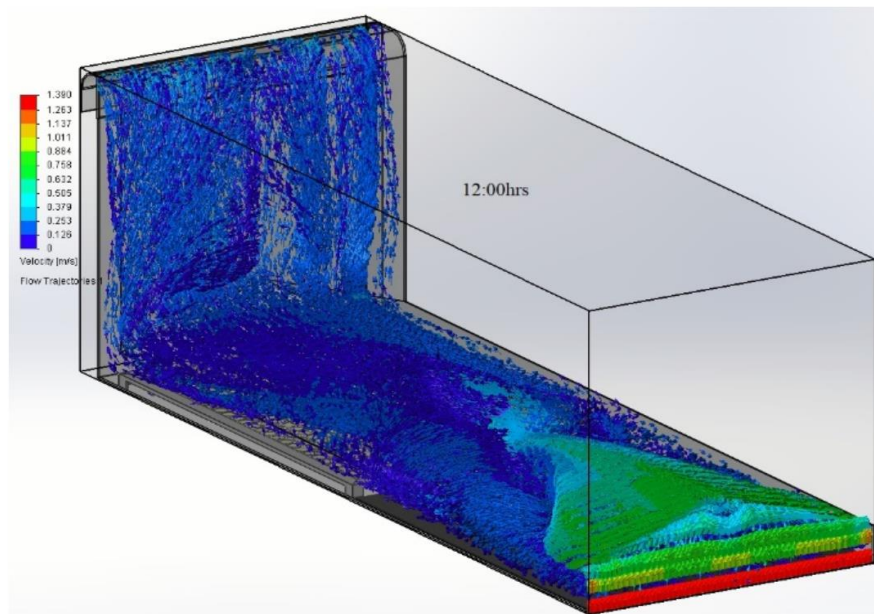
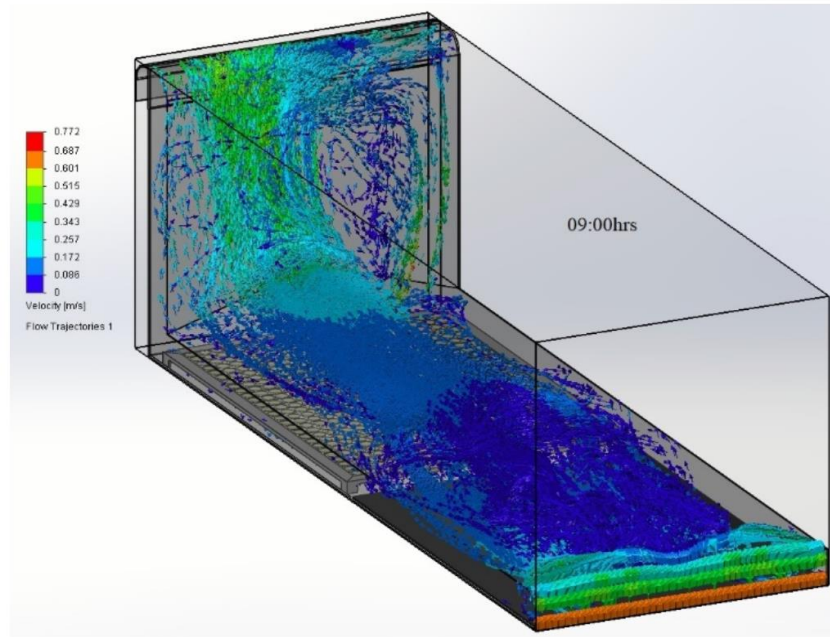


Figure 7. Temperature cut plot

3.1.2 Velocity

Figure 8 shows the velocity trajectories at 09:00, 12:00 and 15:00 hours. The air speed (velocity) picks up as it approaches the chimney exhaust vent. This pattern was anticipated because the flow cross-section reduces. The highest velocity is depicted at the inlet and outlet zones, which is caused by the apertures at both ends. It was also observed that the airflow velocity towards the drying unit produced the lowest velocity profile because the tray (wire mesh) and porous medium (banana slices) arrangement slightly obstructed the airflow stream across the drying unit, resulting in an average air velocity of 0.034 m/s.



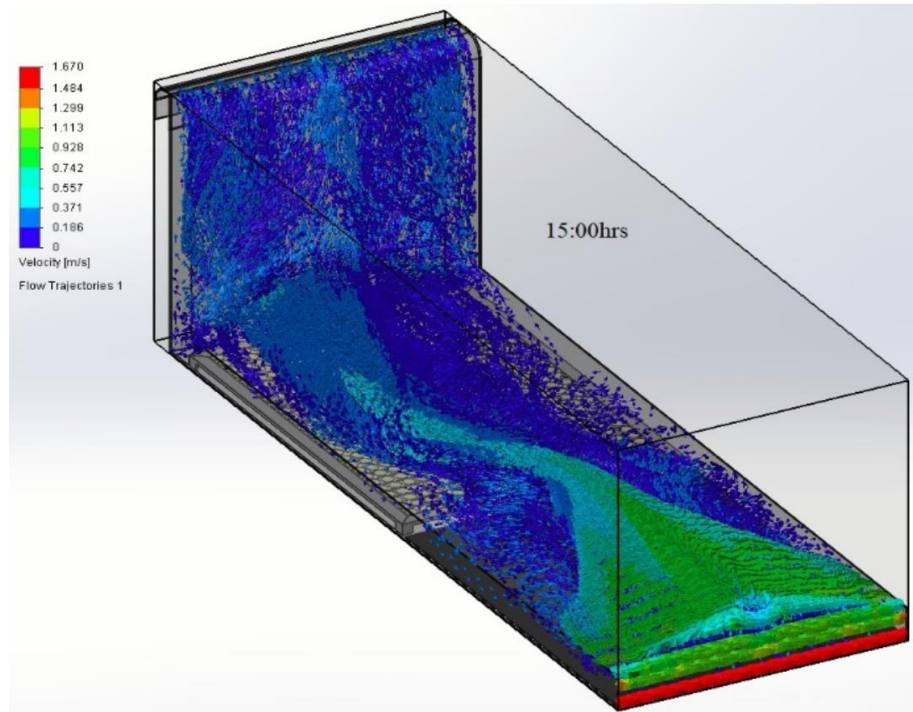


Figure 8. Velocity flow trajectories

Figure 9 shows velocity cut plot at 14:00 hours. The hottest air coming out of the collector forms a recirculation region before flowing to the drying unit. The hot air discharged by the collector rises because it is less dense and collides with each other when it reaches the polyethylene cover causing a disorderly flow field that forms a recirculation region. This flow pattern is in agreement with the cross-sectional temperature distribution depicted in Figures 6 and 7. The contours for the velocity shown in Figure 9 make it possible to appreciate the homogeneity of the temperature through the solar dryer. However, a decrease in the velocity in some parts of the dryer was observed. This was due to the loss in the velocity of the flux produced by the solids inside the chamber, which produced a uniform elevation of the heat.

Regarding the velocity, it was observed that the variation in the drying unit mesh favoured the velocity near the inlet. Hence, it was appreciated that the first pieces of fruit on the wire mesh, took most of the turbulence and backflows. However, when it reached the first bananas at a distance of 1.25 m from the inlet, its velocity dropped sharply to almost zero on the sides of the drying unit. This may have been due to the static resistance to its flow within the wire mesh and product. As the air left the drying unit, its velocity rose sharply but did not reach its initial value, stabilizing at an average of 0.055 m/s in the chimney. This could be attributed to the loss of some of its kinetic energy as it overcame the resistance to its flow through the wire mesh and product. Thus, the air velocity at the point on the wire mesh furthest from the air inlet, is less than that at the point closer. This agrees with the observations by Misha *et al.* (2013) that air velocity decreases as the distance from the inlet increases. Romuli *et al.* (2019) simulated airflow distribution and direction and estimated air mass flow in the inlet to be 0.75 kg/s in an inflatable solar dryer.

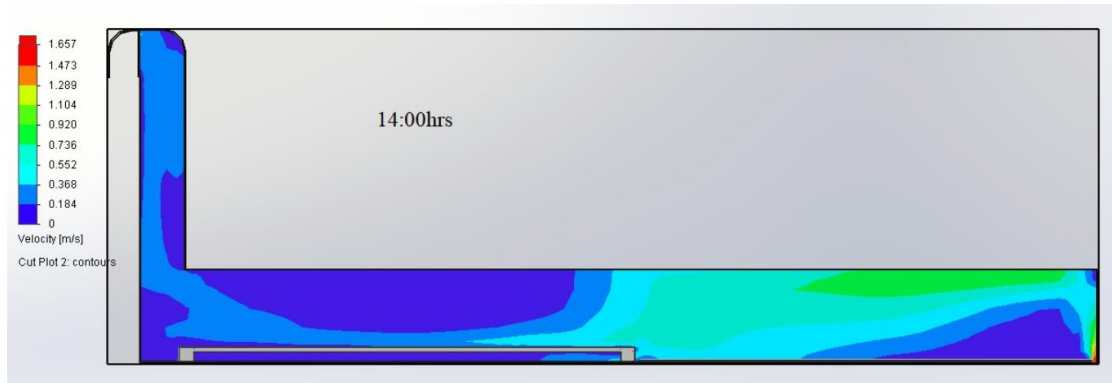


Figure 9. Velocity cut plot

It is also noted from Figure 9 that as the air flows from the drying chamber to the chimney it changes its direction of flow through a 90 degrees turn. According to Brooker et al. (1992), when air in a duct is forced to change its flow direction, both friction and dynamic losses are experienced, contributing to the total pressure losses. It is evident from Figure 9 that the airflow experiences some pressure losses as it moves from the drying chamber to the chimney, as seen by the change in its velocity. To reduce the losses, a curved joint is suggested to reduce the turbulence created as the air changes direction.

3.1.3 Chimney Buoyancy Effect

The chimney buoyancy effect depends on the rise in the temperature produced in the chimney. The simulation showed that the chimney's mean temperature increased by 18.73°C above ambient, thus producing the buoyancy effect. The drying unit air temperatures were higher than the chimney air temperatures despite the chimney receiving solar radiation to heat the air from the drying chamber, further. A major drawback of the bare flat plate type of chimney is its significant thermal losses, which may account for the cooling of the air observed in the chimney (Cherotich & Simate, 2016). The pressure drop that creates the airflow arising from the density difference between the ambient air and the chimney air, and the height of the chimney, can be seen in Figure 10. To cut down on the bare flat plate chimney's thermal losses, it is suggested, that its back and sides be insulated and a glazing added on its front side.

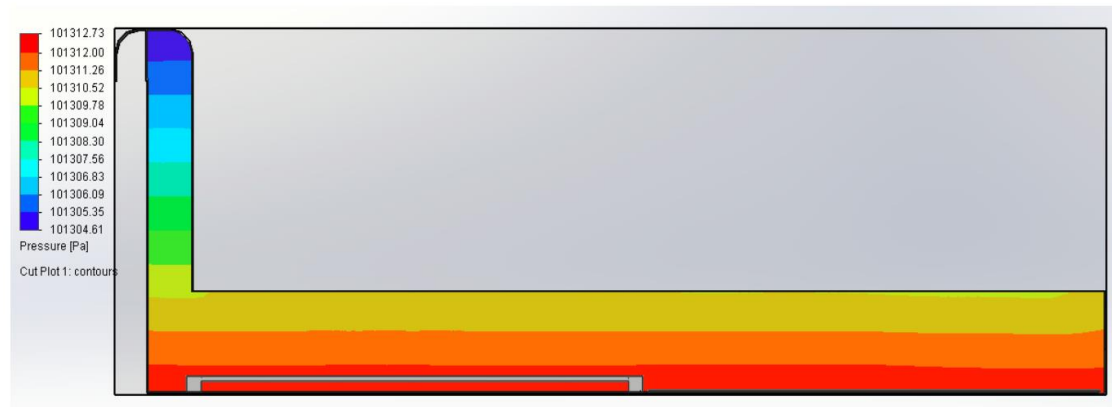


Figure 10. Pressure drop in the chimney

3.2 Comparison of Simulated and Experimental Results

3.2.1 Collector

The simulated and experimental results of the solar collector outlet air temperatures and the global solar radiation against time are shown in Figure 11. The simulated and experimental temperatures showed good agreement with the simulated results being higher by an average of 4.15 °C. The lower values of experimental results were

probably caused by heat loss, which is affected by many factors of the surroundings, as the real conditions are not adiabatic. Consequently, the thermal efficiency of the collector from the simulation was found to be 37.63% which was greater than the efficiency of 33.09% obtained from the experiment.

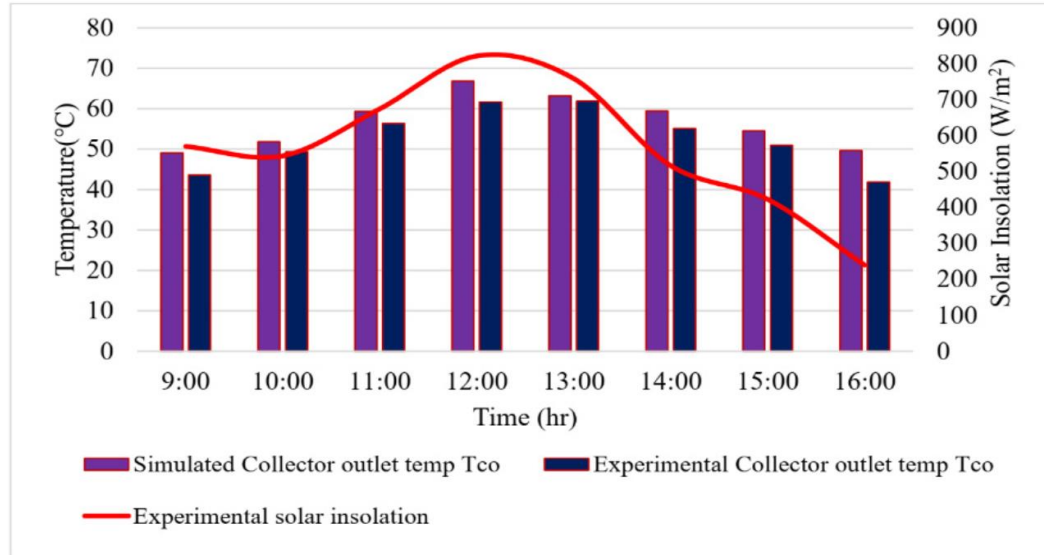


Figure 11. Average simulated and experimental temperatures at the collector outlet

3.2.2 Drying Unit

The comparison of simulated and experimental air temperatures in the drying chamber are shown in Figure 12. The results are in good agreement, with the average temperature difference of 3 °C. The simulated results were consistently higher than the experimental results because the simulation was set to be adiabatic while the experimental setup had some heat losses through some parts that did not have insulation. Both the simulated and experimental temperatures show a steady rise to a maximum of 73.96 and 70.65 °C respectively, followed by a steady decrease.

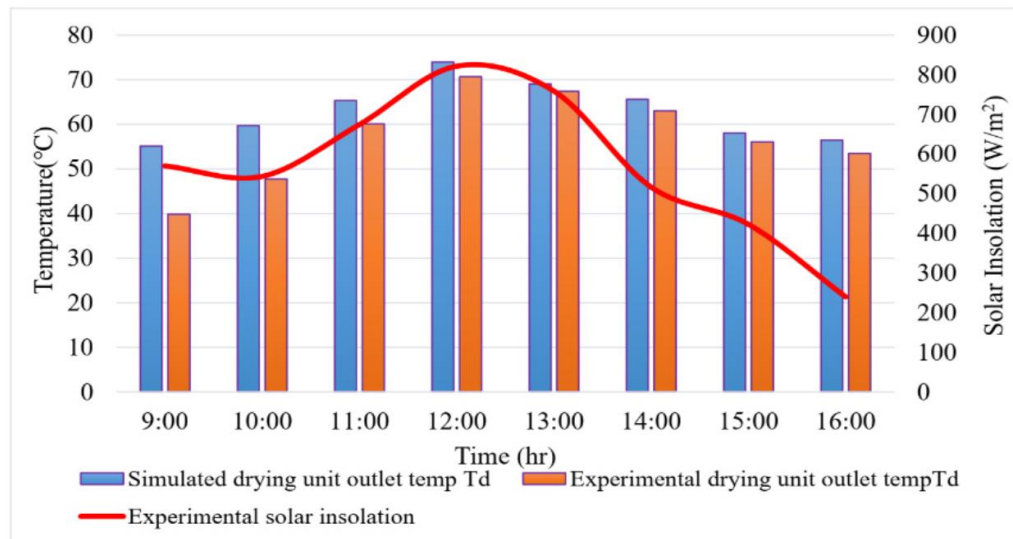


Figure 12. Average simulated and experimental temperatures in the drying unit

3.3 Mean Relative Deviation of Collector Temperature

The mean relative deviation (MRD) of collector temperature was obtained using Equation 1. A comparison between the numerical results and the experimental results shows a good agreement with a mean relative deviation of 5.1% which is acceptable as it does not exceed 10%. Other authors such as Tagne, et al., (2020) found an error of 4.53% which is almost equal to what was found in this study. From the low values of these errors, it can be inferred that the proposed model can predict the temperature profile inside the dryer satisfactorily. The relative error of 5.1 % is acceptable and can be explained by the fact that some real heat losses were not taken into consideration in the theoretical simulation.

4. Conclusion

This paper has set out to simulate, using CFD, the temperature and airflow distribution in a natural convection solar tunnel dryer. The following are noted:

- (1) Although the chimney was receiving solar insolation through its absorber, the air in the chimney did not seem to have benefited from this heating, an indication that there was some loss of heat from the chimney. One way of reducing this heat loss from the chimney is to insulate its back and sides and add glazing on its front side.
- (2) The hottest air coming out of the collector forms a recirculation region before flowing to the drying unit.
- (3) The airflow experiences some pressure losses as it moves from the drying chamber to the chimney, as seen by the change in its velocity. To reduce the losses, a curved joint between the chimney and the drying chamber is suggested to reduce the turbulence created as the air changes direction.
- (4) There existed a decrease in the velocity in some parts of the dryer. This was due to the loss in the velocity of the flux produced by the solids inside the drying chamber, which produced a uniform elevation of the heat.
- (5) The simulation results were validated by comparing them with the results obtained from experiments. The results indicated a good agreement with a mean relative error of 5.1%.

It can be concluded that CFD is an efficient tool that can be used to predict the temperature and airflow distribution in natural convection solar tunnel dryers and has paved the way for further improvements in the design of these solar dryers.

Conflicts of Interest

The authors hereby declare that there are no conflicts of interest regarding the publication of this paper.

Acknowledgments

The authors wish to thank the Heads of the Department of Agricultural and Mechanical Engineering- at the University of Zambia, Dr. V. Kaluba and Dr. V. Musonda together with their entire members of staff, technical and support staff for their generous input.

References

- Al-Neama, M., & Farkas, I. (2016). Influencing of solar drying performance by chimney effect. *Hungarian Agricultural Engineering*, 30, 11-16. <https://doi.org/10.17676/HAE.2016.30.11>
- Bala , B. K., & Wood, J. L. (1994). Simulation of the indirect natural convection solar drying of rough rice. *Solar Energy*, 53, 259-266. [https://doi.org/10.1016/0038-092X\(94\)90632-7](https://doi.org/10.1016/0038-092X(94)90632-7)
- Brooker, D., Bakker-Arkema, F., & Hall, C. (1992). *Drying and storage of grains and oilseeds*. Westport: The AVI Publishing Company.
- Cherotich, S. (2016). *Experimental investigation and mathematical modelling of a natural convection solar tunnel fruit dryer*. Master of Engineering dissertation.
- Cherotich, S., & Simate, I. N. (2016). Experimental Investigation and Mathematical Modelling of a Natural Convection Solar Tunnel Dryer. *International Journal of Scientific & Engineering Research*, 7(5), 597-603.
- Jhersson, C.-R., Amaya, D., & Ramos, O. (2018). Food Dryer Design and Analysis of Velocity and Temperature Profiles. *International Journal of Applied Engineering Research*, 13(18), 13578-13583.
- Kaushal, P., & Sharma, H. (2012). Concept of Computational Fluid Dynamics (CFD) and its Applications in Food Processing Equipment Design. *J Food Process Technol*, 3(138). <https://doi.org/10.4172/2157-7110.1000138>
- Kumar, A., Sreenivaslu, G., P S Raghavendra, R., Kumar, A., & Pattanaik, A. (2019). Experimental Investigation on Performance of Solar Air Heaters With Thermal Storage. *International Journal of*

- Renewable Energy and Its Commercialization*, 5(1), 37-46. <https://doi.org/10.37628/jrec.v5i1.770>
- Mathioulakis, E., Karathanos, V., & Belessiotis, V. (1998). Simulation of air movement in a dryer by computational fluid dynamics: application for the drying of fruits. *Journal of Food Engineering*, 36(2), 183-200. [https://doi.org/10.1016/S0260-8774\(98\)00026-0](https://doi.org/10.1016/S0260-8774(98)00026-0)
- Michael, E. R. (2014). *Unit 03: Glazing - Greenhouse Management Online*. Retrieved May 23, 2022, from https://greenhouse.hosted.uark.edu/Unit03/Printer_Friendly.html
- Misha, S., Mat, S., Ruslan, M. H., Sopian, K., & Salleh, E. (2013). The Prediction of Drying Uniformity in Tray Dryer System using CFD Simulation. *International Journal of Machine Learning and Computing*, 3(5), 419-423. <https://doi.org/10.7763/IJMLC.2013.V3.352>
- Ni, H. (1997). *Multiphase Moisture Transport in Porous Media under Intensive Microwave Heating*. Ph.D Dissertation, . NY, USA: Cornell University, Ithaca.
- Omolola, A. O., Jideani, A. I., & Kapila, P. F. (2015). Drying kinetics of banana (*Musa spp.*). *Interciencia*, 40(6), 374-380.
- Roman, R. N., Lopez, O. A., Garcia, V., Pilatosky, F. I., & Ituna, Y. J. (2019). Computational fluid dynamics analysis of heat transfer in a greenhouse solar dryer “chapel-type” coupled to an air solar heating system. *Energy Sci Eng*, 7, 1123-1139. <https://doi.org/10.1002/ese3.333>
- Romuli, S., Schock, S., Nagle, M., Chege, C. G., & Müller, J. (2019). Technical Performance of an Inflatable Solar Dryer for Drying Amaranth Leaves in Kenya. *Applied Science*, 3, 1-11. <https://doi.org/10.3390/app9163431>
- Sangpradit, K. (2014). Study of the Solar Transmissivity of Plastic Cladding Materials and Influence of Dust and Dirt on Greenhouse Cultivations. *Energy Procedia*, 56, 566-573. <https://doi.org/10.1016/j.egypro.2014.07.194>
- Simate, I. N. (2020). Air Flow Model for Mixed-Mode and Indirect-Mode Natural Convection Solar Drying of Maize. *Energy and Environment Research*, 10(2), 1-12. <https://doi.org/10.5539/eer.v10n2p1>
- Simate, I. N., & Cherotich, S. (2017). Design and Testing of a Natural Convection Solar Tunnel Dryer for Mango. *Journal of Solar Energy*, 1-10. <https://doi.org/10.1155/2017/4525141>
- SOLIDWORKS Corporation. (2010). *Engineering Design and Technology Series: An Introduction to Flow Analysis Applications with SolidWorks Flow Simulation, Instructor Guide*. Concord, Massachusetts USA: Dassault Systèmes - SolidWorks Corporation.
- Tagne, M. S., Ndukwu, C. M., & Azese, N. M. (2020). Experimental Modelling of a Solar Dryer for Wood Fuel in Epinal (France). *Modelling*, 1, 39-52. <https://doi.org/10.3390/modelling1010003>
- Tiris, C., Tiris, M., & Dincer, I. (1995). Investigation of the thermal efficiencies of a solar dryer. *Energy conversion and management*, 36, 205-212. [https://doi.org/10.1016/0196-8904\(94\)00051-Z](https://doi.org/10.1016/0196-8904(94)00051-Z)
- Udomdejwatana, S. (1994). *Thermal properties of Musa suerier and Musa sapientum Linn*, Master's Thesis. Bangkok, Thailand: Chulalongkorn University.
- Vintilă, M., Ghiaus, A. G., & Fătu, V. (2014). Prediction of Air Flow and Temperature Profiles Inside Convective Solar Dryer. *Bulletin of University of Agricultural Sciences and Veterinary Medicine Cluj-Napoca: Horticulture*, 71, 188-194. <https://doi.org/10.15835/buasvmcn-fst:10868>
- Xia, B., & Sun, D.-W. (2002). Applications of computational fluid dynamics (CFD) in the food industry: a review. *Computers and Electronics in Agriculture*, 34, 5-24. [https://doi.org/10.1016/S0168-1699\(01\)00177-6](https://doi.org/10.1016/S0168-1699(01)00177-6)
- Zoukit, A., El ferouali, H., Salhi, I., Doubabi, S., Abdenouri, N., & El kalali, T. (2019). Simulation, design and experimental performance evaluation of an innovative hybrid solar-gas dryer. *Energy*, 189, 116-279. <https://doi.org/10.1016/j.energy.2019.116279>

Copyrights

Copyright for this article is retained by the author(s), with first publication rights granted to the journal.

This is an open-access article distributed under the terms and conditions of the Creative Commons Attribution license (<http://creativecommons.org/licenses/by/4.0/>).